MRC-SL-339

CHARACTERIZATION TECHNIQUES STUDY REPORT

MAGNETIC BUBBLE MATERIALS

Monsanto Research Corporation
St. Louis, Missouri 63166

Roger W. Shaw, Robert M. Sandfort, and Jerry W. Moody

Contract No. DAAH01-72-C-0490

Distribution of this document is unlimited

ARPA Support Office
Research, Development, Engineering,
and Missile Systems Laboratory
U.S. Army Missile Command
Redstone Arsenal, Alabama

Sponsored by:
Advanced Research Projects Agency
ARPA Order Nr. 1999

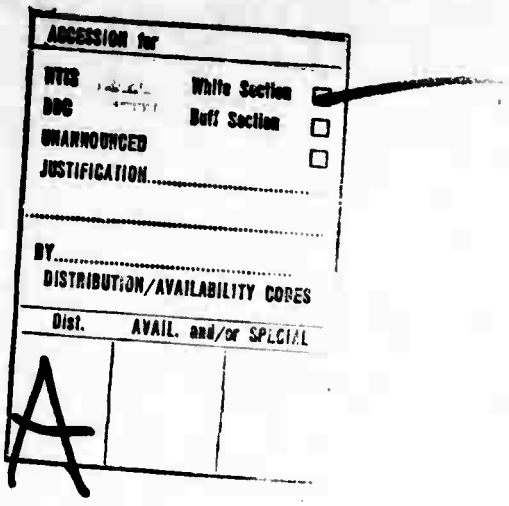

NOTICE

This research was sponsored by the Advanced Research Projects Agency of the Department of Defense under ARPA Order 1999 and was monitored by the US Army Missile Command under Contract Number DAAH01-72-C-0490. Views and conclusions expressed herein are the primary responsibility of the author or the contractor and should not be interpreted as representing the official opinion or policy of USAMICOM, ARPA, DOD or any other agency of the Government.

UNCLASSIFIED
Security Classification

DOCUMENT CONTROL DATA - R & D

(Security classification of title, body of abstract and indexing annotation must be entered when the overall report is classified)

1. ORIGINATING ACTIVITY (Corporate author)
Monsanto Research Corporation
800 North Lindbergh Boulevard
St. Louis, Missouri 63166

2a. REPORT SECURITY CLASSIFICATION
UNCLASSIFIED

2b. GROUP

3. REPORT TITLE

MAGNETIC BUBBLE MATERIALS

4. DESCRIPTIVE NOTES (Type of report and inclusive dates)
INITIAL CHARACTERIZATION REPORT

5. AUTHOR(S) (First name, middle initial, last name)
Roger W. Shaw
Robert M. Sandfort
Jerry W. Moody

6. REPORT DATE
July 1972

7a. TOTAL NO. OF PAGES
177

7b. NO. OF REFS
279

8a. CONTRACT OR GRANT NO.
DAAH01-72-C-0490

b. PROJECT NO.
ARPA Order No. 1999-72

c.

d.

9a. ORIGINATOR'S REPORT NUMBER(S)
MRC-SL-339

9b. OTHER REPORT NO(S) (Any other numbers that may be assigned this report)

10. DISTRIBUTION STATEMENT

Distribution of this document unlimted

11. SUPPLEMENTARY NOTES

12. SPONSORING MILITARY ACTIVITY
Advanced Research Project Agency
Washington, D.C.

13. ABSTRACT

This report presents the results of a study made by Monsanto Research Corporation during the final phase of Contract No. DAAH01-72-C-0490. The intent of the study was to define those physical properties of magnetic bubble materials which need to be characterized, to investigate the known methods for making these characterization, and, finally, to recommend those characterization procedures which appear "best" at this time. Those material properties included in the study were: Substrate and film composition - substrate and film lattice parameter - substrate and film defect identification and location - film thickness - film thickness variations - characteristic length and domain dimensions - saturation magnetization and magnetic fields - domain wall energy - domain wall dynamic properties - anisotropy - coercivity - magneto-striction coefficients - reorientation temperature - Neel temperature - compensation temperature - temperature variation of material parameters - thermal conductivity - refractive index - Faraday effect - Kerr effect - optical and magneto-optical absorption - electrical conductivity - photo conductivity.

Extensive reference to existing literature has been made in an endeavor to keep this report within reasonable size. As a result, a lengthy bibliography has been compiled to which the reader is urged to refer for a more detailed analysis of the measurement procedures discussed here.

DD FORM 1 NOV 68 1473 REPLACES DD FORM 1473, 1 JAN 64, WHICH IS OBSOLETE FOR ARMY USE.

Security Classification

14. KEY WORDS	LINK A		LINK B		LINK C	
	ROLE	WT	ROLE	WT	ROLE	WT
Single Crystal Rare Earth Garnets						
Characterization Methods for Bubble Garnets						
Magnetic Domains						
Memory Devices						

TECHNICAL REQUIREMENT NO. 1533
ARPA ORDER 1999

CHARACTERIZATION TECHNIQUES STUDY REPORT

MAGNETIC BUBBLE MATERIALS

July, 1972

Roger W. Shaw, Robert M. Sandfort, Jerry W. Moody

MONSANTO RESEARCH CORPORATION
St. Louis, Missouri 63166

Contract No. DAAH01-72-C-0490

Monitored By
ARPA Support Office
Research, Development, Engineering, and
Missile Systems Laboratory

Sponsored by
Advanced Research Projects Agency
Washington, D.C., ARPA Order No. 1999

ABSTRACT

This report presents the results of a study made by Monsanto Research Corporation during the final phase of Contract No. DAAH01-72-C-0490. The intent of the study was to define those physical properties of magnetic bubble materials which need to be characterized, to investigate the known methods for making these characterizations, and, finally, to recommend those characterization procedures which appear "best" at this time. Those material properties included in the study were: Substrate and film composition - substrate and film lattice parameter - substrate and film defect identification and location - film thickness - film thickness variations - characteristic length and domain dimensions - saturation magnetization and magnetic fields - domain wall energy - domain wall dynamic properties - anisotropy - coercivity - magnetostriction coefficients - reorientation temperature - Neel temperature - compensation temperature - temperature variation of material parameters - thermal conductivity - refractive index - Faraday effect - Kerr effect - optical and magneto-optical absorption - electrical conductivity - photo conductivity.

Extensive reference to existing literature has been made in an endeavor to keep this report within reasonable size. As a result, a lengthy bibliography has been compiled to which the reader is urged to refer for a more detailed analysis of the measurement procedures discussed here.

Table of Contents

Table of Contents (continued)

Table of Contents (continued)

List of Figures

List of Figures (continued)

List of Tables

1. INTRODUCTION

The concept of a magnetic memory operating without moving parts has been of interest to the computer industry for many years. Indeed, the ferrite core memories in wide use today are such devices but the complexity and resulting cost of their assembly has kept interest in other alternatives high. A number of memory related concepts involving the motion of magnetic domains in metallic ferromagnetic materials have reached the working device level in the form of shift registers, including Hughes Aircraft Dynabit ™ and Cambridge Memories, Inc. DOT™ Systems. Bell Telephone Laboratories has most strongly pursued the concept of moving domain memory devices in insulating, ferrimagnetic materials, starting first with the orthoferrites (prototype - $YFeO_3$) and progressing more recently to the magnetic garnets (prototype - $Y_3Fe_5O_{12}$). In these materials the desirable configuration is one in which the unique easy axis of magnetization is perpendicular to a thin slab or film of the material. In the presence of a magnetic bias field of the proper magnitude along the magnetization direction, cylindrical magnetic domains of opposite magnetic polarity will be stable in these materials. These cylindrical domains, when viewed between crossed polarizers, look like tiny bubbles by virtue of the Faraday effect in the magnetic material. This term "magnetic bubble" has become widely used to describe a cylindrical magnetic domain. A great deal of work has already been done but much work remains in order

to be able to generate, move, and detect bubbles with the speed and reliability required by the computer industry. Many people are now convinced, however, that this can and will be done. Still further development will be required to bring to fruition the potential for logical operations which is inherent in the repulsive interaction which exists between the bubbles. The appeal of a complete, if small, bubble computer is considerable and such efforts will undoubtedly continue.

A very significant part of the development of magnetic bubble technology has been and will continue to be the characterization of the properties of appropriate magnetic materials. Older measurement methods are being adapted to the special requirements of these thin, transparent magnetic bubble films, and, in addition, new methods of measurement are being developed which take advantage of the unique properties of these films, in particular the easily observed Faraday effect in the visible portion of the electromagnetic spectrum. There is no doubt that further refinements will take place in the methods and the properties used to characterize these materials. Improved accuracy, more reliable prediction of device performance, and more rapid data acquisition and analysis are all desirable and will be achieved.

This contract requires the conduct of a study of the state of the art in the characterization of single-crystal,

non-magnetic substrates and single-crystal thin magnetic films, including establishment of all the items required to be characterized, presentation of the known techniques for each of the methods of characterization and identification of the recommended characterization method for each item. The present report has been prepared in fulfillment of that requirement. We have relied upon references to the available literature wherever possible as the traditional and best means of presenting much of the detail of these techniques. In order to increase the usefulness of the report we have also included references to the application of the various techniques to magnetic bubble domain materials wherever possible. For the present purposes these materials are defined as the orthoferrites and iron-containing garnets, with the latter receiving much of the attention because of their more desirable properties -- primarily smaller bubble size and ease of epitaxial growth. The measurement of the following properties of these materials are discussed:

Composition

Lattice constants

Substrate defects

Film thickness and its variation

Film defects

Characteristic length

Magnetization

Domain wall energy

Domain wall dynamics

Ferromagnetic resonance

Anisotropy

Coercivity

Magnetostriction coefficients

Thermal properties

Optical properties

Electrical properties

Not all of these items are felt by the authors to be worthy of routine measurement, but are discussed here more for reasons of completeness than for any reflection on their importance. The authors of this report are Roger W. Shaw, Robert M. Sandfort, and Jerry W. Moody. They would welcome comments, suggestions, and criticism from the readers.

2. COMPOSITION

A knowledge of the chemical composition of the substrate as well as the epitaxial layer is required for the complete characterization and understanding of garnet bubble materials. Impurities or stoichiometric deviations in the substrate can affect the lattice constant of the material. Even small variations of lattice constant can result in significant effects in the epitaxial film. This is especially true for films exhibiting stress-induced anisotropy for which the non-cubic anisotropy depends upon the strains resulting from a deliberate mismatch of the lattice constant of film and substrate. In addition, the chemical components of the substrate can be physically incorporated into films grown by either chemical vapor deposition or by liquid phase epitaxy. For example, Robinson, et al (Ref. 1), observed an interfacial layer between $Tb_{2.5}Er_{0.5}Fe_5O_{12}$ films grown by CVD on $Sm_3Ga_5O_{12}$ substrates. They reasoned that the intermediate layer contained some samarium from the substrate. In the LPE growth of garnet films in PbO-based solvents, there is ample evidence that the surface of the substrate is dissolved before film growth is initiated. The dissolved components can then be reprecipitated as the film grows. Levinstein, et al (Ref. 2) observed intermediate layers in LPE films of $Gd_{3-x}Tb_xFe_5O_{12}$ on $Nd_3Ga_5O_{12}$ substrates. The components of the solution itself are another source of

impurities which can be incorporated in the film. Since the magnetic properties of the film are a sensitive function of the composition, it is important to know not only the major constituents but also what contaminants might be present in the film.

2.1 Film Composition

The problems associated with the determination of the composition of magnetic garnet films have been discussed by Mee, et al (Ref. 3). In general, the films of interest are less than 10μm thick and only a minute quantity is available for analysis. Usually both the film and substrate contain at least gallium in common and separation of film and substrate is not a trivial matter. In typical multi-component films the physical and magnetic properties of the films, such as lattice constant, magnetization, etc., are not specific and, thus, can not be used as a basis for a reliable determination of composition. Most of these problems are avoided by electron probe microanalysis (EPM) for compositional determinations (Ref. 4).

EPM offers three advantages over other means of compositional analysis.

1) The effective volume of characteristic X-ray production is small, typically of the order of $2\mu m^3$. This shallow penetration of the epitaxial layer insures that only the area of interest is considered in the determination.

2) Due to the small area of analysis, it is possible

to perform homogeniety determinations over the surface of the epitaxial layer.

3) Since the technique is non-destructive it is possible to utilize the film in further testing and evaluation subsequent to EPM analysis.

The concentrations of all elements composing the garnet matrix are determined quantitatively with the exception of oxygen. The concentration of oxygen in all determinations is assumed to compose the balance of the composition. This is necessary since the instrument currently used at Monsanto for the analysis does not have the capability to detect elements lighter than aluminum.

For the samples evaluated to date, the concentration of rare earth metals, lead, and iron have been determined by comparison to pure metal forms of these elements. The determination of gallium concentration was made by comparison to gallium phosphide. The purity of the standards used is as follows:

Rare Earths	-	99.9%
Fe	-	Spectrographic grade
Pb	-	Spectrographic grade
GaP	-	Monsanto Semiconductor

Matrix corrections are applied when the sample counts are compared to the standards. The accuracy of the method is approximately 3% of the actual concentration of the metals.

Since the electron beam samples an area only about 2

microns in diameter, the compositional uniformity of the epitaxial layers is determined by taking counts at a number of widely separated points on each layer. The agreement of these determinations is, in general, well within the experimental accuracy of the method. The compositional uniformity of the layers is also checked by measuring the Neel temperature at various points. This measurement is discussed in a later section. Again, the results at various points on a given sample generally agree within the accuracy of the method.

2.2 Trace Impurity Analysis

The oxides (rare earth, iron, gallium, lead, etc.) used in garnet substrate and film growth are now available in high purity from a number of sources. Also, the growth of crystals by the Czochralski method generally effects a further purification (Ref. 5). Thus, impurities in garnet substrates are usually present in trace amounts (with the exception of iridium in the substrate and lead in flux grown films) and, to date, have not been considered a serious problem in garnet bubble material technology. This attitude may change as the technology advances and ever more stringent requirements are placed on compositional control.

The analysis of rare earth garnets (or starting materials) for impurities is relatively straight forward and may be accomplished by a number of well established

methods. These include emission spectroscopy, mass spectroscopy, chemical spectrophotometry and fluorometry, and atomic absorption (see references 6 and 7 for description of these and other methods for trace analysis). It should be pointed out that these methods are destructive but usually require only a small amount of sample. All these methods are capable of accurate determination of trace amounts and the choice of a particular method depends primarily on the availability of specific equipment or personnel.

The analysis of bubble materials for trace impurities has been seldom reported. However, semiquantitative analysis by emission spectroscopy has been performed at Monsanto on selected crystals and materials which were believed to be contaminated by impurities. The technique used is that discussed by Wang, et al (Ref. 8).

2.3 Stoichiometric Deviations

The compositional range of stability of the rare earth garnets is very narrow. In addition, it is probable that the excess components are not distributed uniformly but are concentrated in the growth striations and "core" region of Czochralski grown crystals. It is difficult to determine stoichiometric deviations accurately in such systems so that completely satisfactory analytical techniques have not yet been developed.

The electron microprobe has been used to detect variations in the gallium concentration in wafers of $Gd_3Ga_2O_{12}$. Recently, Braginski, et al (Ref. 9) used the elect on microprobe to study the compositional variation in $Y_3Fe_5O_{12}$ films grown by chemical vapor deposition on $Gd_3Ga_5O_{12}$ substrates. However, this method has not been made quantitative.

Brandle, et al (Ref. 10) have related the lattice constant of $Gd_3Ga_5O_{12}$ to the stoichiometry of the melt from which the crystals were pulled. With this information it is possible to obtain a qualitative estimation of the stoichiometry of a $Gd_3Ga_5O_{12}$ crystal by a precise lattice constant measurement.

3. LATTICE CONSTANTS AND THERMAL EXPANSION COEFFICIENTS

An accurate knowledge of the lattice constant of both film and substrate is one of the most important factors in the successful growth of epitaxial layers and in the interpretation of the magnetic properties of the films. This is especially true for those film compositions which exhibit stress-induced anisotropy. Film and substrate must be matched closely enough to yield smooth, uncracked layers with a high quality interface, but mismatched enough that bilateral stresses, acting through magnetostriction, result in the desired anisotropy. The lattice constant of Czochralski-grown garnets depends upon the conditions of growth and will be found to vary over a relatively narrow range. However, the range of film/substrate mismatch that can be tolerated is so small that the lattice constant of each substrate crystal must be measured and the composition of the film adjusted correspondingly.

The general methods for determining the structure and lattice constant of crystalline substances are well known and need little elaboration here. The reader is referred to any of the many excellent texts on the subject (for example, ref. 11). It is appropriate, however, to outline the specific procedure used at Monsanto to determine the precise unit cell dimensions of the substrates and films, as an example.

The lattice constant, a_o is determined by the x-ray diffractometry procedure published by Pierron and McNeely (Ref. 12). Since the original precision of the method, $\pm$ 0.00001Å, is not needed in this study corrections for the Lorentz-polarization, x-ray refraction and temperature errors are not made. The precision of the procedure used and described herein is $\pm$ 0.0001Å.

The (111) oriented garnet crystal is mounted on the sample holder and the (888), (12 12 12), and (16 16 16) reflections are slowly scanned using Mo radiation. A scanning speed of $0.125°min^{-1}$, corresponding to one inch per minute of recorder chart travel, permits accurate estimate of the 2θ angle at maximum peak intensity to within 0.002°. The d spacings are computed from the 2θ angles and are then converted to corresponding a_o values for the (888), (12 12 12) and (16 16 16) reflections. The a_o values are plotted versus $\cot^2\theta$ so that an extrapolation to high θ angles may be made which will minimize systematic misalignment error. The extrapolated value of a_o at $\cot^2\theta = 0$ yields the cell parameter. If the crystal has been aligned properly, the plot yields a straight line parallel to the $\cot^2\theta$ axis. In routine practice the alignment is considered satisfactory if the difference in a_o values between the (888) and (16 16 16) reflections is no greater than 0.001Å. Alignment is routinely verified by slowly scanning the (888) and (12 12 12) reflections of a standard GaAs crystal, $a_o = 5.65399$. The

2θ values of peak maximum should be 60.23 and 97.63 degrees respectively for Mo $K\alpha_1$ radiation. Fig. 1 is a typical plot for a GGG crystal. In this case the curve extrapolates to an a_o value of 12.3801Å.

The same procedure is used to determine, in situ, the lattice constant of the epitaxial films. In this case two peaks are obtained: one peak corresponding to the strained lattice constant of the film and a second, usually larger in amplitude, corresponding to the strained lattice constant of the substrate. The lattice constants obtained in this manner correspond to interplanar spacings which are perpendicular to the film surface, and in general are different from the unstrained lattice parameters. The lattice dimensions parallel to the film surface, which are of more interest, can be obtained, according to Mee, et al (Ref. 13) by the relationship between parallel and perpendicular strain,

$$\Delta a^{\perp} = \frac{(1 + \mu)}{(1 - \mu)} \quad (a_s - a_f) \qquad (3\text{-}1)$$

where $\Delta a^{\perp}$ is the difference in lattice dimensions obtained from the x-ray analysis, μ is Poisson's ratio for the film composition and a_s and a_f are the unstrained lattice constants of substrate and film, respectively.

The authors feel there is some question as to whether one actually obtains the unstrained lattice constant of the film, a_f, from this analysis. In the data obtained as outlined above, the substrate lattice constant determined in the presence of a thin epitaxial film is different in general from

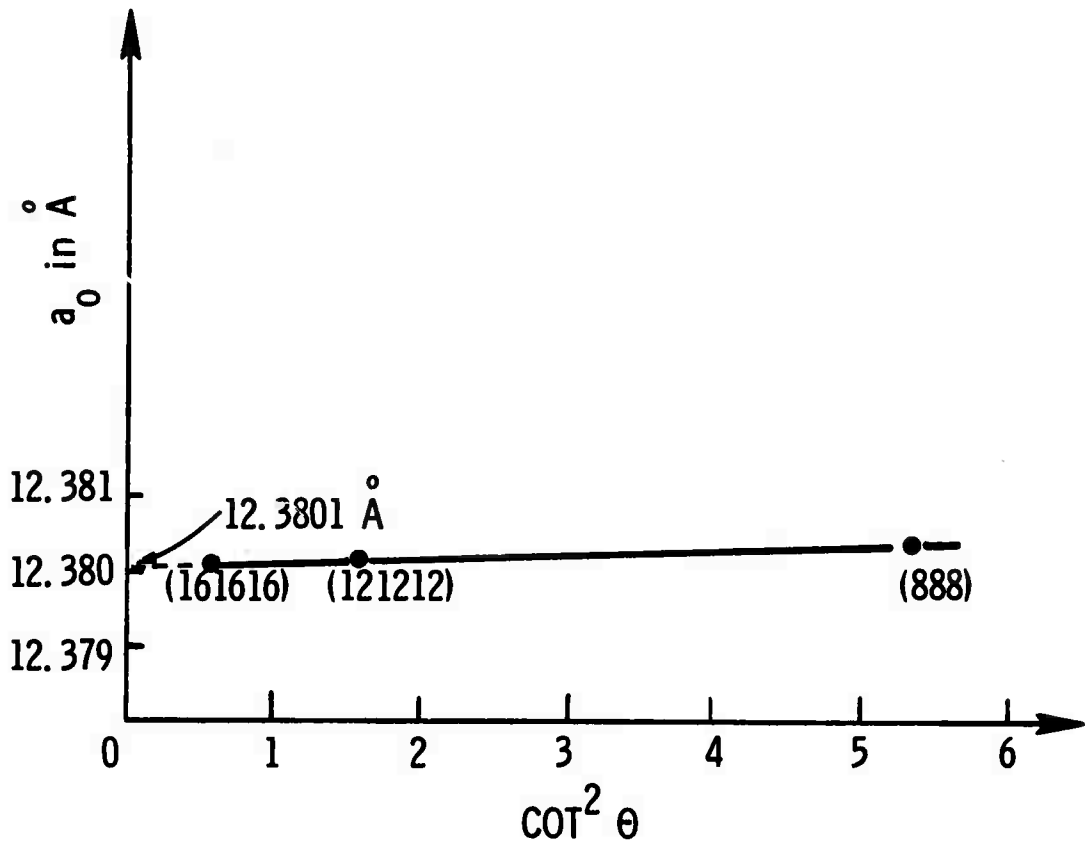

Figure 1. a_o values versus $\cot^2 \theta$ for $Gd_3Ga_5O_{12}$ (Boule 4492)

its value determined separately. It is usually shifted in the direction of the film lattice parameter in agreement with Shick's (Ref. 14) observations. This may indicate that a kind of "average" lattice parameter is being measured for both film and substrate, or that the substrate is in fact strained itself near the interface. We feel that $\Delta a^{\perp}$ is an important parameter, but are disinclined to interpret an unstrained film lattice parameter from $\Delta a^{\perp}$ on the basis of results seen to date. Probably fundamental lattice parameters of this type should be taken from bulk single crystals of identical composition, or from very thick epitaxial layers which are strong enough to be free standing.

For an apparatus equipped with a high temperature cell, the measurement of precise lattice constants at elevated temperatures provides a convenient means of determining the thermal expansion coefficients of the garnets (Ref. 15). If such equipment is not available, the more conventional dilatometry may be used (Ref. 16). This is the method used by Mee, et al (Ref. 17).

4. SUBSTRATE DEFECTS

Although crystals of $Gd_3Ga_5O_{12}$ can now be grown essentially free of all defects, the need for substrate examination and evaluation has not been obviated. The growth of epitaxial magnetic garnet films of device quality requires substrates of the very highest quality. Indeed, most of the defects which impede domain motion in the magnetic film can be traced to defects already present in the substrate before film deposition. Therefore, substrate evaluation will always remain an important part of bubble material technology.

Substrate defects can be introduced either during the crystal growth process or in subsequent cutting, lapping or polishing. Scratches, dust and solvent stains are examples of defects which fall into the latter class. Frequently they can be detected by close visual examination of the substrates and can be avoided by good housekeeping practices and proper polishing procedures. They need not cause the complete rejection of the substrate since the wafer can be repolished or recleaned. Defects which are introduced during crystal growth are more serious. These include strains, inclusions, voids, growth striations and dislocations. Experience indicates that defect-free epitaxial films cannot be grown on substrates containing such defects. Recently, Chaudhari (Ref. 18) discussed the defects in garnet substrates that influence magnetic domain

motion. The detection and evaluation of these defects are discussed in the following paragraphs. It will be apparent that most of the techniques recommended for substrate evaluation depend upon the interaction of defects with light or X-rays. Although the techniques are discussed in reference to a specific defect for which they are especially appropriate, their application can be more general. For example, X-ray topography can not only be used to study striations and banding, but it also reveals dislocations and inclusions. Other examples of complementary methods and how they can be used to advantage will be obvious.

4.1 Strain

The rare-earth gallium garnets are grown by the Czochralski method from RF heated iridium crucibles at approximately 1800°C. Large thermal gradients, both in and above the melt, are natural in such systems. As a result of the thermal stresses, the garnet crystals are often strained. Indeed, one of the most characteristic features of Czochralski grown rare-earth garnets is a highly strained, central "core" which is associated with the development of facets at the solid/liquid interface during crystal growth. (The core can be eliminated by adjusting the growth conditions.)

Strain induces optical heterogeneity and birefringence in the crystal which can be detected by examination

with polarized light. When the crystal is viewed between crossed-polarizers, the strain-induced birefringence manifests itself as color and intensity variations. Fig. 2 illustrates the appearance of a strained $Gd_3Ga_5O_{12}$ crystal when viewed between crossed polarizers. The presence of the central core is readily apparent. For this examination, the ends of the boule must be cut and polished parallel. This qualitative examination for strain is used routinely at Monsanto.

A more quantitative evaluation of the strain in garnet crystals can be obtained by Twyman-Green interferometry (Ref. 19). This method has been widely used for assessing strain in sapphire, ruby (Ref. 20), garnet (Ref. 21) and other transparent crystals. The principal of the Twyman-Green interferometer is shown in Fig. 3. The test crystal is mounted on one arm of the apparatus and the interference pattern is recorded by a camera located on another arm. A variation of one fringe on the interferogram of a crystal of length L with plane parallel end faces is due to an optical path difference of:

$$\Delta(nL) = \frac{\lambda}{2} \qquad (4\text{-}1)$$

where n is the refractive index and λ is the wavelength of the light used.

It should be pointed out that the usual Twyman-Green interferogram integrates the effect of optical inhomogeneities

Figure 2. $Gd_3Ga_5O_{12}$ crystal between crossed polarizers.

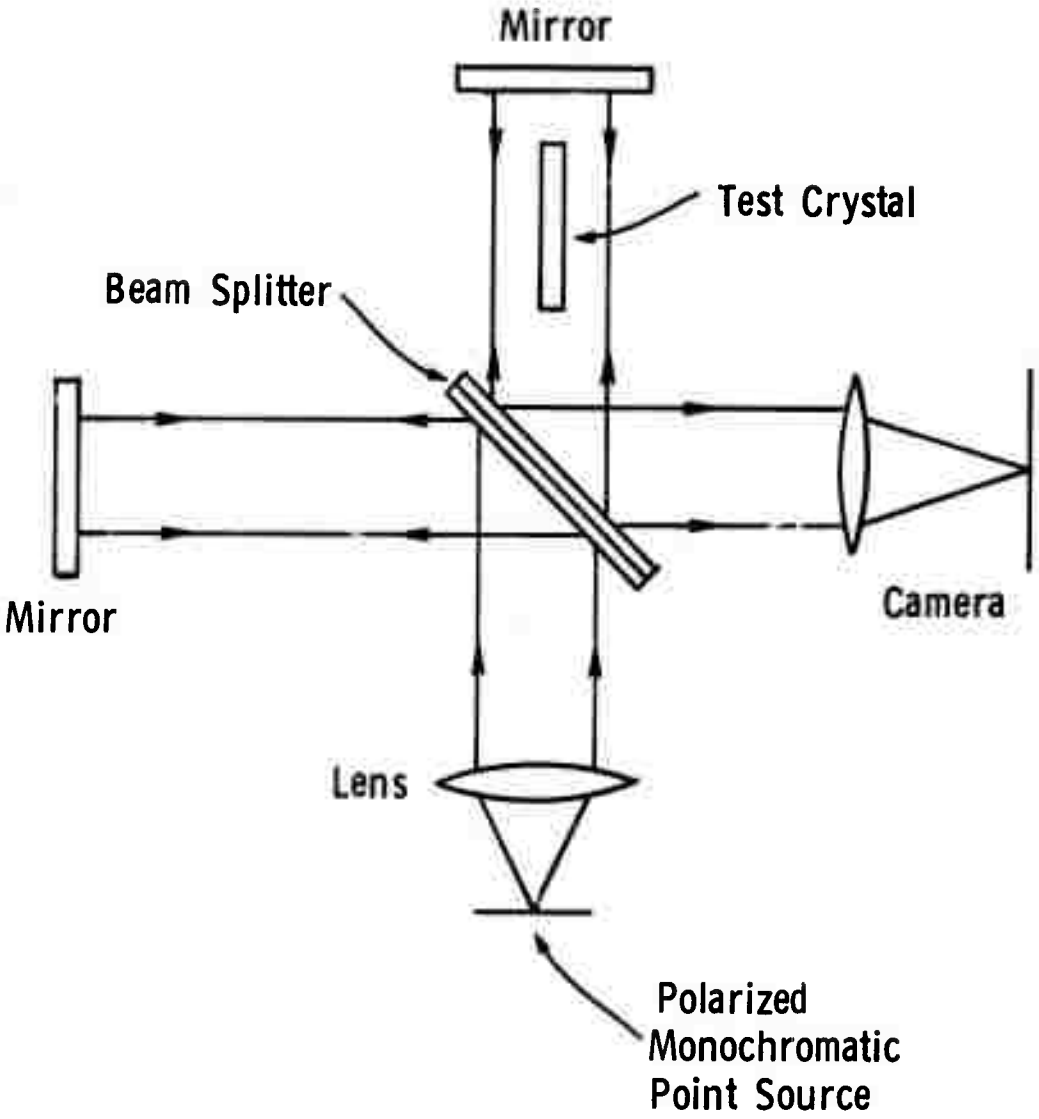

Figure 3. Schematic diagram of Twyman-Green interferometer. After Nestor, ref. 23.

along the entire length of the rod so that the specific source or location of the inhomogeneity cannot be identified. However, more specific information can be obtained by immersing the crystal in an index matching liquid (contained in a cell with flat parallel faces) and viewing from the side.

4.2 Inclusions

The rare-earth gallium garnets are not stable at their melting points in an inert atmosphere. The melts tend to loose gallium via a volatile suboxide (Ref. 22). The decomposition of Ga_2O_3 can be suppressed by maintaining a partial pressure of oxygen above the melt. However, the garnet melts are usually contained in iridium crucibles which are readily oxidized when in an oxygen atmosphere at elevated temperatures. It is difficult to maintain melt stoichiometry and minimize crucible oxidation simultaneously. During the long periods of time required to grow the crystals, the melt tends to become non-stoichiometric and saturated with IrO_2. It is not surprising, therefore, that inclusions of one or more foreign phases are a common defect in garnet crystals.

Brandle, et al (Ref. 10) have discussed the origin and appearance of the most common inclusions found in $Gd_3Ga_5O_{12}$ crystals. Three types of inclusions were identified:

(1) triangular or hexagonal platelets of metallic iridium

(2) dark square or cubic crystals which are believed to be particles of a gadolinium gallium suboxide, probably gadolinium orthogalliate ($GdGaO_3$)

(3) transparent acicular crystals, tentatively identified as Gd_2O_3.

The first two types are by far the most predominant, with the third found only occasionally.

Inclusions in the garnets can be studied most conveniently by optical microscopy. Slices of the crystal polished flat and parallel are required for these studies. Examples of the most common defects are illustrated in the photomicrographs of Fig. 4. The density of the inclusions can be obtained by counting the number of inclusions in a known volume of the wafer.

Tyndall scattering may also be used to measure the density of inclusions (Ref. 20). Here collimated monochromatic light is directed through the crystal, usually along the growth or optical axis. The emergent scattered light (low angle scattering) can be measured by placing a film strip in an arc whose center is the center of the exit end. Alternatively, the large angle scattering can be measured by photographing the light scattered perpendicular to the collimated beam. In this mode, the crystal can be scanned to determine the site and distribution of scattering centers. Nestor (Ref. 23) has described an apparatus to measure large angle scattering for ruby laser rods.

4.3 Dislocations

The energy to create dislocations in the rare earth garnets is large and crystals can be grown essentially free

Figure 4a. Iridium inclusions (200X)

Figure 4b. Gadolinium gallium suboxide particle (1000X)

Figure 4. Common inclusions in $Gd_3Gd_5O_{12}$

of all dislocations. However, dislocations are not uncommon. Dislocations will affect the optical homogeneity of crystals and their presence can be inferred by examination in crossed polarizers. For example, Fig. 5 is a photograph taken of a crystal containing about 10^4 dislocations/cm^2 between crossed polarizers. This photograph may be compared with that of Fig. 2 which is of a crystal containing less than 10 dislocations/cm^2. The strain in the low dislocation density crystal is concentrated in the core region whereas it appears to be distributed throughout the high dislocation density crystal.

Dislocations can be revealed by selective etching. Orthophosphoric acid at 160-170°C is a suitable etchant for the rare earth gallium garnets (Ref. 24). On the {111} planes (the most commonly used plane for epitaxial growth), the dislocation etch pits are six sided with overall triangular symmetry. A typical dislocation etch pit is shown in Fig. 6. This photomicrograph was made with the optical microscope; however, the morphology of the pits would be more apparent under the scanning electron microscope.

4.4 Growth Striations

Czochralski grown garnet crystals usually exhibit distinctive growth striations. It is believed that the striations are slight compositional variations (stoichiometric deviations and/or impurities) resulting from thermal fluctuations in the melt during growth. If such is the case, then corresponding variations in lattice constant

Figure 5. $Gd_3Ga_5O_{12}$ crystal of high dislocation density between crossed polarizers

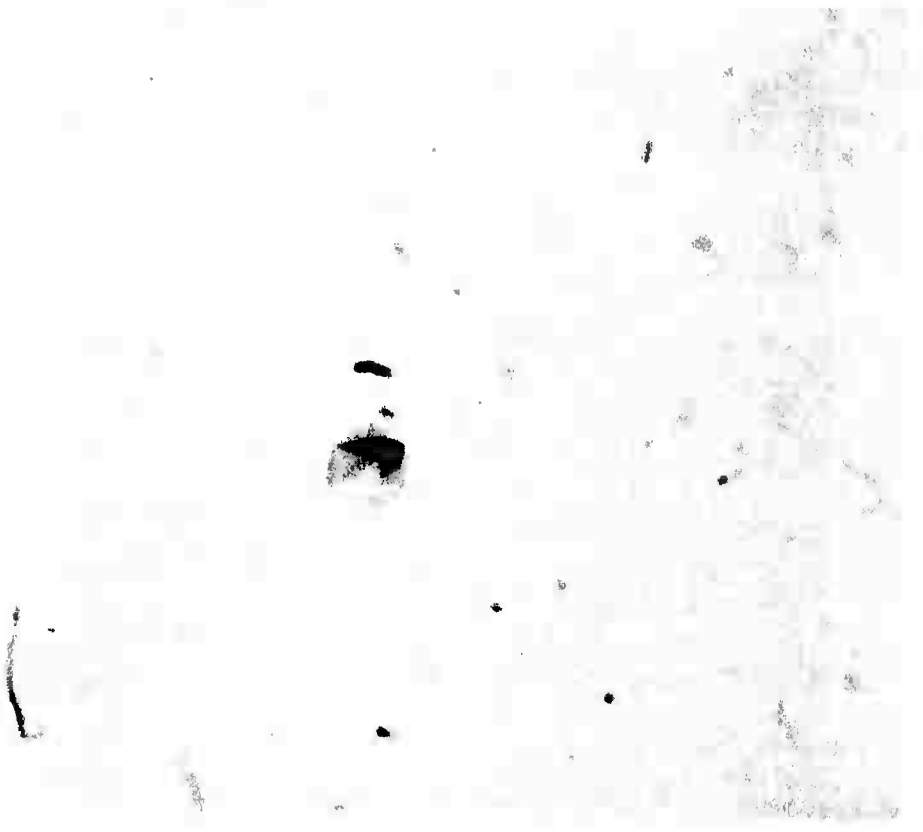

Figure 6. Dislocation etch pit on (111) face of $Gd_3Ga_5O_{12}$ (1000X)

would be expected. The growth striations in the substrate are reproduced in epitaxial films grown by either LPE or CVD. Evidently, the surface of the substrate is slightly attacked before film deposition begins. In some cases, the striations in the film are so pronounced that they impede magnetic domain motion. However, film growth conditions can be adjusted to minimize the replication of the striations to the point where they appear to have no effect on domain motion.

X-ray diffraction topography has proven to be a valuable tool to study the growth striations as well as other imperfections in the rare-earth garnets. The transmission method developed by Lang (Ref. 25) is sketched in Fig. 7 and is illustrative of the general principals of x-ray topography. A narrow collimated beam of x-rays is directed upon the surface of the crystal. The crystal is oriented so that the beam is diffracted from a set of planes with Miller indices (h k l). In the symmetrical case the diffracting planes are perpendicular to the specimen faces and the incident and diffracted beams make equal angles with the specimen. A photographic plate is usually used to record the diffracted beam and a slit prevents the direct beam from reaching the plate. The crystal and plate are mounted so that they can be moved during exposure to record a large area of the sample. Bonse, Hart and Newkirk (Ref. 26) have discussed other modes of x-ray topography.

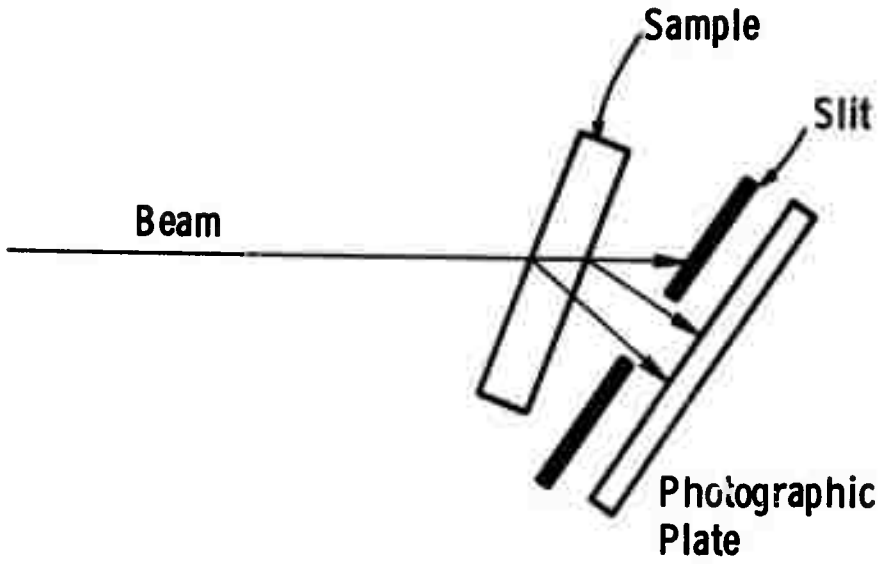

Figure 7. Lang x-ray topographic method

Transmission x-ray topography requires thin sections of garnet (about 100μm thick). Usually it is impractical to use such thin samples for substrates for subsequent epitaxial growth. Other variations of x-ray topography for garnets have been evaluated (Ref. 27) and Glass (Ref. 28) has shown that reflection topography using a double crystal diffractometer is especially useful for the study of both substrates and epitaxial films. Reflection topography is limited, of course, by the effective penetration of x-rays to approximately the first 20 microns near the surface of the specimen.

Much of the information revealed by reflection topography can also be obtained by phase interference microscopy (Ref. 19). The phase interference microscope accentuates small surface irregularities and makes obvious features which cannot be detected by ordinary microscopy. For these studies, the surfaces should be etched as described for the determination of dislocations above.

4.5 Routine Substrate Evaluation

The crystal grower and the epitaxial growth technician need a means of rapidly evaluating candidate substrate materials. The techniques discussed here yield the pertinent information required for judicious substrate selection; however, many of the techniques are complementary and some (x-ray topography, for example) are not really suitable

for routine evaluation. It is felt that an adequate scheme for the routine evaluation of substrate materials would involve the following.

Each boule should be examined between crossed-polarizers. This reveals strain and its general distribution. In some cases, this examination alone can serve as the basis for the rejection of an entire boule.

Representative wafers should then be sliced from the crystal, polished and etched. Microscopic examination with both transmitted and reflected light would reveal inclusions and dislocations. These are the most serious defects commonly found in garnets and largely determine the defect density of the epitaxial film.

Final examination of the wafers under the phase-contrast microscope would reveal the extent of growth striations. With this knowledge, the film grower can adjust growth conditions to minimize banding in the epitaxial film.

5. FILM THICKNESS

The diameter of magnetic bubble domains and the bias field for stable operation in a given film are both functions of the film thickness (Ref.29,30,and 31). Thus, accurate knowledge of the thickness is an important device parameter. It is crucial in assembling a bubble dcmain system with more than a single film that these be matched in thickness to within approximately 1% as well as uniform to that tolerance (Ref.32). In addition, many of the magneto-optic techniques to be discussed later in this report for the determination of other film properties require a knowledge of film thickness. Thus the measurement of this elementary property takes on a considerable importance.

During the stage in which orthoferrites were the most interesting bubble materials available samples were generally sliced out of flux grown bulk samples. At this stage, with the entire thickness an active part of the bubble domain sample, any standard means for the measurement of thin samples (such as a micrometer) was satisfactory for thickness determination. With the advent of uniaxial garnet materials, with their smaller bubbles and correspondingly smaller thicknesses, growth of films on non-magnetic substrates was investigated. At present, the epitaxial growth of a magnetic garnet film on non-magnetic garnet substrate is by far the most widely used means for preparing magnetic bubble samples.

5.1 Edge Viewing Methods

The first method for the determination of film thickness in these samples probably involved breaking the sample and observing the cracked edge microscopically. The magnetic film can be distinguished from the substrate either by its greater optical absorption (in transmitted light) or by etching in hot phosphoric acid to reveal the boundary. This method is useful on rough deposits and requires less equipment than those outlined below but has the obvious disadvantages of being destructive to the sample and of limited accuracy. In addition the garnets do not cleave well so that one must usually deal with a jagged edge and hope for a sufficiently flat region to reveal the boundary sought. Such measurements, because of their directness, have been useful in checking some of the other techniques to be discussed.

A more reproducible and accurate varient of the simple break approach is metallurgical cross-sectioning (Ref. 33 and 34). Because of the hardness of the garnets it is difficult to find a material which is sufficiently hard to avoid faster removal of the material in which the sample is potted and the rounding of the sample's edges which follows. This effect poses a limitation of several percent on the accuracy with which the thickness of a typical film can be measured in this way. In addition the method remains essentially destructive.

5.2 Interferometric Methods

As film uniformity improved non-destructive techniques based upon optical interferometry became possible. In these, a beam of monochromatic light is directed onto the sample and either the transmitted or reflected beam intensity measured as the wavelength of the incident light is varied. Required for the technique are a flat sample surface, good film uniformity over the region sampled, and a significant and sharply defined difference in the index of refraction between the film and the substrate. The fraction of the incident light reflected at the film (index n_f) - substrate (index n_s) interface is given by

$$R_2 = \frac{(n_f - n_s)^2}{(n_f + n_s)^2} \qquad (5\text{-}1)$$

Since this reflected light forms an essential part of the interference phenomenon the requirement for finite $n_f - n_s$ arises. Fortunately the iron ions which are present in the film but not in the substrates of typical garnet samples yield considerable increase in index as well as absorption (see Section 17). Typically, $n_s \sim 1.70$ (Ref. 35) while $n_f \sim 2.35$ in the red portion of the spectrum (Ref. 36) so that $R_2 = 0.026$ which is quite adequate to observe interference effects.

The basic interference effect for thin films is treated in texts on optics (Ref.37 and 38) and will not be repeated here. The optical path difference between the light reflected from the free surface of the film and the

interface with the substrate causes various phase differences to occur as λ, the incident light wavelength, is varied. These, in turn, cause the oscillations in intensity typical of the phenomenon. The effect has been employed in the garnets both in transmission (Ref. 35) and reflection (Refs. 36, 39,and 40). Reflection is to be preferred for the following reasons: 1) The back surface of the substrate is unimportant in reflection while an optical polish is desirable for the transmission measurement. Thus, the reflection technique requires less sample preparation. 2) The oscillations are a larger fraction of the total signal in reflection. This can be seen as follows: The fraction of the total light reflected at the front film surface is

$$R_1 = \frac{(n_f - 1)^2}{(n_f + 1)^2} = 0.16 \qquad (5\text{-}2)$$

Neglecting secondary internal reflections and absorption in the film this fraction interferes with the 0.026 fraction reflected at the film-substrate interface. Taking into account the diminution of this internal beam by the first surface reflection, the internally reflected beam is ~ 14% of the front surface reflected beam. This leads to a maximum fractional variation of the reflected beam due to interference of ~ 28%. Since the transmitted beam, after consideration of reflection at the backside of the substrate, is approximately 70% of the incident beam, the maximum

fractional variation of this beam will be ~ 6.4%. These considerations are qualitatively borne out by comparison of the results (Ref. 35) in transmission and (Ref. 39) in reflection. (See also Fig. 8a)

The calculation of the film thickness from these data follows from a consideration of the extra path length in the film. For normal incidence on a film of index of refraction n, this yields

$$h = \left[2n \left(\frac{1}{\lambda_{i+1}} - \frac{1}{\lambda_i} \right) \right]^{-1} \qquad (5\text{-}3)$$

where λ_{i+1} and λ_i are wavelengths corresponding to successive maxima or minima. In practice an average spacing in $1/\lambda$ is calculated as

$$\frac{1}{\lambda_{i+1}} - \frac{1}{\lambda_i} = \frac{1}{N} \left(\frac{1}{\lambda_{i+N}} - \frac{1}{\lambda_i} \right) \qquad (5\text{-}4)$$

in order to improve accuracy. The use of this equation assumes a constant (or properly weighted average) index, n (an assumption which can be avoided).

Roman, et al (Ref. 36) have assumed a linear variation of n with λ so that the index, $n(\lambda_2)$ at λ_2 is given in terms of $n(\lambda_1)$ at λ_1 and the variation of n with λ as

$$n(\lambda_2) = n(\lambda_1) + \frac{dn}{d\lambda} \left(\lambda_2 - \lambda_1 \right) \qquad (5\text{-}5)$$

$$\text{Then } h = \frac{N}{2} \left(\frac{\lambda_2 \lambda_1}{\lambda_2 - \lambda_1} \right) \left[n(\lambda_1) - \frac{dn}{d\lambda} \lambda_1 \right]^{-1} \qquad (5\text{-}6)$$

where N is the number of intensity oscillations between λ_1 and λ_2. As those authors point out this equation can be used as a guide to choosing the proper weighted average for use in the simpler equation 5-3. Within the visible to near-infrared region $\frac{dn}{d\lambda} < 0$ (Ref.41 and 42) so that an index somewhat larger than those corresponding to the wavelength range used should be employed. While this conclusion appears surprising, because of the nature of the equation it is, in fact, correct as can be seen by direct substitution in equation 5-7. Roman et al quote values of index for three bubble materials as follows:

Material	n at λ = 6330Å
$Gd_{2.3}Tb_{0.7}Fe_5O_{12}$	2.42 ± 0.05
$Eu_1Er_2Ga_{0.7}Fe_{4.3}O_{12}$	2.35 ± 0.05
$Er_2Gd_1Ga_{0.7}Fe_{4.3}O_{12}$	2.36 ± 0.05

The value of $\frac{dn}{d\lambda}$ near 6000Å can be inferred from unpublished values of Tabor as quoted by Shumate (Ref. 40). These are

λ	n
6500Å	2.350
5500Å	2.396

leading to $\frac{dn}{d\lambda} = -4.6 \times 10^{-5}/\text{Å}$. Using this a reasonable estimate of n for equation 5-3 and the convenient wavelength range 6,000 to 10,000Å is 2.45.

Shumate (Ref. 40) has proposed the equation

$$h = \frac{N}{2}\left[\frac{2.396}{\lambda_1} - \frac{2.350}{\lambda_2}\right]^{-1} \qquad (5\text{-}7)$$

where λ_2 and λ_1 are wavelengths corresponding to extrema of the same sign near 5500Å and 6500Å respectively and N is the number of intensity oscillations between these wavelengths. This is the most accurate of the equations quoted here in that the indices used are those measured at or near the wavelengths employed. It also requires the best films since small non-uniformities reduce the oscillations at short wavelengths most strongly. Such an approach, perhaps extended to somewhat longer wavelengths when the full dispersion curve is known, will probably be the most accurate and convenient means of determining bubble film thickness for the foreseeable future.

Systems for the measurement of such interference traces are available from many suppliers of monochromators. A relatively inexpensive committed system, together with typical data, is shown in Figure 8 a & b as assembled at Monsanto. Specific apparatus used has been listed previously (Ref. 39). When used over the full range, the system can approximate the relative accuracy of 1% necessary to match films in multi-film devices. Absolute accuracy is $\pm$ 4%, however, as a result of uncertainty in n and beam divergence (normal incidence is assumed in all of the above equations). Variations in thickness from one point to another on a sample can be handled as described

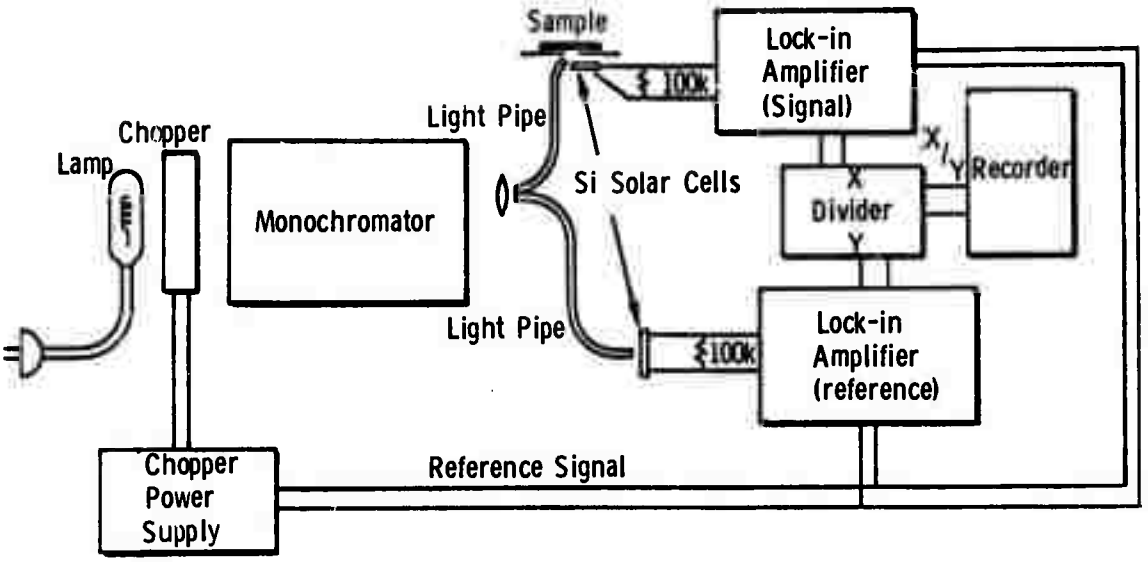

Figure 8a

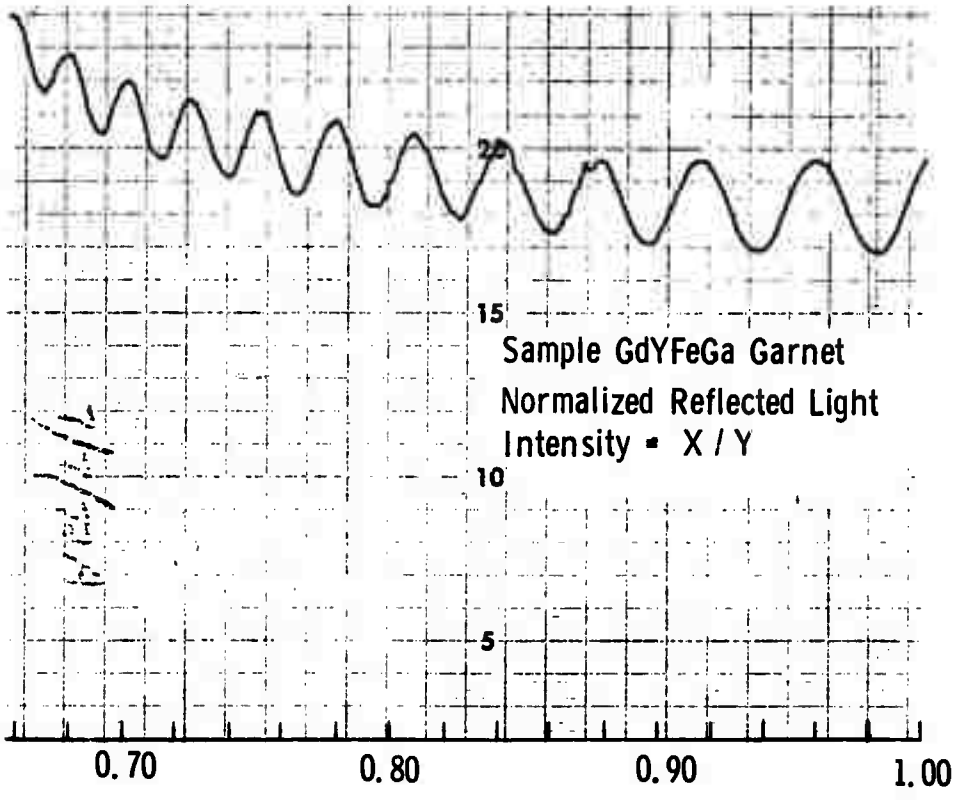

Figure 8b

Figure 8. Thickness system and typical data curve

in the next section.

The system in use at Bell Telephone Laboratories (Ref. 40) differs from this in that the sample is visually observed (by eye in the visible or with the aid of a silicon vidicon tube in the infrared) and the number of interference fringes passing a given point as the wavelength is varied in simply counted. This system has the advantage of providing both thickness and thickness variation information simultaneously but requires the investment in a closed circuit TV system for the infrared region. In addition, as film uniformity approaches the desired flatness, band fringes are no longer visible and the entire surface oscillates in reflectivity as the wavelength changes. In this case the quantitative data provided by a normalized photomultiplier or solar cell system is a necessity in order to find the extrema accurately. It is suggested that a system utilizing photoelectric readout is to be preferred and the separate but simple system of the next section used to determine thickness variations.

6. THICKNESS VARIATIONS

The observation of a broken or cut and polished edge can yield information on thickness variations along that boundary but these destructive techniques are undesirable as production procedures. Fortunately, optical interference again provides a very convenient alternative. Interference effects entirely similar to those described in Section 5 when wavelength is varied would also be observed if the film thickness were varied at constant wavelength. Such an effect is actually observed when regions of different thickness are present in the same sample. In this case the dark bands arising from destructive interference in the reflected light correspond to contours of constant film thickness satisfying the relationship $2\,h\,n = m\lambda$. Once again h is the film thickness, n, the index of refraction at wavelength λ, and m, an integer. The difference in thickness between successive dark bands is then $\Delta h = \lambda/2n$.

The workers at Bell Telephone Laboratories have generally observed the fringes in the infrared region using monochromator illumination and a silicon vidicon tube (Ref. 36). This system permits simultaneous determination of thickness (as mentioned in the previous section) and its variation. While some photographs of these fringe patterns have been made the usual system used at BTL for generating a map of thickness variations has been to mount the sample on a microscope stage equipped with position transducers,

illuminate it with monochromatic light, and generate a map on a X-Y recorder by manually tracing the fringes (Ref. 40).

A more rapid and convenient system is in use at Monsanto (Ref. 39). This consists simply of taking a close-up photograph of the sample illuminated by monochromatic light next to a grid using the system of Figure 9a. The helium filled discharge lamp provides a strong line at 0.5876μm wavelength. This yields a thickness difference between the successive dark fringes of (0.122 $\pm$ 0.005)μm based upon n = 2.40 at this wavelength. These fringes are readily visible to the eye when viewed in this light. This technique has proved invaluable in our efforts to improve film flatness. In order to photograph the interference fringes a glass beam splitter is used as indicated in the figure. A typical result is shown in Figure 9b.

Such a map in itself does not show the sign of the thickness gradient. This can often be determined by visual inspection since a significantly thicker region will appear darker green. If the thickness variations are too small to yield detectable color differences another simple technique is still available. This involves rotating the sample while viewing the fringes under monochromatic light. As the sample is rotated away from a perpendicular viewing angle the dark bands appear to move toward thicker parts of the film. This can be seen as follows: The optical

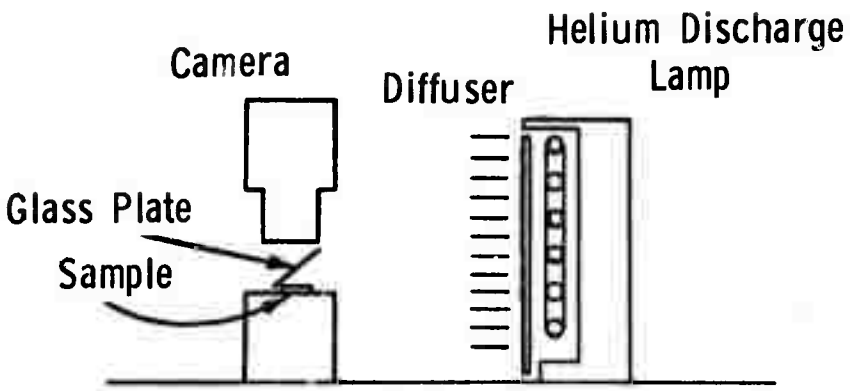

Figure 9a

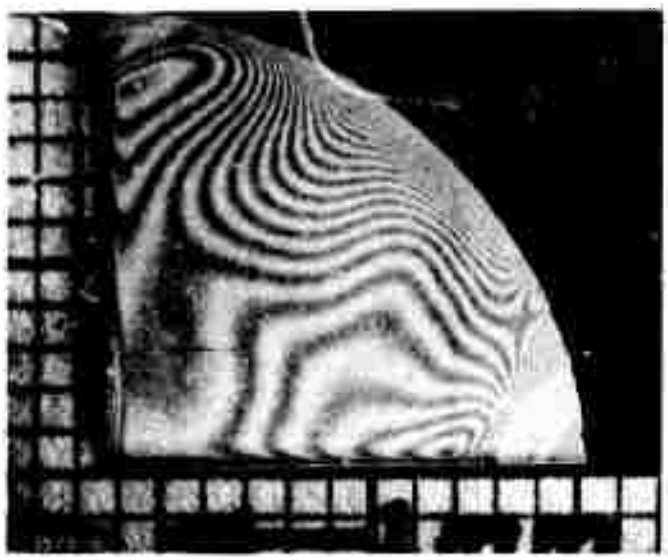

Figure 9b

Figure 9. Thickness variation system and typical thickness map

path difference between the light reflected from the front surface and that reflected from the film-substrate interface is given by Δ (OP) = 2 n h cos θ' where θ' is the angle between the normal to the film and the propagation direction of the light internal to the film (Ref. 37). As the sample is rotated away from the perpendicular, θ' increases from zero and the optical path difference at the spot of thickness h decreases. However, the original dark band will move to a point at which Δ (OP) is the same as it originally was at the spot of thickness h, i.e. it must move in the direction of increasing h.

The combination of variable wavelength interferometry, monochromatic light photography, and visual inspection as a function of angle under the monochromatic light therefore provides complete thickness information at all points of the films. Other monochromatic light sources, such as a sodium lamp or suitably diffused laser beam, are satisfactory for viewing the fringes. The shortest possible wavelength is to be preferred, however, because of its greater sensitivity to small thickness variations. For example, using the 5500Å index quoted by Shumate, successive fringes at that wavelength correspond to 0.115μm thickness difference, to be compared with the 0.122μm figure quoted above for ~ 5900Å. Because of the rapidly increasing iron absorption, 5000Å is an effective lower wavelength limit for the technique.

7. DEFECT DETECTION AND LOCATION

Defects in a magnetic bubble material which impede the motion of bubble domains will, at the very least, reduce device operating margins and, in the worst case, may render the sample useless for device operation. Detection and location of such defects thus becomes an important phase of quality control, both as a check on damage introduced at various stages of sample processing and for the selection of device quality areas.

Several of the standard methods for the study of defects are applicable to magnetic bubble materials. These include etching studies (Reference 24 and 43) X-ray topography (Reference 44 and 45) and microscopic examination (Reference 46). These techniques are essentially the same as those used in the evaluation of substrates and have been discussed in Section 4. We confine our attention below to those non-destructive techniques uniquely suited to magnetic bubble materials. All of these involve the microscopic examination of films or thin slabs in transmitted, polarized light. The plane of polarization is rotated by the magnetic material in a sense dependent upon its magnetization direction (the Faraday effect, see Section 17) and the domain pattern is revealed by placing another polarizer (the analyzer) in the emerging light beam so

as to transmit more of the light passing through one sign of domain than the other. The interaction of domain walls with crystalline defects can then be revealed in a number of possible configurations.

In the orthoferrites it is fairly straightforward to stabilize a single straight domain wall by locating the sample in a region in which the field strength perpendicular to the sample plane is varying sufficiently rapidly with position, i.e., $dH/dx > \beta_c$ with H directed along the z axis normal to the sample plane. Hagedorn (Reference 47) has calculated β_c in terms of the material saturation magnetization, $4\pi M_s$, and characteristic length, ℓ ($= \sigma_w/4\pi M_s^2$ where σ_w=wall energy/cm^2), as

$$\beta_c = 0.016 \frac{4\pi M_s}{\ell} . \qquad 7\text{-}1$$

A very versatile system for the generation of this type of field configuration using two permanent magnets has been described by Shumate (Reference 47) and is reproduced here (Figure 10). When the sample is now moved within this gradient field and the domain wall observed microscopically, defects which interact with the wall will cause distortions from the straight configuration, i.e., from the line corresponding to zero applied field. Examples of such distortions have been shown by Burmeister, et al (Reference 48 and 49). The same

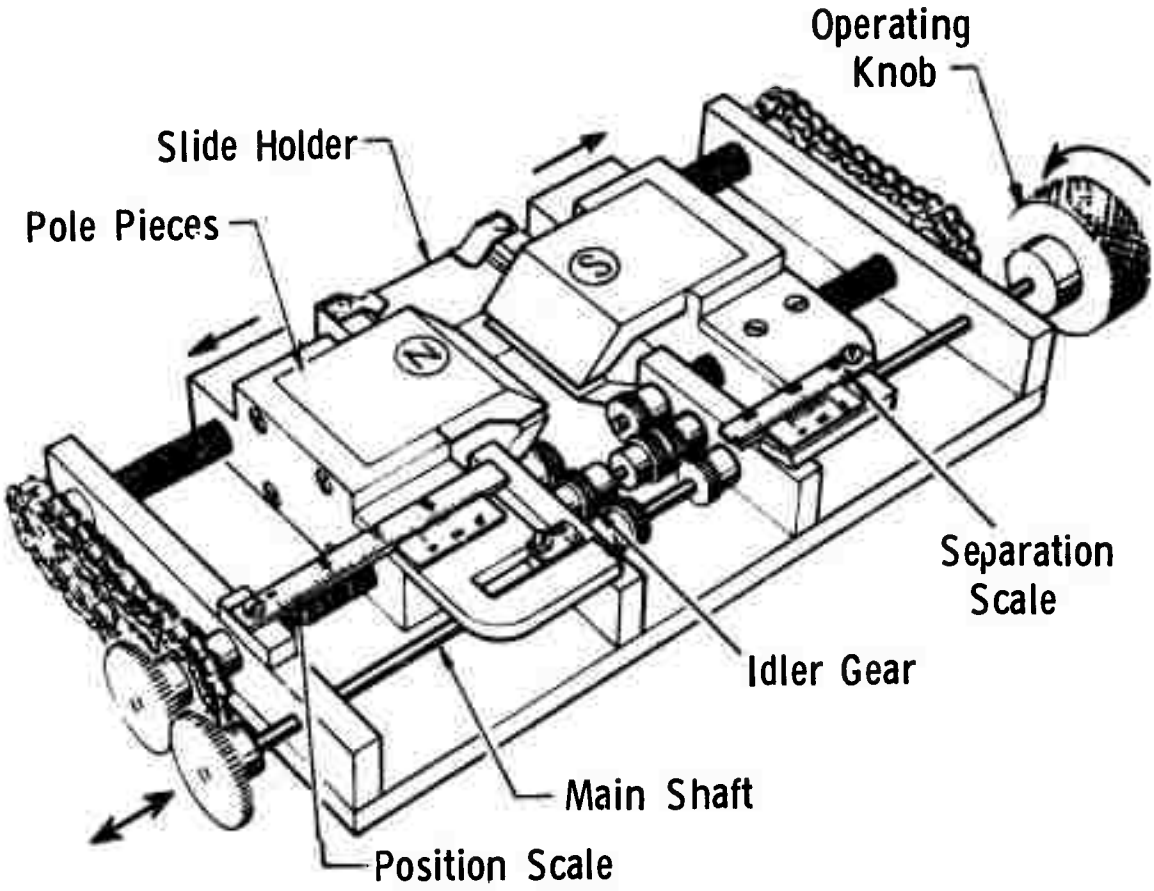

Figure 10. Device for establishing variable gradient field. After Shumate, ref. 47. The sample rests on a slide in the gap between the magnets.

technique has been used by Kurtzig to investigate the interaction of a domain wall with specific defects such as twin and grain boundaries (Reference 50) and dislocations (Reference 44). If the magnitude of the field gradient is known it is possible to calculate the coercivity, H_c, associated with the individual defect as $H_c = \Delta x(dH/dx)$ where Δx is the displacement of the domain wall from its equilibrium position in the gradient field at the time the wall breaks free of the defect. For the cases investigated by Kurtzig, this coercivity was found to be highly anisotropic, as might be expected. Further discussion of defects detected in this way has been presented by Nielsen (Reference 51).

The generation of a single straight domain wall is considerably more difficult in the garnets than it is in the orthoferrites. The garnets are of practical interest because of their smaller bubble size relative to the orthoferrites. This bubble size, in turn, results from lower domain wall energy and higher magnetization. For example, a typical garnet has $\sigma_w \sim 0.2$ ergs/cm^2 and $4\pi M_s \sim 150$G while typical orthoferrite values are $\sigma_w \sim 1$ erg/cm^2 and $4\pi M_s \sim 100$G. The resulting increase in β_c required to generate the single straight wall is nearly a factor of 20 and puts the straight wall technique out of practical reach for many of the garnets. In addition,

as the required gradient becomes larger, the sensitivity (Δx caused by a defect of given pinning strength) goes down and with it the usefulness of the method.

In the presence of a gradient insufficient to bring about a straight wall, a single wall is still possible. This wall will take on the wavy to finger-like forms shown by Hagedorn (Reference 52) depending on the strength of the gradient applied. The passage of such a pattern across a magnetic bubble film is still sensitive to the presence of defects. This technique is being used for the detection of defects at Bell Northern of Canada where it is thought to be more sensitive than the methods to be described below (Reference 53).

Another method for defect detection particularly suitable for the orthoferrites has been developed by Fischer and Shumate (Reference 54). In it a bubble domain is moved across the sample by means of a magnetized probe and distortions of the bubble caused by defects are detected optically. This requires a bias field to be applied opposite to the magnetization in the bubble and the probe which sometimes causes reversal of the probe magnetization and a temporary stop to the scan (Reference 47). The raster scanning mechanism which was built to automate this system makes it a possible production technique

for the orthoferrites. As bubble size becomes smaller, however, the number of passes required in the raster increases and the photoelectric signal involved in a bubble distortion decreases making the technique marginal in the garnets.

Nikitenko, et al (Reference 55) have reported studies of the influence of dislocations on magnetic domains in gallium substituted YIG. The domains were observed by the Faraday effect in the usual fashion while the dislocations were simultaneously observable due to the birefringence brought about by their strain fields. They were able to observe the nucleation and binding of domains to the dislocations but did not determine quantitative binding energies. Their samples were quite thick (0.3 to 2mm) and observations made at 1.2μ wavelength. It seems unlikely that as clear cut defect observations can be made by this technique using the much thinner samples of interest in practical bubble devices.

The most widely used techniques for defect detection in the garnets are based upon the observation of domain motion in an alternating bias field. As described by Geusic, et al (Reference 56) the bias field is cycled slowly with time and points which interfere with the motion of strip domains are detected visually. Two photomicrograph examples are presented

in that paper. Shumate, in reporting on this method (Reference 47), indicated that a 60 Hz sine wave bias is adequate, although judicious addition of a dc bias as well often aids in elucidating weak imperfections and gradients. In this 60 Hz technique a sufficient AC field amplitude is applied to cause appreciable domain motion when viewed in a polarizing microscope. Regions in which domains are still pinned at defects will be decorated by non-moving walls. The technique requires a judicious choice of field amplitude, since a large amplitude will tear domains away from weak pinning sites and those sites will go undetected. In practice the minimum amplitude which causes a blurred condition serves very well to delineate strong defects or those with some spatial extent such as scratches and clusters of point defects. For weaker point defects it is often necessary to go to lower amplitudes, add DC bias, and look for points at which the domain pattern tends not to move or to move in a "snap-action" fashion. Hiskes (Reference 57) and Shumate (Reference 40) have presented photomicrographic examples of this technique. We show an additional example of a line defect in Figure 11.

Chaudhari (Reference 18) has recently described another magneto-optic technique for the detection of defects. An array

Figure 11a. Domain pattern without bias field

Figure 11b. Line defect revealed in oscillating field

Figure 11. Defect detection in oscillating bias field

of bubbles is made to flow as a raft (and presumably generated as well) by a suitably formed pulse coil. Defects are detected by hang up of individual bubbles or by the distortion of the raft from hexagonal symmetry. Several examples and the arguments in favor of this approach have been presented by Chaudhari. Unfortunately no detailed comparisons as to sensitivity or visibility were given. We feel that, while it may be too early for a final decision, the oscillating stripe or moving convoluted wall both provide more useful techniques for the routine scanning of samples for defects.

Defect maps are readily made by connecting the microscope stage to position transducers which, in turn, communicate with an X-Y recorder. The system used at Monsanto and a typical defect map are shown in Reference 39. The sample is manually scanned at 200X by an operator who, upon observing a region of domain wall pinning, centers it in the microscope field of view and presses a footswitch to drop the recorder pen and mark the map. Sixty (60) cycle modulation derived from a variable transformer is quite satisfactory.

It is difficult at this point to say, in any of these techniques, whether all significant defects are being detected or whether some of those detected may, in fact, be too weak to cause problems. What is needed in this regard is a correlated

study of defect strength from the above measurements and bubble propagation errors under a standard circuit mask. The publication of a study of defects using both the convoluted single boundary stabilized by a gradient and the modulated strip domain technique on the same specimens would also be a service. At the present time we recommend the use of either of these approaches for the garnets.

8. CHARACTERISTIC LENGTH AND DOMAIN DIMENSIONS

The characteristic length, ℓ, to be used in the present report follows the notation introduced by Thiele (Reference 29 and 30) and now rather widely used in the literature of cylindrical domain technology, namely, $\ell = \sigma_w/4\pi M_s^2$. Here σ_w is the energy per unit area of a domain wall and M_s is the saturation magnetization. This parameter is clearly a combination of two more basic ones. It is of interest, however, because it governs the scale of domain sizes characteristic of a given magnetic bubble material. Conversely the measurement of certain domain sizes and the sample thickness is sufficient to yield the value for ℓ so that only one further determination (generally $4\pi M_s$) is required to specify both σ_w and $4\pi M_s$. In this report we will devote a separate section to σ_w because there exist a number of alternative approaches to its measurement which are worthy of note.

8.1 Methods Employing Bubbles

The theory of Thiele begins with the assumption of three independent contributions to the total sample energy for a sample containing a single domain, the energy due to domain walls, that due to interaction of the sample with the external field, and that due to internal magnetostatic interactions.

The solutions for the limits of stability of a cylindrical magnetic domain are presented in graphical form and reproduced here as Figure 12. Here S_o (d/h) represents the stability limit against collapse and S_2 (d/h) the stability limit against distortions of twofold symmetry (i.e., strip-out). Thus, cylindrical domains are stable in the area bounded by S_o and S_2. The ordinate for these curves corresponds to the ratio ℓ/h (where h is the sample thickness) and therefore forms the basis for the determination of ℓ from measurements of bubble diameters and sample thickness. For this simplest use of the Thiele theory the diameter either at the strip to bubble transition or at collapse is required. Several difficulties are encountered in carrying out this approach. 1) The accuracy of the strip to bubble transition point is limited both by coercivity effects in real samples and by the ability of the eye to detect small non-circular distortions. 2) Once collapse of the bubble of interest is established it is no longer available for measurement. Thus one must either shift to a nearby (but still "isolated") bubble for the diameter determination or take a series of magnetic field-diameter data as collapse is approached and extrapolate the resulting curve to the collapse diameter using the measured field at collapse. 3) The measurement of domain diameters,

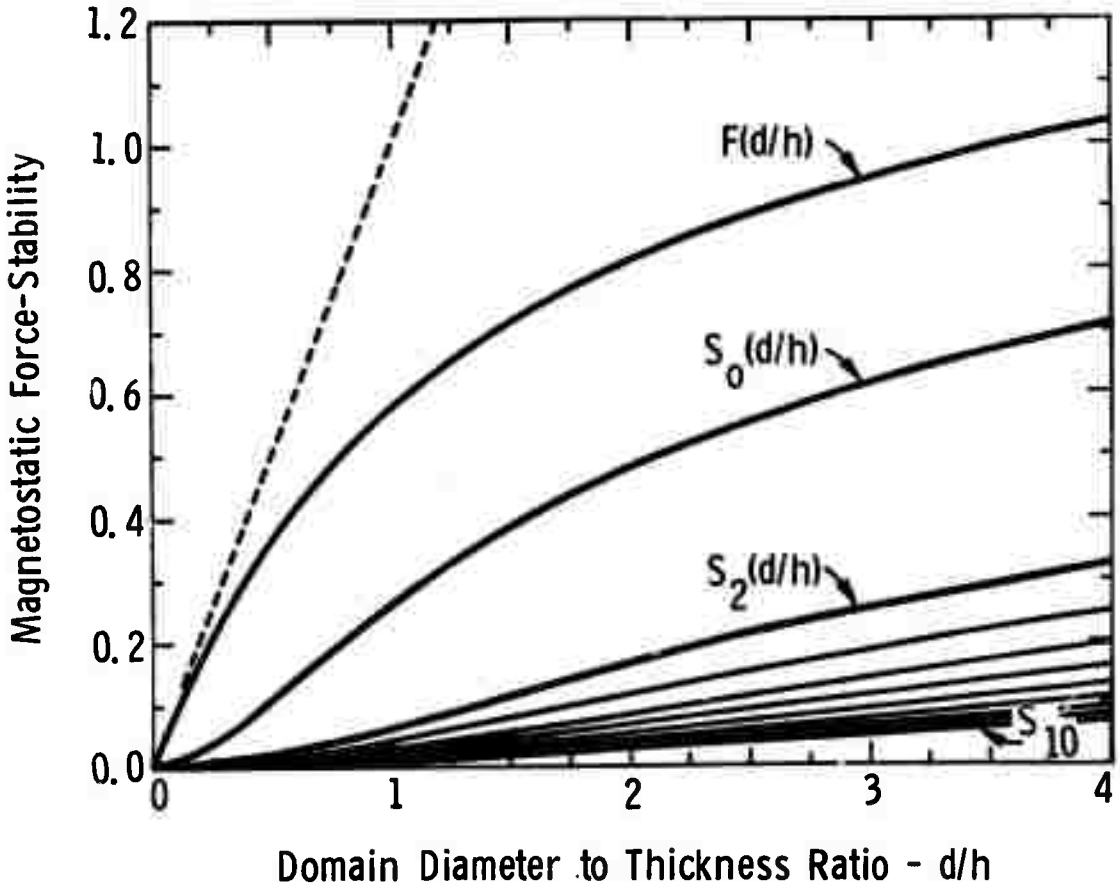

Figure 12. The stability curves for collapse (S_o) and strip out (S_2) for bubble domains and the radial force function F.
After Thiele, ref. 30.

while relatively simple and accurate in the orthoferrites with their large domains (> 25μm), becomes less accurate for the smaller domains of the garnets. Hagedorn, et al (Reference 58), in a test of the accuracy which the Thiele approach permits, quote an uncertainty in bubble diameter of ± 0.2μm which, when coupled to the curve fitting approach to be outlined next, leads to a relative accuracy in ℓ of ± 7%. The experience at Monsanto indicates that a diameter uncertainty of ± 0.5μm is realistic for good but not ultimate optical equipment. The resulting uncertainty in ℓ is not satisfactory in light of the alternatives to be discussed below.

The curve fitting approach of Hagedorn, et al (Reference 58) involves making a least-squares fit of a series of field and corresponding diameter values for a film of known thickness to the equilibrium equation derived by Thiele (Reference 29, Equation 69).

$$\frac{\ell}{h} + \frac{d\,H}{h 4\pi M_s} - F\left(\frac{d}{h}\right) = 0 \qquad (8\text{-}1)$$

The computed curve of the force function $F\left(\frac{d}{h}\right)$ is shown in Figure 12. Careful measurement of a series of ten field-diameter points, when fitted to this equation, yield the

relative ± 7% accuracy quoted above. This method does not hold great promise as a production line technique of reasonable accuracy.

8.2 Isolated Straight Wall Method

A rather unique approach to the determination of ℓ (and, with less accuracy, $4\pi M_s$) has been outlined by Hagedorn (Reference 52). It makes use of the isolated straight wall configuration mentioned in the previous section. As the field gradient needed to stabilize this single wall is reduced, deviations from straightness develop which have a periodicity and critical field gradient characteristic of the sample thickness and the material under test. The characteristic length is a function only of the periodicity of the distortion and the thickness near the onset of this phenomenon and can be determined with good accuracy. $4\pi M_s$ requires a knowledge of the gradient at which the distortion sets in and this is not so well defined. Unfortunately, as mentioned previously, the generation of an isolated, straight wall in the garnets is a difficult project, requiring very large gradients, so that this approach has not been reported for these materials.

8.3 Methods Employing Strip Domains

The normal domain pattern for a magnetic bubble sample in zero applied field is a serpentine array of strips (see,

for example, Figure 11). The alternate regions of magnetization into and out of the sample will have equal width in order to yield a net magnetic moment of zero. This width is a function only of the sample thickness and the characteristic length in the limit of large anisotropy assumed by the theories. Fowlis and Copeland (Reference 59) and Shaw, et al (Reference 60 and 31) have solved the earlier theories of Malek and Kambersky (Reference 61) and Kooy and Enz (Reference 62) to yield ℓ/h from measured values of P_o and h. Here P_o is the spatial period or repeat distance of a set of parallel strip domains measured in the direction perpendicular to the strips. The results of these calculations are shown in Figure 13 and are presented in tabular form in Table 1.

As mentioned above, the equations upon which these results are based make the assumption of high anisotropy, i.e., $H_A >> 4\pi M_s$. Here H_A is the uniaxial anisotropy field which is related to the frequently used anisotropy constant K_u as $H_A = \frac{2K_u}{M_s}$. The above inequality is not fully achieved in practical materials nor is it, in fact, desirable. As Hagedorn and others (References 63, 64, and 65) have pointed out the domain wall mobility is inversely proportional to K_u so that a high anisotropy implies low mobility, quite undesirable in a magnetic

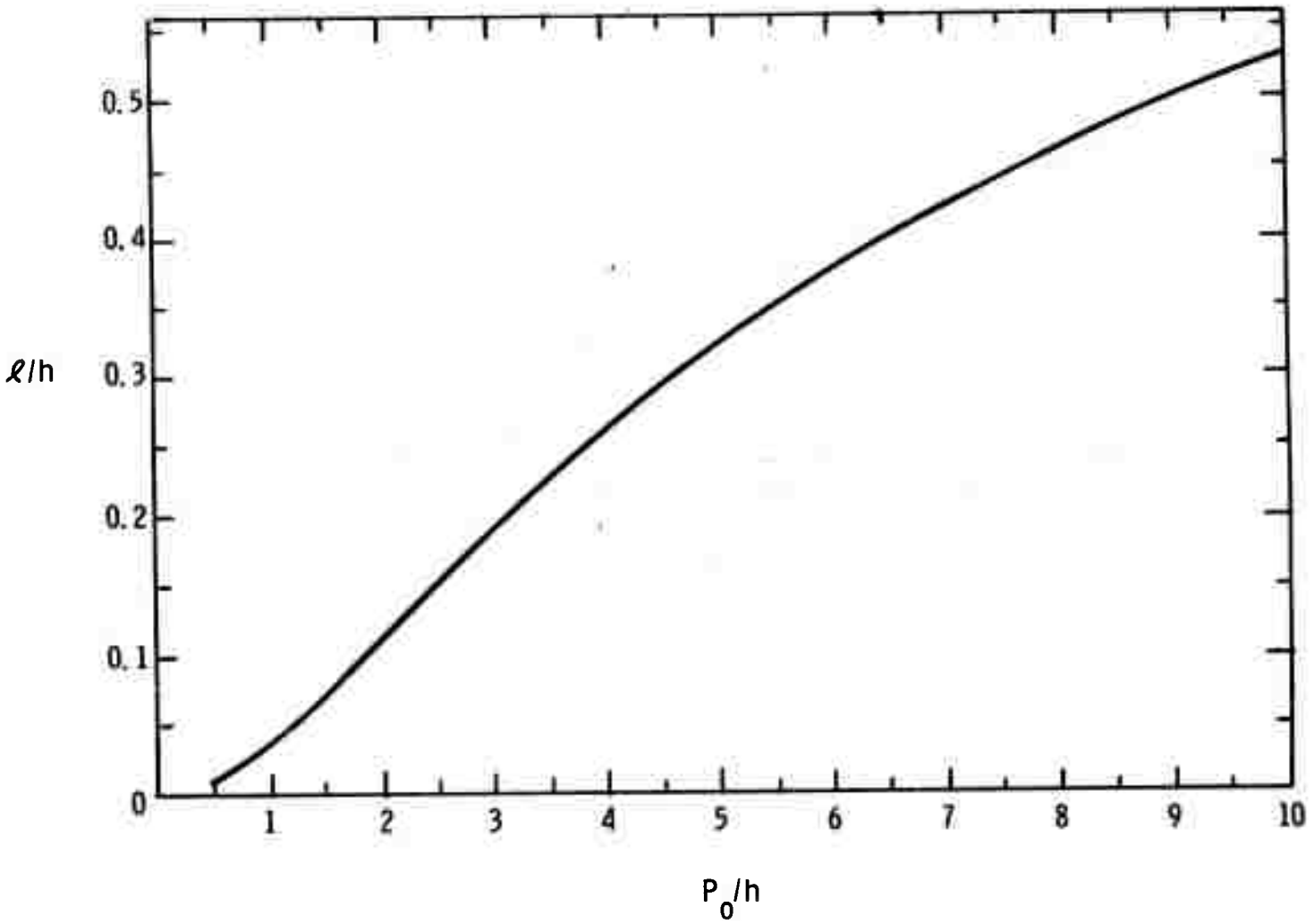

Figure 13. Characteristic length divided by thickness vs. strip domain period at H = 0 divided by thickness. After Kooy and Enz, ref. 62.

TABLE I

Characteristic length, ℓ, divided by thickness, h, vs. strip domain period, P_o, divided by thickness.

P_o/h	ℓ/h	P_o/h	ℓ/h
0.50	.0085	6.20	.389
0.60	.0122	6.40	.398
0.70	.0166	6.60	.406
0.80	.0216	6.80	.415
0.90	.0273	7.00	.424
1.00	.0335	7.20	.433
1.20	.0473	7.40	.441
1.40	.0626	7.60	.448
1.60	.0788	7.80	.457
1.80	.0956	8.00	.465
2.00	.1126	8.20	.472
2.20	.1295	8.40	.478
2.40	.1464	8.60	.485
2.60	.1629	8.80	.493
2.80	.1789	9.00	.500
3.00	.1945	9.20	.508
3.20	.2100	9.40	.514
3.40	.2247	9.60	.521
3.60	.2387	9.80	.526
3.80	.2525	10.00	.533
4.00	.2660	10.50	.546
4.20	.2790	11.00	.562
4.40	.2915	11.50	.575
4.60	.304	12.00	.588
4.80	.315	12.50	.602
5.00	.327	13.00	.613
5.20	.338	13.50	.625
5.40	.348	14.00	.637
5.60	.360	14.50	.648
5.80	.370	15.00	.659
6.00	.379		

bubble device material. The Thiele theory for bubble domains was also based upon this assumption of large anisotropy. In this case the recent results of Lin and Tu (Reference 66) and particularly those of DeBonte (Reference 67) extend the theory to finite anisotropy. At Monsanto we have carried out more accurate calculations including finite anisotropy effects for strip domains based upon the Equations 1 through 3 of Kooy and Enz. The equilibrium equation which results is

$$\frac{\ell}{h} = \frac{2\mu}{\pi^3\alpha^2} \sum_{\substack{n=1 \\ n \text{ odd}}}^{\infty} \frac{1}{n^3} \frac{\sinh(n\pi\alpha)\left[\sinh(n\pi\alpha) + \sqrt{\mu}\cosh(n\pi\alpha) - n\pi\alpha\sqrt{\mu}\right]}{\left[\sinh(n\pi\alpha) + \sqrt{\mu}\cosh(n\pi\alpha)\right]^2} \qquad (8\text{-}2)$$

Here $\mu = 1 + 4\pi M_s/H_A$ and $\alpha = \frac{h}{P_o}\sqrt{\mu}$. (Ref. 68)

The results of this calculation for values of μ = 1.0, 1.25, and 1.5 (i.e., $H_a/4\pi M_s = \infty$, 4, and 2) are given in Table 2 . Note that the total variation of ℓ/h near the practical, interesting range $\ell/h \sim 0.25$ (for example, at $P_o/h = 4.0$) is only 4%. Nevertheless, as measurements become more accurate such an effect should be taken into account.

Essentially all domain size measurements are presently being done in polarizing microscopes equipped with a graduated eyepiece. The entire optical system is calibrated by placing an accurately ruled slide on the microscope stage in place of

TABLE II

Characteristic length divided by thickness vs. strip domain divided by thickness for several values of anisotropy field divided by $4\pi M_s$.

$H_A/4\pi M_s$ =	∞	4	2
P_o/h	ℓ/h	ℓ/h	ℓ/h
0.50	.0085	.0080	.0076
0.60	.0122	.0115	.0110
0.70	.0166	.0157	.0149
0.80	.0216	.0205	.0195
0.90	.0273	.0258	.0246
1.00	.0335	.0318	.0304
1.50	.0706	.0683	.0660
2.00	.1126	.1109	.1088
3.00	.1945	.1961	.1967
4.00	.2660	.2708	.2746
5.00	.3268	.3342	.3406
6.00	.3791	.3882	.3965
7.00	.4245	.4350	.4446
8.00	.4647	.4760	.4866
9.00	.5005	.5126	.5239
10.00	.5329	.5454	.5572
15.00	.6591	.6729	.6861
20.00	.7496	.7640	.7776

the sample. The resolution of the microscope ($\pm$ 0.5 to $\pm$ 0.2μm as discussed above) is generally the limitation on this calibration so that 1% accuracy in a measurement of 100μm is quite possible.

Experimentally, the domain period, P_o, at zero field can be measured with much greater accuracy than can an individual domain diameter. This is the result of three factors: 1) The strip domain period is greater than the bubble diameters by approximately 2 for the operating bubble size and 4 for the collapse size. 2) It is usually possible to arrange the zero field strips into a parallel array, either by oscillating them with an AC bias field until a useful pattern develops (this procedure is aided by the application of an in-plane field component), or, as suggested by Fowlis and Copeland, by "combing" them with a magnetic probe. Once such an array has been formed, the distance for twenty or more periods can be measured and an average value computed very conveniently. 3) Effects of finite coercivity are more readily minimized in the strip pattern than for bubble domains since a finite AC bias field can be applied and gradually brought to zero without fear of collapsing the domains of interest. By the judicious use of these techniques an overall accuracy of 4%

in ℓ is readily achieved. At present we recommend the strip domain measurement at H=0 as the most convenient and accurate approach to the determination of ℓ.

9. SATURATION MAGNETIZATION, $4\pi M_s$, AND MAGNETIC FIELDS

The study of magnetization probably dates back to the ancient Greeks or Chinese (Ref. 69). Since that time a great many techniques have been developed for its measurement and many of these have been applied to the investigation of orthoferrites and garnets. As the development of magnetic bubble domain devices has progressed toward smaller bubbles and thinner samples some of these techniques have lost their usefulness, particularly for thin films on more massive paramagnetic substrates. Others, more compatible with the magneto-optical approach used for other parameters, have been developed. In the present report we will touch on these earlier methods only briefly, saving most of our attention for those techniques of particular use in the magnetic bubble area. Furthermore, excellent reviews of these earlier methods already exist in the literature (Ref. 70, 71, and 72).

9.1 Traditional Methods

The force on a magnetized sample placed in a non-uniform magnetic field forms the basis of one class of magnetization measurements (Ref.73 and 74). Bozorth, et al (Ref. 75) adapted this technique to the low temperature study of a number of rare-earth orthoferrites. This system involved the force on the sample in the field of an electromagnet with specially formed pole pieces. These provided a field gradient normal to the net field direction and

caused a force on the sample toward the higher field region. This force was balanced by passing a current through a small coil riding with the sample and just balancing the sample magnetic moment. The system was calibrated by replacing the sample with one of known magnetization, in this case iron. Such a means of calibration has been frequently used. Force systems of similar types have been employed in the study of garnets, as well as the orthoferrites (Ref. 76, 77, and 78).

The induction of current in a coil when a magnetic sample is moved in its vicinity dates back to the development of Faraday's law in 1834. The effect has been used numerous times in the study of materials presently of interest for magnetic bubble applications (Ref. 79, 76, 77, and 80). The availability of lock-in amplifiers and other adaptable AC electronics has caused recent interest toward continuous generation of an alternating induction signal. In these either the sample (Ref.81 and 82) or the pick up coil (Ref.83 and 84) are vibrated and the signal detected by means of a lock-in amplifier. The vibrating sample system has been used by Heinz, et al (Ref. 85) for garnet films on paramagnetic garnet substrates but, because of the low saturation magnetization of practical magnetic bubble films, accuracy in these cases is limited.

A magnetized sample, when placed in a magnetic field which is not parallel to the easy magnetization direction of the sample, will experience a torque. In applying this

principle to the measurement of magnetization and anisotropy, a counter-torque is generally applied by means of current carrying coils to the same shaft on which the sample is mounted. Such null deflection systems with automatic recording features have been described in detail by Croft, et al (Ref. 86), by Penoyer (Ref. 87), and by Byrnes (Ref. 88). An instructive schematic diagram, presented by Chikazumi (Ref. 89) is reproduced as Figure 14. The paired photocells, B, generate an unbalance signal when a torque is applied which is amplified and applied to the coil, C, in such a way as to restore the position of the entire specimen, coil, mirror assembly to very nearly its original position. The current required is a measure of the torque applied and is plotted vs. the direction of the applied field by the X-Y recorder. For small applied fields (smaller than that required to rotate the natural M_s within the sample significantly) this torque is a measure of M_s. At fields high enough to force M_s into parallelism with H the torque becomes a measure of the anisotropy in the magnetic energy (see Section 13).

The torque magnetometer approach has been used frequently both in the study of orthoferrites (Ref. 90, 91, 92, and 93) and the garnets (Ref. 94, 95, 96, 97, and 98). Because the torque method is applicable to the determination of magnetic anisotropy as well as magnetization, several of these references as well as others cited in

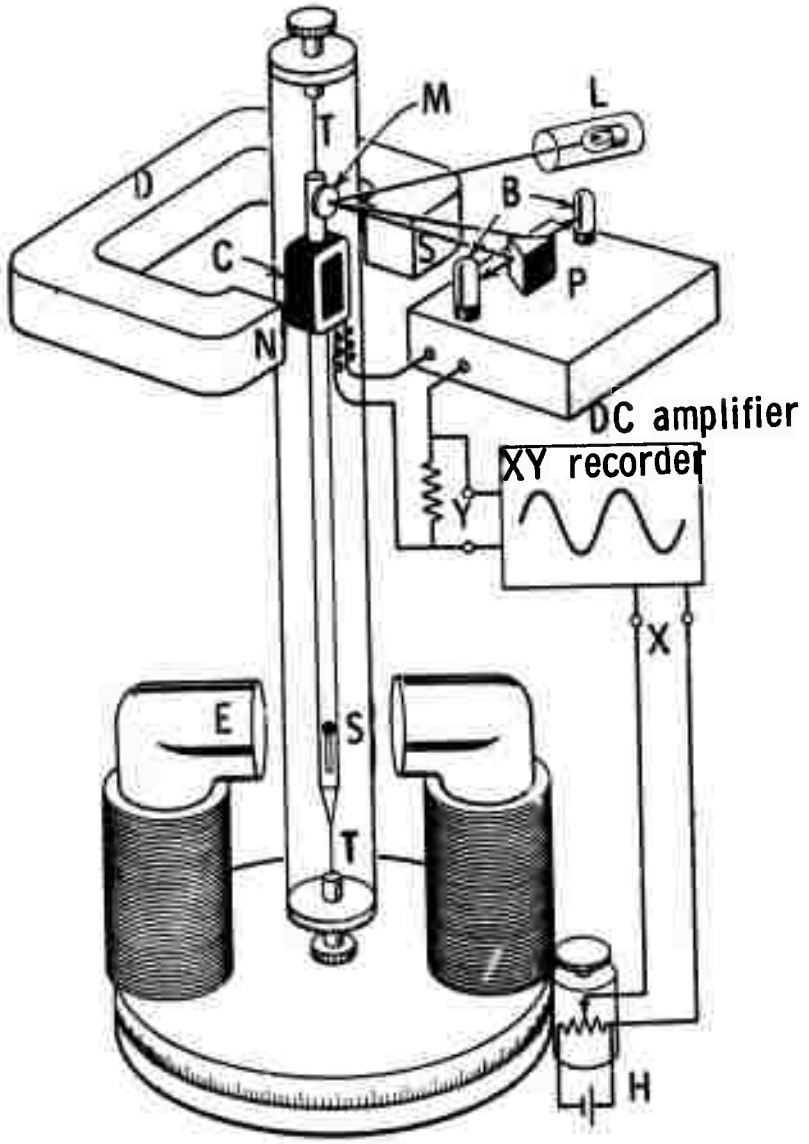

Figure 14. Automatic torque magnetometer. After Chikazumi, ref. 89.

Section 17 deal primarily with anisotropy. Lacey has recently inaugurated a torque system in which the effects due to paramagnetic substrate and magnetic film can be separately determined for epitaxial samples (Ref.99 and 100). There are sensitivity problems, however, for the low anisotropy materials most desirable as magnetic bubble films and, in any case, the separation of film and substrate effects requires considerable analysis of the torque versus applied field data.

9.2 Magneto-optical Methods

Magneto-optical approaches to the determination of magnetization are particularly appropriate for thin, optically transparent bubble domain samples. This is especially true since the entire fledgling industry depends upon microscopic examination of the behavior of magnetic domains via the Faraday effect for the evaluation of both materials and circuits for use with these materials. Techniques for the determination of magnetization from optically observed behavior in various magnetic fields derive from the same theoretical approaches which were central to the determination of characteristic length (Section 8). Either the behavior of magnetic bubble domains or strip domains may be employed. We consider first the use of bubble domains.

The theory of Thiele (Ref.29 and 30) yields the equilibrium equation for bubble domains quoted in Section 8 (Equation 8-1). Once the characteristic length and thickness

have been determined by the methods discussed previously each pair of values for applied field and bubble diameter serve to determine $4\pi M_s$ through this equation. Hagedorn, et al (Ref. 58) have carried out a least squares fit to this equation of careful measurements of domain diameter and applied field (10 each) and conclude that relative determinations of $4\pi M_s$ to within $\pm$ 3% can be made using this approach. Note that, because of the nature of this equation, the accuracy of $4\pi M_s$ is considerably better than that for ℓ determined in the same way ($\pm$ 7%). It still does not meet the requirements laid down by Bobeck, et al (Ref. 32) of 1% reproducibility in $4\pi M_s$ for devices. It also has all of the difficulties associated with it that were mentioned in Section 8 for the determination of ℓ from bubble dimensions.

Fowlis and Copeland, in their search for rapid means of evaluating bubble material parameters, have suggested that only the bubble collapse field, H_o, and the zero field domain period, P_o, be measured for the determination of $4\pi M_s$ (Ref. 59). They quote a calculation of Goldstein, based on the theories of Malek and Kambersky (Ref. 61) and Thiele, which relates these quantities to $4\pi M_s$. The results are shown in the curve of Figure 15. In contrast to the technique which uses only bubble measurements, the relative accuracy of the $4\pi M_s$ value is lower than that for ℓ here, being estimated by Fowlis and Copeland as 7% for $4\pi M_s$ and 5% for ℓ.

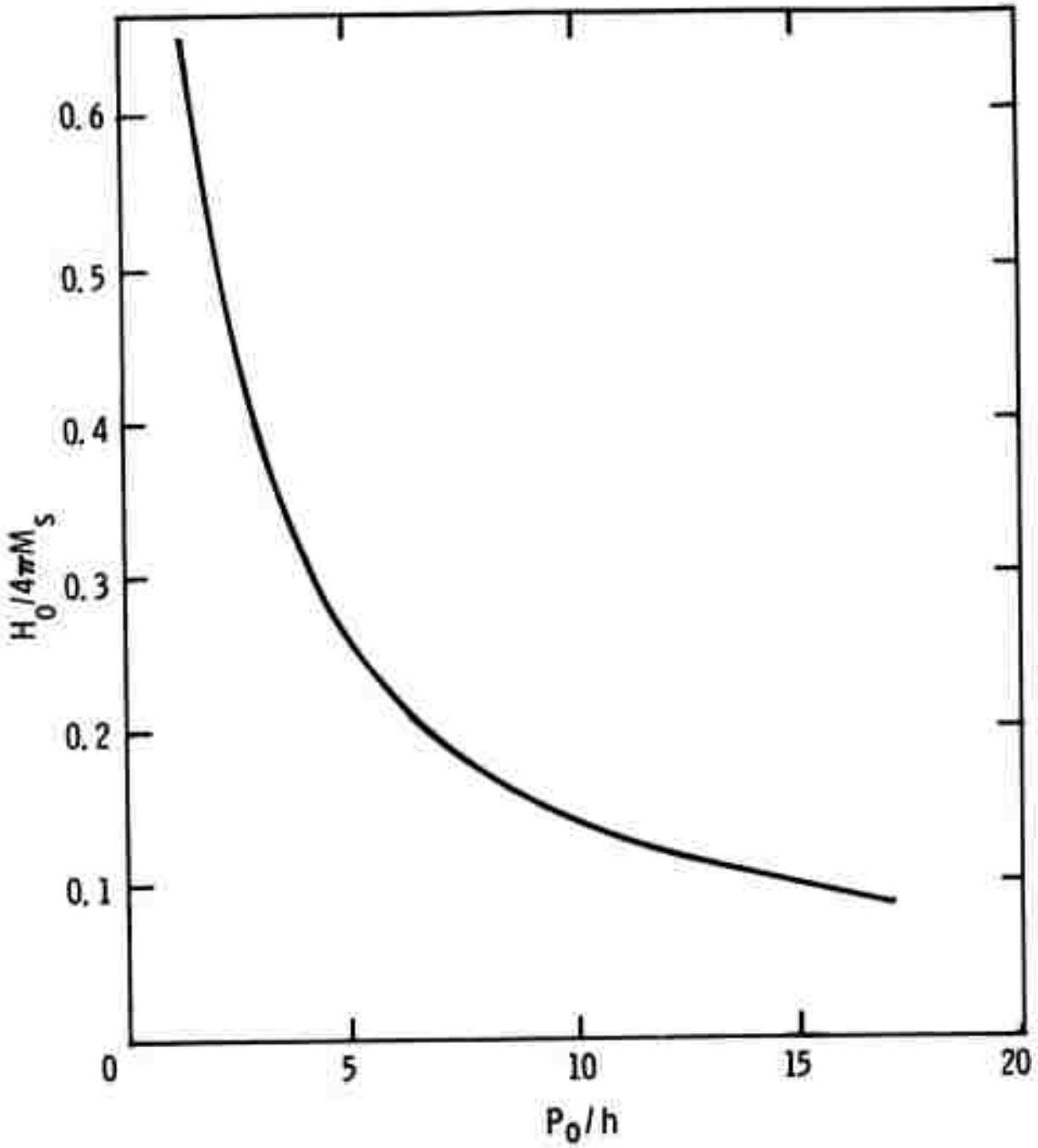

Figure 15. Bubble collapse field, H_o, divided by $4\pi M_S$ vs. strip domain period, P_o, at H = 0 divided by thickness, h. After Fowlis and Copeland, ref. 59.

One caution concerning the use of the bubble collapse field (and, indeed, all bubble measurements) should be made here. As discussed by Bobeck recently (Ref.101) and observed at Monsanto and at Hewlett Packard Companies (Ref.102) there appears to be more than one type of bubble capable of at least metastable existence within a given bubble film. Bobeck has termed all of those which are not in harmony with the Thiele theory "hard" bubbles, since a larger magnetic field is required to collapse them. They apparently differ from "ordinary" bubbles primarily in their wall energy density. Their formation seems to be favored when bubbles are formed using fast rise-time field pulses such as are frequently employed in the measurement of mobility (see Section 11). Thus one can be misled in the measurement of collapse field appropriate to the Thiele theory. Generation of bubbles by methods less energetic than fast, high field pulses are to be preferred. Such a recommended technique would be the cutting of strip domains with a fine magnetized wire.

One further magneto-optical method remains to be discussed, namely, the use of the full hysteresis curve (M/M_s vs. H). This curve is readily obtained for small regions of the samples by mounting a photomultiplier or other optical detector at the eyepiece of a polarizing microscope equipped with bias field coils. Cycling the bias field to saturation while recording the bias coil current versus photomultiplier output using an X-Y recorder yields a curve like Figure 16. A quantitative

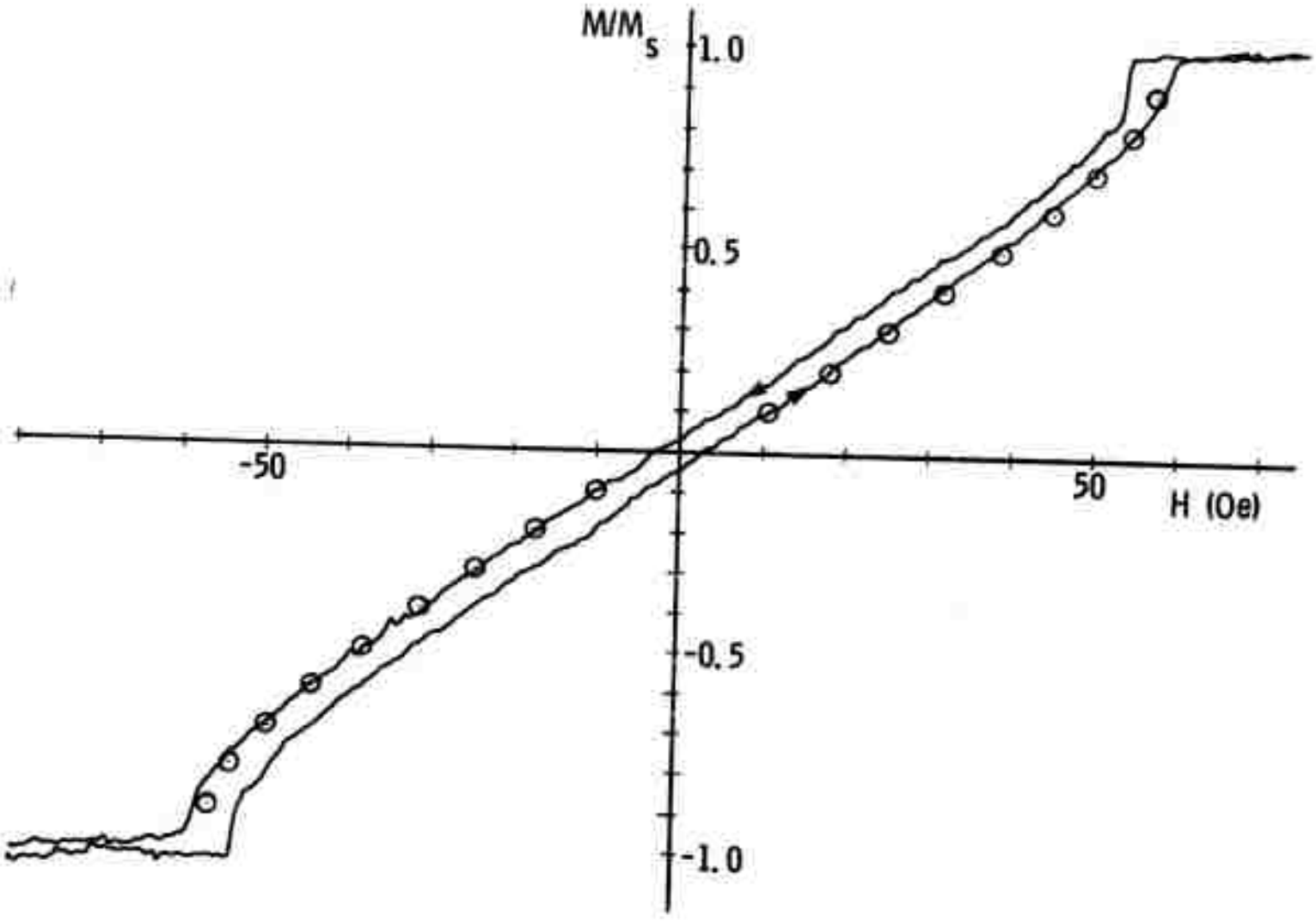

Figure 16. Hysteresis curve (M/M_S vs. H) for film of $Gd_{.87}Y_{1.18}Ga_{.9}Fe_{4.1}O_{12}$

M/M_s vs. H curve then requires only a knowledge of the bias coil calibration and reasonable assurance that the M/M_s curve (for which $M/M_s = 1$ is usually apparent) is linear. This is a good approximation as long as the polarizer-analyzer pair is not too close to extinction. A somewhat more elaborate temperature controlled Faraday hysteresigraph has been described by Beck (Ref.103) and applications of a similar system to garnets described by Mee (Ref.104and105). Both of these systems use He-Ne laser sources while we have found that, if a properly equipped microscope is available so that the highly collimated beam is not required, better signal to noise can be obtained using an incandescent (quartz-iodine) source with a photo-multiplier with cutoff in the red (such as the R.C.A. 6199 with S-11 surface).

The interpretation of the hysteresis curve in terms of $4\pi M_s$ involves recourse to theory, such as that of Kooy and Enz (Ref. 62). Craik (Ref.106) has outlined a method based on the initial slope of the curve and unpublished curves. Shaw, et al (Ref. 60) have solved Equations 9 and 10 of Kooy and Enz for the values of $H/4\pi M_s$ corresponding to 0.1 intervals in M/M_s. The results for high anisotropy materials ($H_a >> 4\pi M_s$) are shown in Figure 17. The procedure for determining M_s then involves reading values of M/M_s and H from the hysteresigraph for a sample of known P_o and h. The origin for H is moved to the right on the

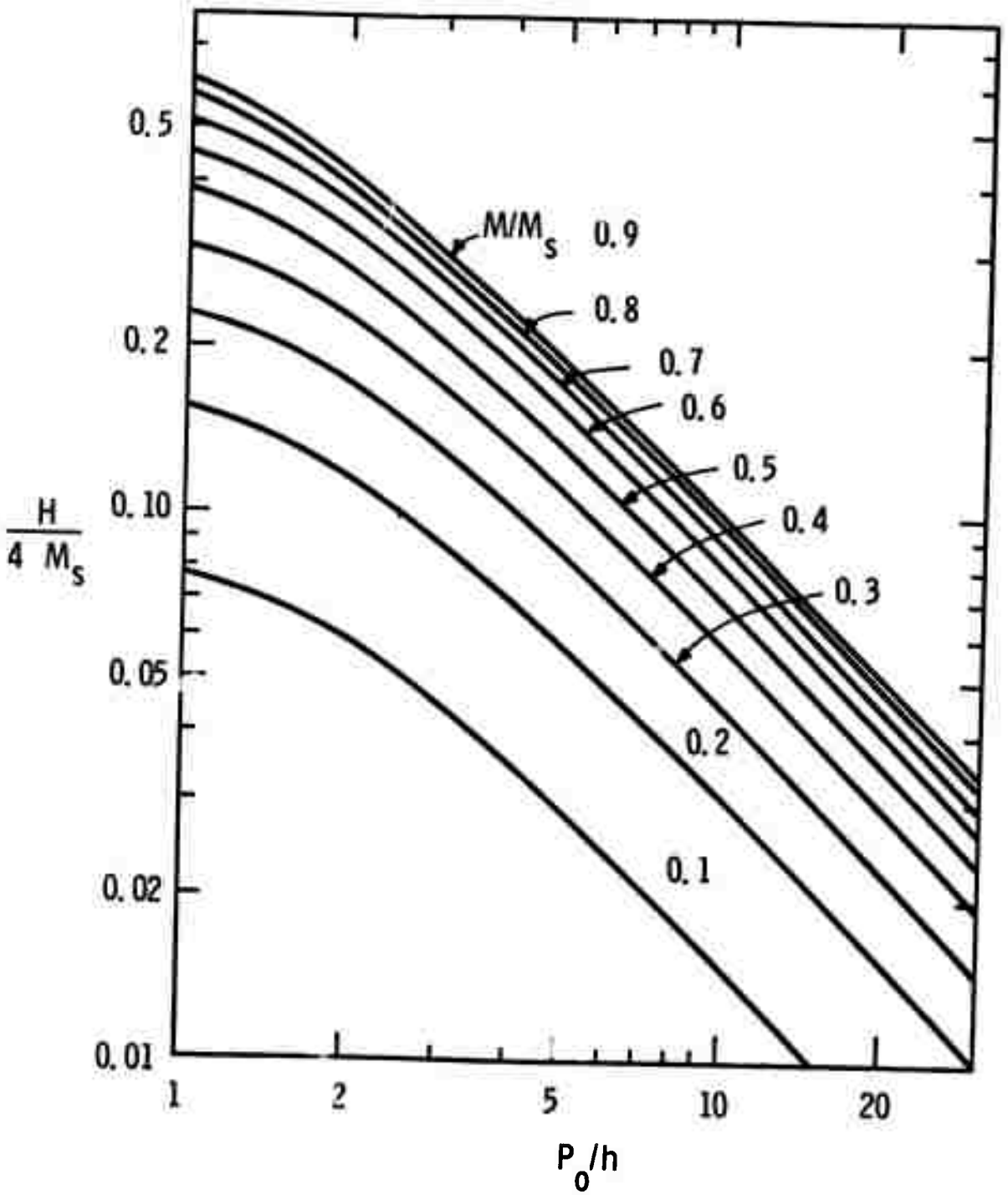

Figure 17. The applied field H necessary to achieve various magnetization ratios M/M_S for samples exhibiting zero field strip domain repeat distance P_O. After Kooy and Enz. Note the normalizations of the axes.

hysteresis loop by one half the loop width at H = 0 and the M/M_s read from the rising portion of the curve. The theoretical curves then permit determination of $H/4\pi M_s$, and from that $4\pi M_s$, for a particular sample at a particular M/M_s value. Figure 16 illustrates the agreement between the theory (points) and an experimental curve (continuous line). The use of all 18 M/M_s and H values results in a reasonably accurate value of $4\pi M_s$. We estimate that relative measurements of $4\pi M_s$ can be made from sample to sample of the same composition with this technique to within $\pm$ 3%. The term "relative" here means we ignore uncertainties in index of refraction (which enters the determination of h), in bias coil calibration, in graduated eyepiece calibration, and in approximations in the theory since these errors, if present, will enter each determination of $4\pi M_s$ in the same way.

Calculations are presently in progress at Monsanto (Ref. 68) which begin from the more accurate Equations 1-3 of Kooy and Enz and take into account finite anisotropy down to $H_A = 2(4\pi M_s)$. Preliminary results indicate that the largest changes in Figure 17 will occur for large M/M_s and small P_o/h where they will amount to an increase in $H/4\pi M_s$ of approximately 4%. In the other extreme of this figure the changes are less than 1%. We feel that the hysteresis curve approach, utilizing either the procedure just outlined or a direct, least-squares fit to the

theoretical equations, is the most accurate means for determining the magnetization of the thin epitaxial films needed for magnetic bubble technology. The greater convenience of the method of Fowlis and Copeland will, however, cause it to be used for more routine measurements.

10. DOMAIN WALL ENERGY

The two previous sections outline methods for the determination of $\ell \equiv \sigma_w/4\pi M_s^2$ and $4\pi M_s$. Together, then, they provide the data needed to calculate the domain wall energy per unit area, σ_w. Our primary concern in this section will be the discussion of other methods which have been devised to more or less directly determine σ_w. First, however, we briefly mention its relationship to other magnetic parameters.

The form of domain wall which normally occurs in the garnets (and for some orientations in the orthoferrites) was first investigated by Bloch (Ref.107and108). In this Bloch wall the individual spins are progressively rotated as one traverses from one domain to the next, the spin orientation always lying in the plane of the wall. In a crystalline film of uniaxial anisotropy with easy axis normal to the film (a first approximation to the situation in a magnetic bubble film) the net magnetization then undergoes a 180° rotation between adjacent domains. Two terms contribute to the increase in energy which this configuration causes, being offset by the decrease in magneto-static energy resulting from the breakup into domains. These two terms arise from isotropic exchange and uniaxial anisotropy characterized by the constants A and K_u, respectively. Upon minimizing the total energy with respect to the rate of rotation of the local moment, one finds a total wall energy per unit surface area given by a combination of isotropic exchange and anisotropy as

$$\sigma_w = 4(AK_u)^{1/2} \qquad (10\text{-}1)$$

The width of the wall (defined as that width required to encompass the total 180° rotation if the maximum rate of rotation at the wall center were maintained throughout) is given in this same context as

$$\ell_w = \pi(A/K_u)^{1/2} \qquad (10\text{-}2)$$

As already mentioned the anisotropy constant is related to the field required to force the magnetization into the hard direction, H_A, as $K_u = H_A M_s/2$. Thus the present section, together with those dealing with M_s and H_A (Sections 9 and 13) permit the complete characterization of magnetic bubble films in terms of these basic parameters.

Kurtzig and Shockley (Ref.109) developed a method for the determination of domain wall energy in the orthoferrites which involves the increase in wall length brought on by the application of a particular type of inhomogeneous field. They considered straight wall strip domains with an array of parallel wires laid across the domains at right angles. Application of equal but opposite current to adjacent wires of this set caused a spatially periodic distortion of these straight walls. Although the calculations and experiments were carried out under conditions permitting several simplifying assumptions (the conductors were far enough from the sample to yield only spatially sinusoidal field variations, the amplitude of wall motion was small compared

to width, the domain walls always contained the easy axis of magnetization) the expressions remained formidable and will not be reproduced here. The method, averaged over ten determinations on five samples of $ErFeO_3$, yielded 1.95 ergs/cm^2 $\pm$ 5%. The total variation among the ten cases cited was 14%. For the materials with smaller domain dimensions presently of interest this approach would be considerably less accurate since much smaller domain motion would need to be measured.

Nemchik and Charap (Ref.110and111)have investigated the behavior of an array of bubble domains in GdIG and developed two additional means of obtaining σ_w. In this case a sufficient density of bubbles was formed by means of a pulse coil to inhibit the tendency to run out into strip domains at low fields. Thus, even at zero bias field, the domain array was that of nearly circular bubbles.* Charap and Nemchik have also made use of the fact that GdIG has a compensation temperature near room temperature (T_c = 9.6°C) (Ref.105). This leads to a large variation with temperature of nearest neighbor bubble spacing and bubble size at zero applied bias field. By fitting variable temperature data to theoretical curves and assuming that the domain wall energy

---

* Cape and Lehman (Ref.112and113) and Kaczer (Ref.114)have considered the energetics of bubble and strip domain patterns. They showed that the energy difference between such a bubble array and the strip pattern is not large and discussed the barriers separating the two patterns.

itself is not a function of temperature near T_c, they have derived values of σ_w from each of these temperature variations. Cape and Lehman point out an error in their computation, however, so that at the present time we can only say that, done properly, the method appears capable of $\sim$ 20% accuracy in materials having significant temperature coefficients in the region of interest. Such variability with temperature is not desirable in a device film, of course.

In considering the alternative approaches to the measurement of domain wall energy per unit area, the best balance of speed, convenience and accuracy is found in the determination of ℓ and $4\pi M_s$ by the methods already discussed and the calculation of $\sigma_w = \ell 4\pi M_s^2$.

11. DOMAIN WALL DYNAMIC PROPERTIES

The parameter most commonly used today for the specification of dynamic domain wall response is the domain wall mobility, μ_w. This is defined in terms of the wall velocity, v, the field required to first cause wall motion, H_o, and the instantaneous applied field, H, as

$$\mu_w = \frac{v}{H-H_o} \quad . \tag{11-1}$$

This parameter has direct bearing on the speed with which bubbles can be moved in a device and therefore on the maximum data rate possible. As work has progressed, however, it has become clear that, in high mobility materials, a strict proportionality between domain wall velocity and net drive field holds only for small $H-H_o$ (Ref.115and116). For this reason as well as others to be mentioned later, the present section will extend beyond the measurement of mobility only.

Attempts to relate mobility to other parameters characteristic of the materials under study have met with limited success. An excellent review of this situation has recently been presented by Hagedorn (Ref. 63) and it is not the function of the present publication to repeat these details. The reader is also referred to the earlier reviews of Dillon (Ref.117) and Kittel and Galt (Ref.118). The one relationship which appears to be well established is a proportionality of mobility and domain wall width as given by equation (10-2).

11-1 Methods for Bulk Samples

The classic method (since about 1950) for the measurement of domain wall motion has been discussed in considerable detail by Galt (Ref.119). It involves cutting a "picture-frame" ring with each leg of the sample oriented along a direction of easy magnetization. Such a structure is illustrated in Fig. 18. In this case the domain wall can be propagated through the sample in a direction normal to the plane of the "picture-frame" by means of a coil wound on one leg of the frame. The motion of the domain wall can be detected by the emf generated in another similar coil. Considerable care must be exercised to insure that only one wall of the moving type is present. This sometimes requires careful proportioning of the sample in order to favor a particular wall (Ref.120). The wall velocity is then determined by applying a pulse of current to the drive coil and measuring the magnitude, V, of the voltage pulse generated in the pick-up coil. Ideally this is a flat, square pulse from which the wall velocity follows using Faraday's law and the system geometry:

$$v = \frac{V}{N8\pi M_s W \times 10^{-8}}. \qquad (11\text{-}2)$$

Here N is the number of turns in the pick up coil, W is the dimension of the sample leg perpendicular both to its axis and the direction of wall motion, and the units are mixed: v-cm/sec; V-volts, M_s-Gauss, and W-cm. The mobility then follows from equation (11-1).

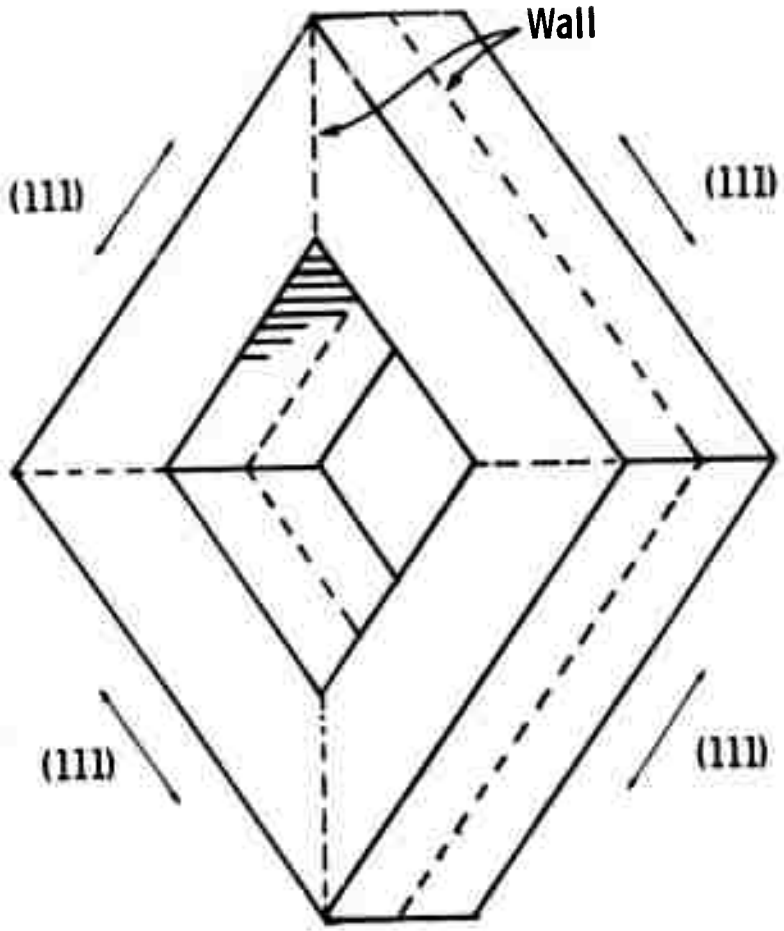

Figure 18. "Picture frame" geometry for domain wall mobility measurement. After Galt, ref. 119.

This technique, without the use of a full "picture-frame" sample, has been applied to yttrium orthoferrite by Umebayashi and Ishikawa (Ref.121) for temperatures down to 77°K. Yttrium iron garnet was measured using the full frame configuration by Hagedorn and Gyorgy (Ref.122) and by Wanas (Ref.123) down to 4.2°K. A difference of a factor of 4 - 7 between these results probably resulted from the presence of multiple domain walls in the earlier measurements. Wanas also observed the decrease in mobility brought about by the addition of small amounts of Si, a clear indication to today's crystal grower of the need for purity.

Response of single crystal toroids of YIG doped with Yb^{3+} and Er^{3+} ions has been investigated by Harper and Teale (Ref.124 and125). Because of the sample geometry used they suspect the presence of multiple domain walls and therefore work with switching times rather than mobilities. The temperature dependences observed (large peaks in switching time below approximately 100°K) are certainly reflections of the damping introduced by the Yb and Er rare earth ions, however.

While this "picture-frame" technique is an excellent one for the study of domain wall dynamics its chief drawback, sample preparation, should be obvious. Such complex samples cannot be formed from the thin films needed for devices nor, in fact, could they be formed at all from uniaxial material and still maintain the easy axis orientation in all legs.

Thus the approach may remain quite useful for fundamental studies but has no place in the routine characterization of films for bubble devices.

It is not necessary to have a closed magnetic loop such as the "picture-frame" geometry, of course, in order to induce an electrical signal as a result of domain wall motion. Asti, et al (Ref.126,127 and128) have made use of ellipsoidal samples placed within a coil which is in turn within a larger solenoid. A pulsed field is generated by means of a capacitor discharge through the solenoid and a signal proportional to the rate of change of sample magnetization is developed in the pick up coil. Effects not associated with the sample are bucked out by a matched compensating coil also within the solenoid. A number of ferrites have been studied in this way but, once again, application to thin films is not convenient.

Vella-Coliero, et al (Ref.129 and130) have measured the real and imaginary parts of the susceptiblity of small, bulk crystals of garnets using a modification of a nuclear magnetic resonance system (Ref.131). They determine a relaxation frequence, ω_c, at which the imaginary term in the susceptibility has a maximum while the real part has fallen to 1/2 of the low frequency limit, χ_o. The domain wall mobility is then calculated as

$$\mu_w = \frac{\chi_o \omega_c d}{2M_s} \qquad (11\text{-}3)$$

where d is the domain width in the sample. For two series of Tb and Dy additions to $Gd_3Fe_5O_{12}$ agreement to within 10% with the method of Bobeck (see below) is indicated but no indication of absolute accuracy is given.

In the second of these papers (Ref.130) the authors have investigated a series of high mobility $Y_{3-x}Gd_xFe_5O_{12}$ samples and have observed a resonant behavior near 100 MHz. Such a resonance implies a domain wall inertia and thus an effective mass for the wall. The mass per unit area was calculated from the resonant frequency ω_r as

$$m = \frac{4M_s^2}{\omega_r^2 \chi_o d} \qquad (11\text{-}4)$$

The results indicate that m rises from $\sim 2 \times 10^{-11}$ to 12×10^{-11} gms/cm^2 as the yttrium content increases and clearly demonstrates a means of evaluating this wall mass in suitable materials. In addition, mobility values calculated from equation (11-3) increase from $\sim$ 5000 to 12000 cm/sec Oe for the same composition change. These are the highest room temperature mobilities reported to date. Henry (Ref.132) has pointed out that wall mass effects may become significant in device applications of such materials.

11-2 Pulsed Field Methods for Thin Film or Platelet Samples

The application of a pulsed field to the thin platelet or film samples of interest for bubble devices does lead to measurable effects. Middelhoek (Ref.133) has described a

system appropriate for Ni-Fe films in which wall position was detected via the Kerr effect. The change in position of a single wall in an initially saturated film following a series of field pulses was interpreted in terms of a velocity. The mobility followed as the slope of the velocity vs. pulsed field amplitude curve. Other results in Ni-Fe films have recently been reported by Konishi (Ref.134). In magnetic bubble materials, domain walls are usually detected via the Faraday effect. Seitchik, et al (Ref.135) have discussed a technique used in the orthoferrites in which the variation of light passing through the sample (and passing through the usual polarizer-analyzer pair) is measured as a short risetime field pulse is applied. In order to minimize inductive effects a small (20 turns, 1.8mm diameter) coil was used and sampling and time averaging techniques applied to the resulting signal to improve the signal to noise ratio. The relaxation time, t, of the domain walls to their new configuration in the pulsed field must be considerably longer than the rise time of the applied pulse and the field pulse amplitude must be less than 1/2 of the saturation field to maintain accuracy. In this case starting with strip domains

$$\mu_w = (X_o/H_o)\ t^{-1} \qquad (11\text{-}5)$$

where X_o is the equilibrium displacement of a wall in an applied field H_o. Shaw, et al (Ref. 39) have discussed a

means of calculating X_o/H_o from a knowledge of the h, P_o, and $4\pi M_s$ using Fig. 17. At Monsanto, the Seitchik method has been used extensively in mobility measurements in thin film magnetic garnets. Efforts to extend this method to high mobility materials have yielded values to approximately 1,000cm/sec Oe in garnets from 2 turn or 5 turn coils which allow pulse risetimes of 1 and 2 nsec, respectively. A mercury-wetted reed pulser (Spencer Kennedy Laboratories Model 503A) with 0.5 nsec risetime is used to drive these coils in a strip-line configuration. Accuracy is estimated at $\pm$ 25% in the high mobility range while the value of the mobility is a function of pulse amplitude as expected from the results of Calhoun, et al (Ref.115) and Bonner, et al (Ref.116). Shumate (Ref. 47 and 40) and Shaw, et al (Ref. 39) have discussed the use of this approach in the garnets. Nemchik and Charap (Ref.136) have discussed a similar approach which, however, starts with a zero field bubble array rather than strip domains.

Another approach to the mobility which also employs a pulsed field and Faraday rotation is the bubble collapse method of Bobeck (Ref.137). More detailed analysis of the method (but including some approximations) has been presented by Callen and Josephs (Ref.138). The technique involves the application first of a DC bias field which stabilizes isolated bubble domains. One of these is now subjected to a further bias pulse driving it toward collapse. Although

this total field ($H_{bias} + H_{pulse}$) may be large enough to cause collapse if applied as a constant bias field for a pulse of sufficiently short duration the bubble will still be present and return to its original size after the pulse terminates. This is a result of the finite speed with which the domain wall can move toward collapse during the pulse. The pulse amplitude and duration at which collapse just takes place (i.e. reducing either quantity results in the continued existence of the bubble) forms the basis of the measurement. It is important to realize that the minimum instantaneous diameter from which a bubble can recover is smaller than the static diameter for collapse, being approximately one half of that static dimension for a bias field equal to the strip to bubble transition field. The original Thiele paper (Ref. 29) discusses this dynamic stability limit but more explicit consideration of the limit as it applies to the present method has been given elsewhere (Ref.139 and140). Shumate (Ref. 47) has reported Rossol's observations of the dynamically allowed range of diameters using stroboscopic techniques. If the pulse is applied to a bubble initially at the strip to bubble transition the total distance traveled by a wall to just reach collapse is $\Delta r \cong r_{S-B} - r_o/2$. Bobeck suggests plotting the inverse of the pulse duration, T, necessary to bring about bubble collapse vs. the field pulse amplitude H_p. Some of his original data (Ref.137) is reproduced in Fig. 19.

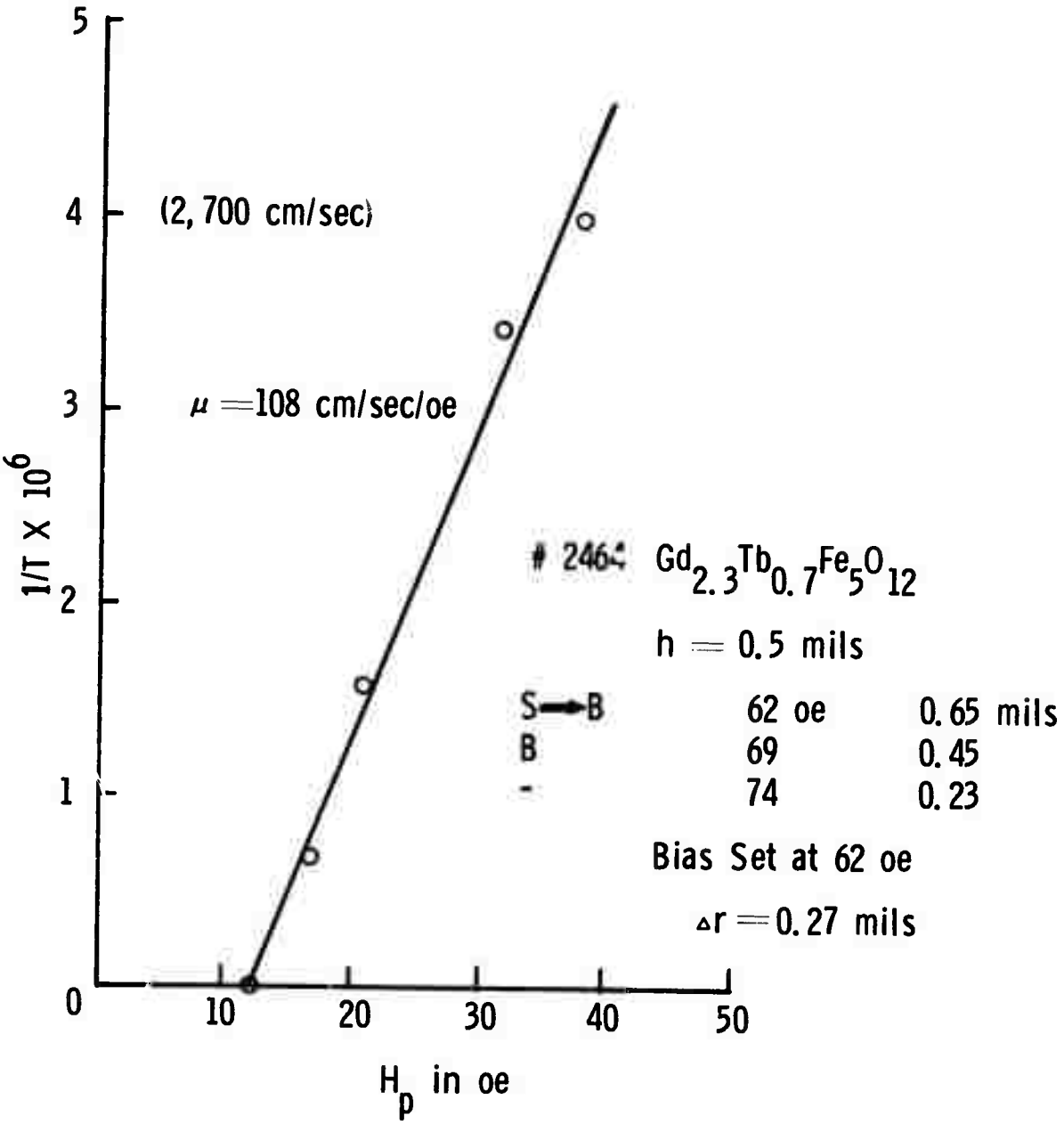

Figure 19. Bubble collapse data for a uniaxial garnet. After Bobeck, ref. 137.

The mobility is then calculated as:

$$\mu_w = \frac{(\Delta r)\ \Delta(1/T)}{\Delta H_p} \qquad (11\text{-}6)$$

The approach of Callen and Josephs (Ref.138) is couched in terms of fields and pulse lengths only (with all variables elegantly normalized). For pulse fields considerably above those required to cause collapse their method yields

$$(\mu_w T)^{-1} \cong a_1 + a_2 H_p \qquad (11\text{-}7)$$

where a_1 and a_2 are functions of H_c , $4\pi M_s$, ℓ, and h. This can be cast in the same form as the Bobeck approach by differentiation in which case

$$\mu_w \cong \frac{1}{a_2} \frac{\Delta(1/T)}{\Delta H_p} . \qquad (11\text{-}8)$$

In the present notation

$$a_2^{-1} = \frac{2(4\pi M_s)\ h\left\{[1-3/4\ (\ell/h) + (H_1/4\pi M_s)]^2 - 4H_1/4\pi M_s\right\}^{1/2}}{3H_1} \qquad (11\text{-}9)$$

which replaces Δr in the Bobeck expression. Here H_1 is the DC bias field applied.

This approach has been widely used and has the advantages of yielding results on a wide variety of materials and requiring a minimum of additional equipment. Calhoun, et al (Ref.115) have used it to study the variation of velocity with pulse amplitude in high mobility Ga-YIG where they find $\mu_w \sim \sqrt{H_p}$. Such a phenomenon suggests that the mobility (usually measured at small pulse amplitudes) is not the most

useful parameter for predicting device performance. Velocity measured at a pulse amplitude characteristic of the contemplated device would be much more realistic as a starting point in such a prediction. Several authors (Ref. 141 & 142) have recently reported results on various Y-RE garnets indicating a velocity saturation effect. Both the bubble collapse (Ref.141) and step function response (Ref.142) methods were used. Slonczewski (Ref.143) has attacked this problem on a theoretical basis.

There are a number of areas of concern in the application of the bubble collapse method. First (and probably least important) the dynamic collapse radius mentioned above is a function of the DC bias field, being $r_c/2$ only at the strip to bubble transition field and approaching r_c as the DC bias is raised toward the collapse field. Second, Cape (Ref. 144) has pointed out that the Bobeck expression actually involves a linear approximation to an exponential (the exponential approach of the bubble radius to its new equilibrium) and, as such, requires pulse fields considerably greater than the minimum necessary to bring about collapse. The same idea is involved in producing the approximation, equation (11-8), from the theory of Callen and Josephs above. Cape also has some more subtle restrictions on the Bobeck method which would seem to require that the initial radius (and therefore H_1) must be quite close to the collapse value. If this is true the accuracy of the method would be seriously impaired.

Third, the matter of different kinds of bubbles ("hard" bubbles) raised earlier becomes particularly troublesome here. The bubble under study must be annihilated in such a measurement and it is very tempting to reduce the bias and pulse the coil hard in order to generate new bubbles. Unfortunately this seems to be the very best way to generate these anomalous bubbles which do not behave in quantitatively the same way that "ordinary" bubbles do and lead to considerable scatter in the data. The best way to avoid this problem seems to be each time to cut the strips with a fine wire as mentioned earlier.

11.3 Methods Utilizing the Isolated, Straight Domain Wall

In the orthoferrites an isolated wall can be generated by applying a sufficiently strong gradient. Such an arrangement has been used in the study of mobility by Rossol (Ref.145 and146) and Shumate (Ref.147). Rossol's approach has been to apply an alternating field in addition to the gradient and stroboscopically determine the total displacement, X, of the wall. As the frequency of the constant amplitude alternating field is raised the wall velocity increases until it becomes limited by the mobility of the material. The angular frequency, ω_c, at which the wall displacement has fallen to $1/\sqrt{2}$ of its low frequency value, X_o, is determined from a frequency vs. displacement plot. The mobility is then given by

$$\mu_w = \frac{X_o \omega_c}{H_{AC}} \qquad (11\text{-}10)$$

Rossol has reported mobility for a number of the rare-earth orthoferrites including values as high as 50,000cm/sec. Oe in carefully prepared $YFeO_3$ at 77°K.*

Shumate (Ref.147 and149) has used a similar, straight wall technique in which the alternating field is replaced by a square pulsed field of duration such that the domain wall does not reach its new equilibrium before the pulse is removed. The wall approaches its new position, X_o, during the pulse according to the equation

$$X(t) = X_o \left[1 - \exp\left(-\mu_w H_p t/X_o\right)\right] \qquad (11\text{-}11)$$

Thus measurements of the maximum displacement for various pulses of known duration and amplitude serve to determine μ_w. Steady rather than stroboscopic illumination has generally been employed. For the orthoferrites this technique appears to be the most accurate available, the reported reproducibility on a given sample of high quality being several parts per thousand and the absolute accuracy, 5%. Shumate investigated the anisotropy of mobility - arising from the presence of Bloch and Neel walls for different wall orientations in the orthoferrites (Ref.150) - and the

---

* Marsh, et al (Ref.148) have briefly described a related technique in which an isolated bubble is modulated in size by an AC bias component and the field amplitude required for constant amplitude in radius is measured.

changes of mobility brought about by annealing and x-ray irradiation (Ref.149 and151). (See also ref.152).

The difficulties in generating the field gradient needed to yield a single straight wall in the magnetic bubble garnets have already been discussed (see Section 7). This limitation severely restricts the application of this technique for today's magnetic bubble materials. So far as the authors are aware no analysis of the corrugated or finger like wall which occurs in the garnets at reasonable gradient fields has been attempted so that the approach cannot be recommended for general use.

11.4 Bubble Translation Methods

Several schemes have been proposed for the study of the dynamic translational response of bubbles. Such a measurement is to be desired in that cylindrical domain walls are, in fact, the ultimate moving element in this subject, not individual strip domain walls. Heinz, et al (Ref. 35) (see also ref.153) have employed conductor loops deposited directly onto the bubble film surface. These were pulsed so that a net field difference was established which tended to transfer a bubble from one to the next. Approximating this as a constant gradient $\Delta H/\Delta x$ between the loops and knowing the minimum pulse duration, t_o, required to transfer a bubble of diameter, d, between loops of spacing r they were able to calculate the approximate domain mobility

$$\mu_d \cong \frac{r}{dt_o \ (\Delta H/\Delta x)} \qquad (11\text{-}12)$$

Here $\mu_d = \mu_w/2$. Such a system is useful in the garnets but requires the deposition of the conductor pattern (or the close approach as such a pattern on a separate microscope slide) as well as the above approximations for its application.

Copeland and Spiwak (Ref.154) have employed a single straight conductor to generate the translating gradient field. They present theoretical results indicating that the driving force is constant to within 20% for bubble center positions within half of the bubble radius. They also consider various conductor to sample spacings and sample thicknesses. In the experiment the bubble is driven using a bipolar square wave so that it remains within the region mentioned (two other conductors carrying direct current are also present to contain the bubble). In arriving at mobility values these authors also identify the drive field H_F as $H_F = R\ \Delta H/\Delta X$ for a bubble of radius R. Mobilities obtained by this method agree to within 10% with those measured by Shumate using the straight wall method. Unfortunately the method appears to be limited to the orthoferrites (Ref.155).

Rossol has applied the stroboscopic approach to the study of bubble motion under a permalloy disk (Ref.156) and in a simple T-bar circuit (Ref.157) (again on orthoferrites). In the former, the phase lag between an in-plane rotating field and the bubble motion was measured as a function of the rotation frequency. After considerable analysis

of the disk-bubble interaction, the mobility was calculated and agreed well with that found by the straight wall technique. In the T-bar circuit, the time delay between various positions for a circulating bubble in the device was measured and a velocity obtained for each region of the device. In this case the field gradients and corresponding mobility again required detailed analysis which was not presented. The method is, in fact, of more usefulness in the design and analysis of magnetic overlays for devices than for material characterization.

Vella-Coleiro and Tabor (Ref.158) have recently proposed a pulsed gradient system of considerable accuracy for use in the garnets. This involves the used of two parallel conductors carrying current in the same direction which, when pulsed, yield a gradient field at their center which drives a bubble perpendicular to their direction. In order to reduce the effect of the decreasing field seen by the bubble as it moves in the pulsed field they superimpose a linearly increasing field component by means of an additional conductor in the form of a rectangle. This ramp contribution to the field must be computed and properly adjsuted for each measurement of bubble motion vs. pulsed field gradient. Further, the total travel is limited to $\sim$ 10% of the distance between the conductors in order to remain in a region of reasonably constant gradient ($\sim$ 3%). For the circuit described this

total travel is 5μm so that its measurement will pose a significant limitation on the overall accuracy of the method. One further limitation comes from the decrease in gradient as the distance from the plane of the conductors increases, being approximately 13% at 10μ and limiting the technique to samples of about this thickness. Within all of these limitations the method yields the mobility (and the dynamic coercivity, H_c) from the equation

$$v = \Delta X/\Delta t = 1/2\ \mu_w \left(\frac{1.60Id}{D^2} - \frac{8}{\pi} H_c \right) \qquad (11\text{-}13)$$

where I is the current in the parallel conductors and D is their spacing. Several measurements under various pulse conditions are of course necessary to determine both μ_w and H_c. Cape (Ref.144) has proposed a similar system using two wires without the ramp field refinement. He has also discussed some of the real world difficulties which occur with such a system.

11.5 Conclusions

In closing this section on the many approaches which have been made to the measurement of domain wall dynamics, several points should be made.

1. The relationship between domain wall velocity and drive field is not always linear, particularly for materials composed of ions with nearly zero orbital angular momentum. The highest mobilities occur for drive fields which are too small to be practical. At

useful drive fields the domain velocity saturates in many cases which results in a low effective mobility. Therefore the concept of a mobility loses much of its usefulness. If mobility values are quoted they should be accompanied by a drive field value or by an assurance that the value is independent of drive field over a specified range. The preferable approach would seem to be to quote velocity vs. drive field values or curves.

2. It would appear at this point that the bubble translation method of reference 158 is the best approach to the accurate measurement of velocity vs. drive field while the step function response of linear walls is most convenient as a quality control test in a production situation. In spite of the many techniques which have been proposed, however, it seems likely that the ideal method for routine evaluation of dynamic properties of bubble materials is still to come.

3. Even when reliable mobility or velocity data are in hand, the prediction of device operating speeds and margins remains a formidable and imprecise task. Several useful discussions have been presented, however, and are listed here as references 159, 160, and 161.

12. FERROMAGNETIC RESONANCE (FMR)

This phenomenon can be pictured in terms of the precession of the total magnetic moment of the specimen around the direction of an applied magnetic field. When a transverse field is applied at the frequency of this precession, energy is absorbed as the system is excited (in a quantum mechanical picture) to higher Zeeman levels. YIG and the related rare-earth garnets present a nearly ideal system for the study of this phenomenon for they are good insulators, possess strong FMR lines, and are theoretically tractable. Because of this and because commercial microwave applications exist for YIG the literature on this subject is enormous. Our review here will be necessarily very incomplete but will touch on those aspects of particular relevance to magnetic bubble applications. These include the relationships of FMR frequency and applied field to anisotropy and of the FMR linewidth to mobility and other dynamic properties of domains.

The most useful experimental configuration for the present purposes is that generally referred to as perpendicular resonance. In it a static magnetic field H is applied perpendicular to the film plane and an oscillating field (generally in the microwave range) is applied in the plane of the film. The condition for the lowest frequency mode in this case is given by

$$\frac{\omega}{\gamma} = H - 4\pi M_s + H_A \qquad (12\text{-}1)$$

(Ref.162,163,164, 35, and 13). Here ω is the resonance frequency and γ, the gyromagnetic ratio. This equation can be pictured in the following elementary way: The resonance condition for an ion is simply, $\omega = \gamma H_{total}$ where H_{total} is made up of three terms: 1) The externally applied field, H, assumed large enough to saturate the sample, 2) the demagnetizing field, $- 4\pi M_s$, which is the internal magnetic field generated by the free magnetic poles on the surfaces of the films and 3) the anisotropy field, H_A, which, by its very definition, plays the role of an additional bias field resisting the tendency of the microwave field to tip the net magnetization away from the film normal. The full spectrum of higher excitations in FMR is very rich, as the above references show. In addition there are a number of effects of sample geometry and orientation which we will not discuss. (See, for example references 165and166). For the films of interest in this report the magnetization is low enough that these higher frequency modes are not strong.

Heinz, et al (Ref. 35) have pointed out that equation (12-1) is directly relevant to the conditions for bubble stability and mobility. In order to have bubbles with magnetization normal to the film plane the condition

$$H_A \gtrsim 4\pi M_s \qquad (12\text{-}2)$$

must be satisfied (Ref. 29). This can be read directly from the FMR results as

$$H_A - 4\pi M_s = \frac{\omega}{\gamma} - H > 0 \qquad (12\text{-}3)$$

An additional consideration is that increasing anisotropy causes a reduced domain wall width and with it decreased mobility so that maintaining $2 \lesssim H_A/4\pi M_s \lesssim 8$ is desirable. FMR, coupled with a measurement of $4\pi M_s$ as described earlier and published values of γ, provides useful knowledge of H_A and this ratio. Pearson, et al (Ref. 95, 96, and 97) have reported detailed comparisons of anisotropy data from FMR and torque measurements for the garnets. The phenomenon of growth induced anisotropy in the garnets, which has given the crystal grower much wider latitude in designing new bubble materials, was investigated using FMR by LeCraw, et al (Ref.167). FMR has the capability of providing $4\pi M_s$ and γ values if several frequencies or orientations are used but such an approach is quite involved and does not lend itself to routine characterization.

It is worth pointing out that the connection between static torque magnetometer measurements and FMR is quite close. This results from the fact that FMR detects the condition in which maximum energy can be pumped into the magnetic system. Since such a system is associated with an angular momentum a torque is required to bring this about. Thus the starting vector equation for the FMR calculation is

$$\frac{d\bar{M}}{dt} = \gamma \bar{M} \times \bar{H} = \gamma\bar{\tau} \qquad (12\text{-}4)$$

where $\bar{\tau}$ is the torque. As demonstrated by Pearson and Cooper (Ref. 95 - see also ref.168) for Tb doped YIG, the field for resonance is given by

$$H_{res} \alpha \frac{\partial \tau}{\partial \theta} \qquad (12\text{-}5)$$

which is also the second derivative of the crystal energy with respect to angle. Here θ is the angle which the applied field makes with a crystal axis. Unfortunately, such a simple relationship only holds for spherical samples, reducing its usefulness in the present context.

The connection between domain wall mobility and FMR linewidth was developed largely during the 1950's by workers at Bell Telephone Laboratories (Ref.119,169,118, and120). Hagedorn and Gyorgy (Ref.122) noticed a discrepancy between damping factors derived from mobility and FMR measurements for high mobility materials and developed a new theory for wall damping in such materials. Their prediction of velocity proportional to the square root of the drive field has recently been verified by Calhoun, et al (Ref.115).

Harper and Teale (Ref.125) pursued the connection between mobility and FMR and, by making some simplifying assumptions, have deduced the equation

$$\mu_w \cong \frac{A^{1/2}}{\Delta H} \frac{\omega}{1 + (\omega t)^2} F(\sigma_1, \sigma_2) \qquad (12\text{-}6)$$

where ΔH is the linewidth; ω, the resonant frequency; t, the relaxation time for the excited states of the crystal and $F(\sigma_1, \sigma_2)$ a function of crystalline anisotropy and the orientations of M_s on both sides of a domain wall. It is clear that a number of measurements would be necessary to extract numerical values of mobility from such an approach.

So far as we are aware, no one is attempting to do that on a routine basis. However, this connection has been of great use in the search for improved magnetic bubble materials. Because of the large amount of work done by Dillon and others (Ref.170,171,172,173, and 94) linewidth information on many of the rare-earth garnets and rare-earth doped YIG are readily available. This information provides valuable guidance in choosing rare-earths necessary to adjust the magnetic and lattice parameters. It indicates, among other things, that the large linewidth ions Tb, Dy, and Ho are to be avoided in applications demanding high mobility.

The apparatus and techniques for FMR are well established and, at least for room temperature work, largely available on an off-the-shelf basis today. Kip (Ref.174), Soohoo (Ref.166) and Seiden (Ref.175) have discussed apparatus for this measurement. Fig. 20 illustrates a simple system as shown by Seiden. In it the power reflected by the sample is detected in the crystal detector and, after amplification, recorded directly. For weak signals such as those arising from dilute systems of magnetic ions more sophisticated methods such as those used in electron paramagnetic resonance are available (Ref.176).

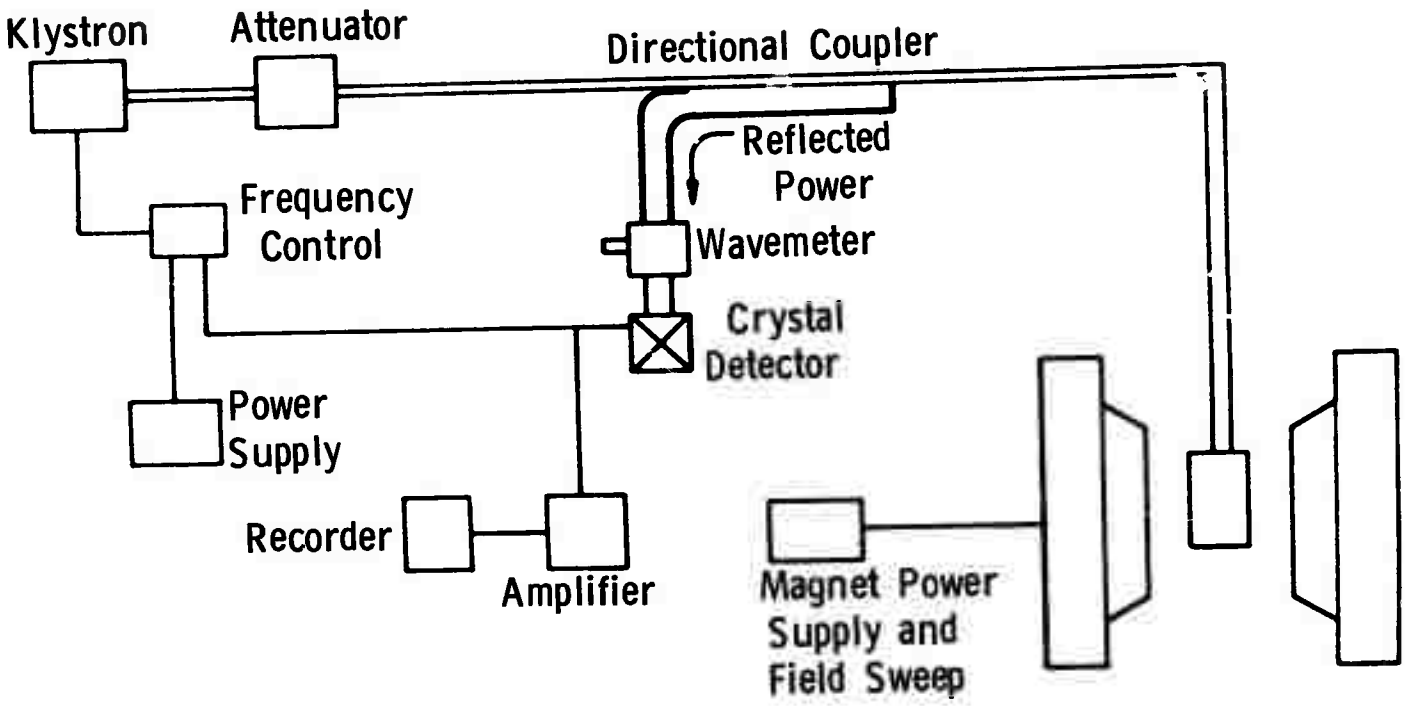

Figure 20. Diagram of simple FMR apparatus for microwave frequencies. After Seiden, ref. 175.

13. ANISOTROPY

The magnetic anisotropy, as mentioned previously in this report, is represented by the anisotropy field required to pull the magnetization into the hard direction, H_A, or the related uniaxial anisotropy constant, $K_u = H_A M_s/2$. While this uniaxial anisotropy, favoring a magnetization direction normal to the plane of the bubble film or platelet, is essential for the bubble device, it is an over-simplification to ignore other forms of anisotropy which may be present. We therefore present a very brief introduction to the subject here. More extensive discussion can be found in a number of references (see for example, ref.177 and178).

The orthoferrites have an orthorhombic crystal structure and exhibit a very high anisotropy, M_s lying along the c direction at room temperature for most of the single rare-earth compositions. (The lattice parameters obey the inequality $a < b < c$.) The exception is $SmFeO_3$ for which the a direction is preferred (Ref. 90,179, and180). Such a direction is also preferred below the reorientation temperature in other orthoferrites (Ref.181 and section 16). Away from this temperature the anisotropy field has been estimated at approximately 10^5 Oe (Ref.182). This gives rise to a large wall energy and the large bubbles which have been the major drawback of orthoferrites for devices. By growing mixed rare-earth orthoferrites with Sm it is possible to come close enough to the reorientation temperature to reduce this

anisotropy and the bubble size to some extent but only at the expense of temperature stability.

The garnets are basically cubic crystals which, in the absence of other factors, exhibit typical cubic dependence of energy upon magnetization direction,

$$E = K_1 (\alpha_1^2\alpha_2^2+\alpha_2^2\alpha_3^2+\alpha_3^2\alpha_1^2) + K_2\alpha_1^2\alpha_2^2\alpha_3^2+ \ldots \quad (13\text{-}1)$$

Here α_i is the direction cosine between the magnetization direction and the ith. cubic axis. Pearson (Ref. 96) has measured K_1 and, where possible, K_2 for most of the single rare-earth garnets. Generally K_1 is negative leading to easy directions for the magnetization of <111> . (See also ref. 64). Because of the high symmetry exhibited by this expression garnets were not at first looked upon as likely prospects for bubble devices. It has proved possible, however, to generate sufficient uniaxial anisotropy to markedly change those prospects. Both stress, generated by polishing or mismatch with the underlying substrate (Ref. 104 and 3) and particular growth direction and constituents - termed growth induced anisotropy (Ref.183, 64,184, and185)- have been shown to yield the necessary uniaxiality. This uniaxial anisotropy can be described as a series of terms in the energy once again:

$$E = K_{u1}\sin^2\theta + K_{u2}\sin^4\theta + \ldots \quad (13\text{-}2)$$

Here θ is the angle between the magnetization and the easy axis. The total anisotropy energy of a garnet in general then will be given by the sum of equations (13-1) and (13-2).

For device purposes the most important anisotropy is between the film normal direction and the lowest energy direction approximately in the film plane since it is this difference which will determine the bubble stability. This difference is here referred to as K_u.

13.1 Non-Optical Methods

Two of the standard methods for the measurement of magnetic anisotropy have already been discussed in some detail. These are torque magnetometry (Section 9) and ferromagnetic resonance (Section 12).

One other recently developed method deserves mention here. Flanders and Doyle (Ref.186 and187) have developed a rotating sample magnetometer and applied it to the measurement of anisotropy in GdIG platelets. The voltages induced in pickup coils near the rotating sample are detected using a lock-in amplifier synchronized to the rotation frequency or one of its harmonics. Reference186 discusses a number of sample configurations to be used depending upon the sample anisotropy and the property desired. It indicates that a rotating sample system may have advantages over vibrating sample or coil systems of ruggedness and simplicity while still maintaining comparable sensitivity. Such a system should be applicable to epitaxial films on paramagnetic substrates but with the same general limitations discussed for torque magnetometry in Section 9.

13.2 Magneto-Optical Methods

Kurtzig and Hagedorn (Ref.188) have described a visual technique in which a variable field is applied in the plane of the sample. The Faraday contrast between adjacent domains decreases as the field is increased and the field at which the contrast is undetectable is taken as H_A. The author claims 10% accuracy for this method. They report results for both CVD and LPE grown films including the observation that annealing at temperature in excess of 1200°C removes essentially all of this non-cubic anisotropy of LPE films but does not affect the (strain induced) non-cubic anisotropy of CVD films. This visual method is not entirely satisfactory in that the rotation of magnetization into the hard direction is a gradual function of applied field without a well defined visual cutoff. In addition saturation of the sample by a small normal component of the applied field also leads to loss of contrast, and could be misinterpreted as H_A, although it is true that in this case the two domain types will not maintain equal areas. A more quantitative approach is desirable.

Such a method has been developed by Shumate (Ref. 47 and 40). (See also reference 39). It involves applying a field H_x in the plane of the sample, once again, with the addition of an alternating field H_z normal to the sample. As long as domain walls are present they move in synchronism with this alternating component (providing a domain wall motion term to the susceptibility) and their motion is

readily detected using a silicon or photomultiplier detector and lock-in amplifier. Once the walls have been eliminated a significant spin susceptibility remains (the spins being readily turned from the hard direction) which gradually falls to zero as the in-plane field is increased further. It is convenient to add provision for a DC component to H_z - H_z(DC) (normal to the sample) by use of a suitable power supply for the coil which provides the alternating field. Such a system is shown schematically in Fig. 21a.

At this point there are at least two ways to determine H_A from the system output. In the approach favored by Shumate, H_z(DC) is adjusted to yield saturation of the sample. This eliminates the domain walls and leads to zero signal until H_x reaches approximately H_A when the spin susceptibility reappears as shown in Figure 21, curve The peak in this curve is then identified as $H_A - 4\pi M_s$, when consideration is given to the shape anisotropy or demagnetizing factor of these thin films. The field at which this peak occurs is, in fact, a function of the strength of H_z(DC) as shown in the figure. Shumate (Ref. 189) has calculated a correction curve which takes account of this effect and should be available shortly. The present authors, as an alternative to this correction, adjust H_z(DC) until the wall susceptibility contribution extends to the maximum H_x. This approach amounts to using H_z(DC)

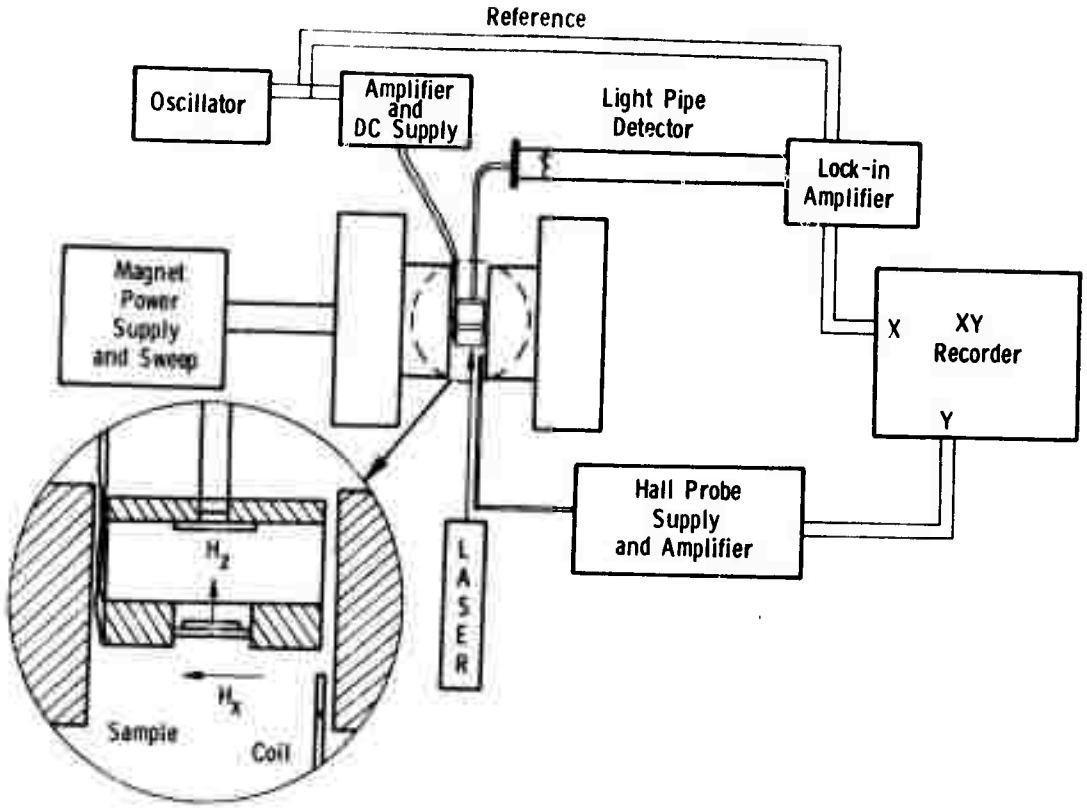

Figure 21a

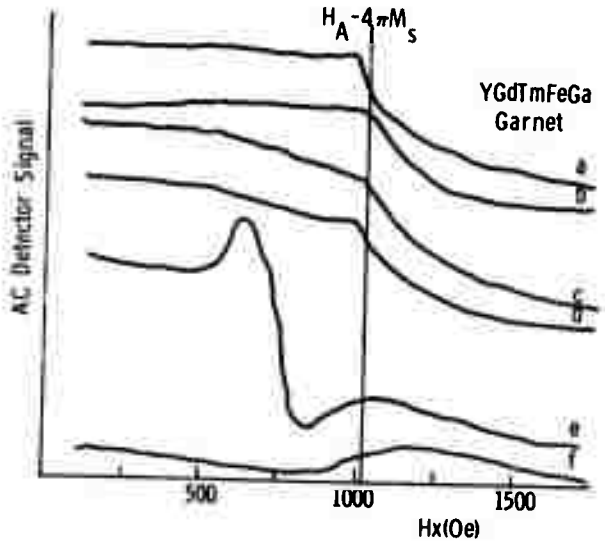

Figure 21b

Figure 21. Anisotropy measurement system (a) and typical data curves. The curves correspond to the following values of H_z (in Oe): a -50, b -17, c 0, d +17, e +56, f +90.

to make small adjustments in the total field direction until that direction coincides with the crystalline hard direction. The maximum in-plane field which still yields wall motion is then taken as $H_A - 4\pi M_s$. Figure 21 shows several curves taken at different values of H_z(DC) by this technique. Three or more such curves are required to pinpoint $H_A - 4\pi M_s$, but these can be obtained rapidly due to the substantial signal available. Partly because of uncertainties in interpretation this method is estimated to yield H_A to $\pm$ 10% but is felt to be the best routine method for its determination in epitaxial thin films at the present time. If the work of Shumate (Ref. 189) removes this interpretational uncertainty, accuracy of $\pm$ 3% seems quite possible. Shumate (Ref. 40) has also used this technique to study the in-plane anisotropy of magnetic bubble films, thereby further extending the usefulness of this method. With possible minor modifications in the future it appears to be by far the most convenient approach to the study of anisotropy in films for bubble devices.

14. COERCIVITY

The coercivity, H_c, is the field in excess of the equilibrium value which is required to cause a domain wall to move, i.e., one half of the hysteresis loop (M vs. H) width. As such it represents an energy dissipation mechanism to be held to a practical minimum. It is well known that in most magnetic materials the hysteresis loops for small field excursions are not ideal parallelograms in which no change in M occurs until the major hysteresis loop is intersected. Rather, the minor loops continue to exhibit decreasing slope near H=0 as the extent of the excursions is reduced. The magnetic bubble materials are rather well behaved in this respect but such effects do make the coercivity a somewhat nebulous parameter.

14.1 Full Hysteresis Loop Methods

Historically the coercivity has been measured as the half width of the full hysteresis curve, i.e., the M vs. H loop which extends to saturation in both positive and negative applied field directions. Such a hysteresis curve has been presented in Figure 16 for a bubble garnet and similar curves have been published by C. D. Mee (Ref.104and105) and others (Ref.190,191, and192). All of these references employed the Faraday effect as discussed in Section 7 and elsewhere (Ref.193,194, and103). In addition, several of the methods discussed for the measurement of magnetization (Section 9) will yield hysteresis curves and a measure of

the coercivity. These include mutual induction effects (Ref.195), torque magnetometry (Ref. 93) and vibrating sample magnetometry (Ref.179). The ballistic measurement of the applied field required to yield zero net magnetization has also been used (Ref.196). However, the Faraday effect remains the best method for the measurement of the hysteresis loop and, from it, the coercivity for thin, optically transparent samples.

14.2 Microscopic Coercivity Methods

Bobeck, et al (Ref.153) have proposed a technique which is, once again, closely related to the bubble domain phenomenology. They make use of the repulsive interaction between bubbles to yield a measure of the smallest force required to move a bubble. This is done by bringing two bubbles together (by means of a magnetic probe, for example) and then allowing them to repel to the relaxed distance, ℓ_{12}. By approximating the field of a bubble as that of a dipole at the interaction distance a coercivity is derived as

$$\frac{H_c}{4\pi M_s} = \frac{3\pi r_o^3 h}{8\ell_{12}^4} \qquad (14\text{-}1)$$

where r_o is the bubble radius. The difficulties in using this technique for accurate measurements in materials where the bubble diameter is small are immediately evident from the high powers to which the microscopic distances are raised.

Ignoring the relatively small uncertainty in h, standard error propagation yields

$$\Delta H_c/H_c = \left[9(\Delta r_o/r_o)^2 + 16\ (\Delta \ell_{12}/\ell_{12})^2 \right]^{1/2} . \quad (14\text{-}2)$$

Thus these uncertainties are amplified by these large exponents making the technique impractical when r_o and ℓ_{12} cannot be measured to high precision.

Another approach to the coercivity on a microscopic scale was developed by Kurtzig (Ref. 50) and discussed in connection with defect detection in Section 7. It is based upon the generation of a straight wall by a gradient field and, in the garnets, suffers from the difficulties already described.

The Bobeck reference (Ref.153) mentions another approach to coercivity on a microscopic scale which is a more workable alternative for the garnets. If any of the bubble translation methods for the measurement of mobility are used at low pulsed gradient fields a limit can be found below which no bubble motion takes place. Thus, for example, in Equation 11-12 the coercivity is determined by extrapolating the velocity vs. pulse current curve to v=0 (at I_o) and then solving the resulting equation to yield

$$H_c = \frac{0.2\pi I_o d}{D^2} . \quad (14\text{-}3)$$

Such a method is far less sensitive to the uncertainties in

bubble diameter and is accomplished at the same time that the mobility is being determined. This technique for mobility measurement (Ref.158), when used with the superimposed ramp field in order to maintain the field at the bubble constant, is judged to be too complex to be used in routine characterization, unfortunately. For such purposes we recommend the following method for the determination of coercivity with the recommended mobility technique as a separate measurement.

14.3 Partial Hysteresis Loop Method

The hysteresis methods discussed above are somewhat misleading for the purposes of magnetic bubble devices in that the loops, when carried to saturation, are influenced by nucleation processes at the edge of the film and by local defects which may not be in the area of interest. Minor hysteresis loops which do not progress to saturation are a better measure of the local coercivity but the low signal to noise ratio becomes a serious limitation on accuracy. Luff (Ref. 53) Shaw, et al (Ref. 39) and Shumate (Ref. 40) have used an AC technique which takes advantage of the narrow band capabilities of the lock-in amplifier. In it the domain walls are driven by an alternating bias field and the modulated Faraday signal detected using a photomultiplier and the lock-in amplifier. A schematic diagram of the apparatus for this measurement is shown in Figure 22. The resulting signal is plotted versus the

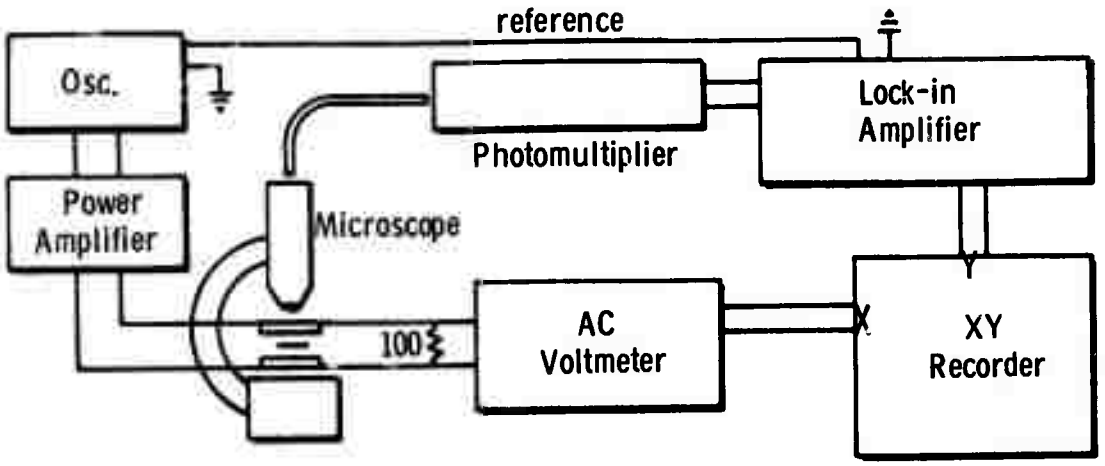

Figure 22a

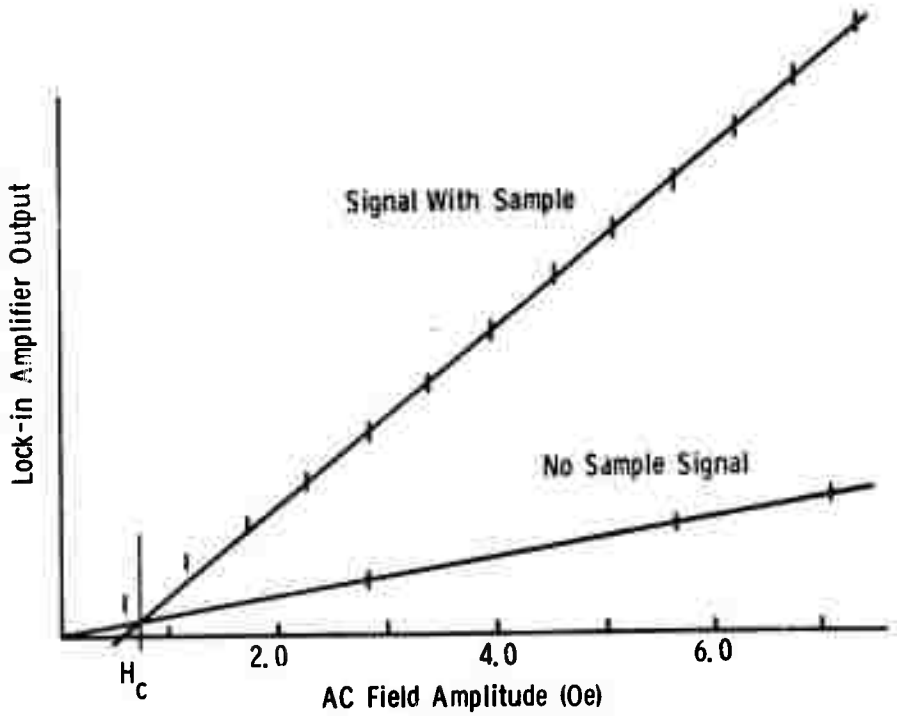

Figure 22b

Figure 22. Coercivity system

alternating field amplitude. If the hysteresis loops were ideal parallelograms in which no change in M occurred across the top and bottom of the loop, then the lock-in amplifier signal would fall to zero at an alternating field amplitude of H_c and remain zero for all smaller amplitudes. The typical data of Figure 22 show that this is not quite fulfilled but that a linear portion of the curve is apparent which can be extrapolated to zero lock-in signal to yield H_c. The short vertical lines on this figure are the data points taken by setting the recorder pen down for approximately 10 time constants of the lock-in amplifier filter circuit. The "no sample" curve is similar data taken with no sample in the microscope and results from Faraday rotation in the microscope optics (Ref. 39). Such an effect can be avoided by using laser illumination and avoiding the use of a microscope entirely or by using long working distance optics and a small coil (Ref.155), but cross checks have indicated the present technique is as accurate and it is more convenient to carry it through while the sample is in the microscope for other measurements.

15. MAGNETOSTRICTION COEFFICIENTS

In single crystal magnetic materials the magnetocrystalline anisotropy energy depends on the state of strain of the crystal lattice. When the lattice deforms under the influence of a given stress, the increase in elastic energy induces a change in the anisotropy energy so as to minimize the total energy of the system. The material parameters which characterize this change in anisotropy energy are the magnetostriction coefficients, λ_{100} and λ_{111}. The magnetostriction phenomenon is reciprocal in the sense that the dimensions of the crystal depend on the direction of magnetization relative to the crystal axes. For materials with cubic symmetry, such as the ferrimagnetic garnets, the magnetically induced dimensional change can be expressed as

$$\frac{\Delta \ell}{\ell} = \frac{3}{2} \lambda_{100} \left(\alpha_1^2 \beta_1^2 + \alpha_2^2 \beta_2^2 + \alpha_3^2 \beta_3^2 - \frac{1}{3}\right)$$

$$+ 3 \lambda_{111} \left(\alpha_1 \alpha_2 \beta_1 \beta_2 + \alpha_2 \alpha_3 \beta_2 \beta_3 + \alpha_3 \alpha_1 \beta_3 \beta_1\right), \quad (15\text{-}1)$$

where α_1, α_2, α_3 are the direction cosines of the magnetization direction referred to the cubic axes, and β_1, β_2, β_3 are the direction cosines of the direction in which $\frac{\Delta \ell}{\ell}$ is measured. The change in elastic energy resulting from the crystal dimensional change $\frac{\Delta \ell}{\ell}$ may be regarded as a first order correction

to the anisotropy energy, and as such, adds a term to Equation 13-1. Physically, the significance of Equation 15-1 may be considered in the following light: It may be energetically favorable for the crystal to deform in a given direction, if, as a result, the anisotropy energy is lowered by more than the elastic energy is increased.

Magnetostriction in magnetic bubble materials is important for two primary reasons: 1) In thin layers of ferrimagnetic garnets, magnetostriction has been utilized extensively to induce sufficient uniaxial anisotropy for the material to support magnetic bubble domains (References 3, 35, 197, and 198); 2) local variations in the state of strain of the crystal lattice (for example, near a dislocation, lead to local inhomogeneities in magnetocrystalline anisotropy, and interfere with bubble propagation.

The earliest technique used to measure the magnetostriction coefficients of ferrimagnetic garnets was employed by Callen et al (Reference199) to measure the constants of single crystal YIG. The method utilizes a strain gauge apparatus first employed by Goldman (Reference200) to measure magnetostriction constants of polycrystalline rods and strips. In this technique a thin metallic foil with attached leads is bonded to a magnetic

sample. A similar device is bonded to a dummy ceramic block in close proximity to the first so that both will experience the same temperature and magnetic field environment during measurement. The resistance of the foil gauges as a function of strain has previously been calibrated (usually by the manufacturer, e.g., Budd Company, who then quotes a gauge factor) so that, when the active and the dummy gauges are connected as two legs of a D. C. Wheatstone bridge, resistance changes due to sample strains as small as 10^{-7} can be detected. This strain gauge technique was also used by Iida (Reference201) to measure the magnetostriction coefficients of $Tb_3Fe_5O_{12}$ and $Eu_3Fe_5O_{12}$, by Clark (Reference202) to measure the constants of dysprosium, holmium and erbium iron garnets, by Iida (Reference203) to measure the constants of all of the rare earth iron garnets, by Belov, et al (Reference204) to measure the constants of thulium orthoferrite in the reorientation temperature range, and by Gyorgy, et al (Reference205) to measure several partially substituted Sm orthoferrites. The data of Clark and Iida are not in precise agreement at room temperature, the absolute magnitude of Clark's magnetostriction values being higher in general. Current magnetic bubble literature (Reference 64) quotes Iida's data almost exclusively, but this may be due more to a consideration of where the work was performed (Bell Laboratories) than to accuracy considerations.

Callen, et al (Reference199) points out that magneto-resistance effects in the metallic foil at low temperatures makes strain gauge measurements taken at liquid nitrogen temperature somewhat in error. These authors proposed an alternate measurement technique in which the sample was sandwiched between a metal support plate and an aluminum plated silica disk which served as one plate of a capacitor. A Be-Cu ring placed around the sample served as the other capacitor plate. The whole capacitor assembly was made part of a free-running Hartley oscillator whose frequency was monitored. For small changes in sample length induced by rotating the assembly in a magnetic field, the magnetostriction coefficients are proportional to frequency shift of the oscillator. A strain of 10^{-7} produced a frequency shift of about 10 Hz when operated at 5 MHz. This method eliminates magnetoresistance effects as well as effects due to changes in gauge factor as a function of temperature, but the distributed capacity of the oscillator must be known accurately, and there are the additional bonding problems which arise because of the different thermal expansion coefficients of the sample, support, and capacitor plates.

Another technique for measuring the magnetostriction coefficients, in a sense the reciprocal of the methods discussed thus far, was employed by Petrakovskii (Reference206) to measure the constants of Ga-YIG. This method consists of mounting a single crystal spherical sample in a press which was integral with a specially designed waveguide section. A known amount of stress could be applied to the sample by loading the press with weights. Small shifts in the ferromagnetic resonance peak which resulted from the uniaxial compressive stress were detected by an X-band spectrometer (adapted to fit this purpose) which could resolve shifts of as little as 0.005% in the location of the peak. The advantages of this technique are that only relatively small samples are required ($\approx$ 1 mm), the method is relatively simple to instrument, the measurement results in accuracy comparable to the strain gauge method, and the technique can be automated. On the other hand, only those materials can be measured which exhibit a narrow ferromagnetic resonance line (which many of the ferrimagnetic bubble garnets do not).

All of the techniques discussed are applicable only to bulk single crystal materials, while most present day bubble materials are thin epitaxially grown films which are being stressed by the substrate on which they are grown. The stress

level is generally too poorly known to obtain accurate magnetostriction constant measurements from the shift in the ferromagnetic resonance line as a function of stress. Added to this problem is the fact that most useful garnet materials contain relatively complex mixtures of rare earth and yttrium ions as well as gallium ions partially substituted for iron on tetrahedral sublattice sites. These compositions would have to be grown as bulk single crystals to enable measurement of magnetostriction constants by the strain gauge technique. Giess, et al (Reference198) have discussed a few of the problems involved in attempting to use the bulk single crystal iron garnet magnetostriction coefficients to interpret observations of thin film gallium substituted rare earth iron garnets. As these authors point out, what is normally done is to assume the magnetostriction coefficients in a gallium substituted iron garnet are not diminished by gallium, and that for a mixed rare earth garnet the magnetostriction coefficients are a linear combination of those of the single ion rare earth garnets. The latter assumption probably isn't bad, but the former is almost certainly in error. There really is no accurate way to measure magnetostriction constants in thin films of bubble garnets. Measurements using FMR or the strain

gauge technique should be performed on bulk single crystals having compositions identical to those of the bubble garnet films for which the magnetostriction coefficients are desired.

16. TEMPERATURE EFFECTS

The temperature characteristics of bubble materials are relevant for a variety of reasons, the most important of which relates to the eventual device application in which they may be used. The bubble diameter is a function of all the magnetic parameters which characterize a sample of bubble material, and all of these parameters are functions of temperature. If the operating temperature of a bubble device varies, then, unless careful precautions have been taken, so will the bubble diameter. In the worst case, the change in bubble diameter with temperature will result in bubble collapse or runout at some point in the bubble device.

16.1 Reorientation Temperature Range

In the rare earth orthoferrites, the easy axis of magnetization undergoes a continuous reorientation from the crystallographic c to the a axis in a certain region of temperature known as the reorientation temperature range. This fact along with the non-alterable magnetization and high anisotropy of the orthoferrites eliminated them from consideration as useful bubble domain materials. Because of the drastic nature of the change in anisotropy with temperature in the reorientation range, several methods could be used to measure its onset and its temperature extent. Sherwood, et al (Ref.182) used a torque magnetometer in a variable temperature mode to detect the reorientation temperature

range. Gyorgy, et al (Ref.207) used both variable temperature torque and vibrating sample magnetometers for reorientation range measurements in Sm and Tm orthoferrites. Rossol (Ref.208) made an exhaustive study of the reorientation temperature range in thulium orthoferrite by making visual measurements of domain size and then using the theory of Malek and Kambersky (Ref. 61) to obtain wall energy as a function of temperature. All of these measurement methods have previously been described so no further discussion will be given here.

16.2 Neel and Compensation Temperatures

The temperature at which the transition from ferromagnetic to paramagnetic behavior occurs in magnetic materials is known as the Curie temperature. In ferrimagnetic materials this temperature is also known as the Neel temperature. The rare earth garnets exhibit an additional significant temperature dependent effect. The rare earth and octahedral iron sublattices align antiparallel to the tetrahedral iron sublattice, and the various sublattices have different temperature dependences. As a result, most of the garnets experience a temperature where the oppositely directed sublattice magnetizations cancel, resulting in zero net moment. This temperature is known as the compensation temperature.

The Neel temperature of orthoferrites and garnets has been measured by a variety of techniques nearly all of which involve monitoring the magnetization as the temperature is increased through the Neel temperature. The most cumbersome

in terms of experimental apparatus is the neutron diffraction technique used by Koehler, et al (Ref.209) to measure the Neel temperature of polycrystalline Nd, Ho and Er orthoferrites. These authors discuss the design and operation of their apparatus in an earlier article (Ref.210). Treves (Ref. 92) has done Neel temperature measurements on most of the orthoferrites by torque magnetometer and Mossbauer spectroscopy. Eibschütz, et al (Ref.211) have also measured Neel temperatures in all the orthoferrites by means of the Mossbauer technique with an accuracy estimated to be $\pm$ 1°K. Eibschütz, et al (Ref.212) had previously measured the Neel temperatures of the orthoferrites by differential thermal analysis which relies on a specific heat anomaly at the Neel temperature. Using NiO as a reference, they claimed an accuracy of $\pm$ 2% for those Neel temperature determinations.

The above references represent some of the more unusual approaches to the measurement of Neel and compensation temperatures. In fact, most measurements of these properties in ferrimagnetic garnets have used torque magnetometer and ferrimagnetic resonance measurements as functions of temperature to determine Neel and compensation temperatures in bulk single or polycrystalline garnet materials. The reader is referred to the excellent bibliography following chapter 3 in von Aulock's Handbook of Microwave Ferrite Materials (Ref.213).

The technique used at Monsanto to measure the Neel temperature is a magneto-optical one similar to that

described by Kurtzig, et al (Ref. 65). This method involves the modulation of the Faraday effect by oscillating domain walls which are being driven by an AC bias field. The garnet sample is situated in a heating stage and as the stage temperature is raised to the Neel temperature the Faraday susceptibility drops sharply to zero, allowing a measurement precision of $\pm$ 1°K. This method is rapid, simple and accurate and should become the most widely used technique for determining Neel temperature in the garnets.

A somewhat similar but less accurate technique is to observe the domain pattern visually as the sample temperature is raised to the Neel temperature. In the vicinity of the Neel temperature the domains will disappear. Unfortunately, the contrast is low near the Neel temperature and the exact temperature of the ferrimagnetic to paramagnetic transition is difficult to determine in this way. Accuracies of no more than $\pm$ 5% should be expected with this method.

Epitaxial layers with a highly defected film-substrate interface will spontaneously demagnetize in an array of bubbles when brought down from above the Neel temperature as domains nucleate at every defect as well as at the sample edge. This fact has been used by Hsu (Ref.214) to find the Neel temperature in EuEr iron gallium garnet films. A film previously saturated at room temperature is heated to near the Neel termperature, then cooled and the type

of domain pattern (bubbles or strips) is noted. This procedure is repeated in small temperature increments until the Neel temperature is reached. Unfortunately not only is this method tedious, but in high quality samples of the type required in bubble devices, the film-substrate interface is not defected, and the layer does not spontaneously demagnetize into an array of bubbles. Therefore this technique is not recommended.

16.3 Temperature Variation

It is important to know how the magnetization and/or bubble diameter varies with device operating temperature, as pointed out earlier in this section. The functional dependence of bubble diameter on temperature has been observed visually in most cases (Ref.208and215). Magnetization as a function of temperature can be obtained from any of the techniques of section 9 applied at the temperatures desired. For the magneto-optical techniques, heating stages for microscopes are available from several commercial sources (a Leitz 350°C stage is used at Monsanto) which can be useful above room temperature in this application. A better approach over somewhat more limited range is to employ a thermoelectric heating/cooling device. This device has several advantages: the new equilibrium temperature is attained rapidly, both heating and cooling are accomplished electrically, and it is economical to instrument. The chief disadvantage is that temperature excursions are limted to about $\pm$ 50°C in the region of

room temperature. In most cases, knowledge of bubble bias field and diameter variations in this temperature range along with Neel and/or compensation point data is enough to evaluate the material in question in light of its eventual performance in a device related environment. Temperature dependence of several of the other properties of magnetic bubble films, including characteristic length, domain wall energy, coercivity, and mobility, are also measurable with such a system.

16.4 Thermal Conductivity

One additional thermal characteristic, thermal conductivity, is worth mentioning briefly since it may become important in bubble device packaging. Luthi (Ref.216) measured the thermal conductivity of single crystal YIG at liquid helium temperatures using a standard thermal conductivity apparatus which consisted of carbon resistors for temperature measurement cemented to the rectangular YIG specimen and a Dahlohm resistor cemented to the specimen for heating. One end of the specimen was cemented to a copper bar which was immersed in liquid helium. Luthi's results indicate a thermal conductivity varying from about 6mw/cm°K at 1.5°K up to about 50mw/cm°K at 5°K. An absolute accuracy of 20% is claimed for these data. Douglass (Ref.217), using a nearly identical apparatus, measured the thermal conductivity of YIG over a temperature range from 0.4 to 20°K in the presence of magnetic fields of from 0 to 20K Oe. His data indicates a maximum in thermal conductivity

of approximately 1000 mw/cm°K in the vicinity of 20°K. Douglass' data agree well with those of Luthi (Ref.216) in the common range. Slack and Oliver (Ref.218) have recently published results for several non-magnetic Al and Ga garnets as well as YIG for temperatures between 2°K and 300°K. These authors quote a room temperature thermal conductivity for YIG of 0.09 W/cm°K and an accuracy of about 10% using a refined version of the same apparatus discussed above (Ref.219). In all likelihood, this parameter will vary little from one ferrimagnetic garnet to another, obviating the need for its routine measurement. Sufficient accuracy should be obtained in most instances if the value of thermal conductivity of YIG is used in calculations involving other garnets.

17. OPTICAL PROPERTIES

Optical methods have been discussed as possible means of detection or "read-out" in magnetic bubble memories (Ref.220and221). As Strauss concludes, optical readout is probably not the most attractive method, particularly with the advent of the small bubbles available in garnets. Nevertheless, for the person involved in characterizing such materials optical methods are extremely convenient and because of this, these properties take on considerable interest. In particular, the index of refraction enters the thickness measurement and the Faraday rotation is central to all of the optical study of domain dimensions and behavior. Other optical properties , such as the rare earth spectra, impurity and lattice mode spectra, Kerr effect and Zeeman and Stark spectroscopy, possess some potential usefulness and a great deal of basic literature, but are peripheral to the central theme of this report. As such, they will be given only brief consideration. A third class of optical properties -- those relating to the instruments used in these measurements are very important to the worker in this field but outside of the scope of this report. Some references of a review nature may be helpful, however, and are presented here: Monochromators - (Ref.222), microscopes - (Ref.223), light sources (Ref.224), fiber optics (Ref.225and226) and optical detectors (Ref.227).

17.1 Refractive Index

The first measurements of the index of refraction of the garnets involved the measurement of reflectivity (Ref.228). Solving equation 5-2 for n yields

$$n = \frac{1 + \sqrt{R}}{1 - \sqrt{R}} \qquad (17\text{-}1)$$

where R is the fraction of the incident light intensity which is reflected and the equation considers only one sample surface. In this reference natural single crystal faces were used and later surfaces presumably did not contribute to the reflected beam. The resulting index for YIG and ErIG was quoted at 2.2 $\pm$ 0.2 in the 0.6 to 1.0μm wavelength range. Geometric and surface quality effects tend to limit the accuracy of this approach and, in addition, there is always the suspicion that the surface layer from which reflection takes place may not be representative of the bulk material. For the thin samples of current interest here, there are the additional difficulties of reflection and interference from the other surfaces present.

Johnson and Walton (Ref. 41) measured the infrared index for YIG and $Y_{1.5}Gd_{1.5}Fe_5O_{12}$ by forming prisms from flux-grown crystals and measuring the deviation of the beam through them. As discussed in optics texts (Ref.229) one normally adjusts the prism for minimum deviation of the refracted beam in which case

$$n = \frac{\text{Sin } (\delta_{min} + \alpha)/2}{\text{Sin } \alpha/2} \qquad (17\text{-}2)$$

where δ_{min} is the minimum angle through which the incoming beam is bent by the prism and α is the angle between the two faces of the prism. These authors present values of n between 1.4μm (n=2.209) and 5.5μm (n=2.103) with a mean deviation of 0.003. No detectable difference was found between the two garnet compositions.

Grant (Ref. 42) published reflectivity data for YIG and YGG over the wavelength range 6000Å to 1700Å. Due to surface and alignment difficulties, however, his absolute values are uncertain to ~ 30% so that the index values resulting from Equation 17-1 are not directly useful. Unfortunately, the wavelength range covered by Johnson and Walton does not permit a sufficiently reliable extrapolation into Grant's range to fix his absolute values much better although it definitely indicates that they are too low. When used with the index values of Roman, et al at 6328Å (see below), the data of Grant do serve to indicate the further growth in n at shorter wavelengths.

Kahn, et al (Ref.230) calculated the real and imaginary parts of the index of refraction using Grant's reflectivity results and their own Kerr effect values. The absolute values are subject to the uncertainties already mentioned in connection with Grant's data.

Grismore and Rhodes (Ref.231) have reported reflectivity

measurements on Gd and Tb iron garnets in the energy range 2 to 5.5eV (6200 to 2260Å wavelength). They employed light polarized in the plane of incidence and made measurements at two angles of incidence, ϕ, in order to determine both the real part, n, of the index of refraction and the imaginary part, k, (sometimes called the extinction coefficient) which becomes significant in this strongly absorbing range. For this polarization the reflectivity is given by

$$R = \frac{(n - \sec\phi)^2 + k^2}{(n + \sec\phi)^2 + k^2} \qquad (17\text{-}3)$$

The computed values of n for TbIG show some structure but are approximately 2.15 ± 0.05 between 2 and 3eV. Unfortunately they did not compute n and k for GdIG below 3eV and, indeed, it would appear that the very low reflectivities measured at $\phi = 70°$ for this compound would require unreasonably large n values at 2eV (~ 2.7). Neglecting absorption and using only their value of R at $\phi = 20°$, we compute $n = 2.42$ at 2eV. Their curve indicates $n = 2.52$ at 3eV making our value at lower energy appear reasonable. This difference in n between TbIG and GdIG indicates that significant errors may result from assuming a constant n for all garnet compositions. A systematic study of the variations with composition would be of considerable value.

The Brewster angle method employed by Roman, Spiwak, and Baron (Ref. 36) makes use of the polarizing effect upon reflection at the air-garnet film interface. Theory shows that light polarized in the plane of incidence has zero reflectivity at a certain angle of incidence. This angle, ϕ_B, measured from the normal to the reflecting surface is known as Brewster's angle and is given by (Ref.232)

$$\tan \phi_B = n \qquad (17\text{-}4)$$

for light incident from vacuum (or air to ~ 0.03% accuracy) onto a surface of index n. Thus, an accurate measurement of the angle corresponding to this zero of reflected light intensity yields an accurate measure of n. The use of a laser, with its highly collimated beam, aids in improving the accuracy of the measurement. For the case of films on substrates of different index and for thin samples generally, the measurement is complicated by the presence of the reflected beam from the other surfaces. In general these will add a component which will not go to zero at the Brewster angle and may, in fact, give rise to interference effects. These will go to zero, of course, at the Brewster angle. For a thick film in the visible (a region of significant absorption, see below), the proper angle will correspond to a minimum in the reflected intensity of the correct polarization.

An alternative approach, due to Abeles (Ref.233and234) takes advantage of the zero reflectivity and the fact that

this effect is reciprocal (i.e. also occurs for light progressing along the same path from within the sample). For a film thin enough to neglect absorption, the angle ϕ_B above can be found as that angle at which the substrate with film gives the same reflected intensity as a similar bare substrate. Both approaches to the measurement of the Brewster angle are subject to the possible criticism that they only sample the surface region. However, when used in combination they appear to yield the best method for the measurement of refractive index of magnetic bubble materials.

Current refractive index measurements at Bell Labs are being made by W. J. Tabor on bulk samples of the same compositions as those of interest for films (Ref.155). The method employed is very closely related to the thickness measurements of films already discussed. The samples are prepared with two very flat opposite faces slightly non-parallel to one another. The interference fringes produced in monochromatic light together with the difference in thickness across the sample are sufficient to yield the index of refraction. For N interference fringes between points of thickness difference, Δh, the index is given as

$$n = \frac{\lambda N}{2\Delta h} \qquad (17\text{-}5)$$

This method is also applicable to films, of course, when Δh can be obtained with sufficient accuracy by some other means.

Microscopic measurements on broken or polished edges of a tapered thick film is such a method. For typical films, however, the Brewster angle method appears preferable.

The same techniques described here for the garnets are applicable to the orthoferrites without further complication. Infrared reflectivity data have been reported by Antonov, et al (Ref.235) who analyzed them to yield $n = 2.35 \pm 0.05$ at $\lambda = 2.0\mu m$. This is approximately 0.16 higher than YIG at the same wavelength. More detailed analysis of erbium orthoferrite has been carried out using the Kerr effect (see below) by Jung, (Ref.236) based upon theoretical work of Argyres (Ref.237) and others (Ref.238 and 239). The results are presented as the real and imaginary parts, ε_1 and ε_2, of the dielectric constant over the range 3600 to 7000Å. Analyzing these on the basis of the Equations (Ref.240)

$$n^2-k^2 = \varepsilon_1 \quad \text{and} \quad nk = \varepsilon_2 \qquad (17\text{-}6)$$

one finds $n = 2.50$ at 5000Å and $n = 2.32$ at 3900Å.

17.2 Faraday Effect

In the case of the orthoferrites the measurement of Faraday rotation of the plane of polarization is complicated by the simultaneous presence of birefringence in the crystal. This causes the plane of polarization to oscillate as the wave progresses through the crystal rather than turning unidirectionally as it would under the influence of the Faraday effect alone. The analysis of this situation is sufficiently complex and excellent discussions so readily available that it would be pointless to try to condense them here. Some of these discussions are given in references 241,242,243,244, and245. The second of these indicates that all of the rare earth orthoferrites, with the exception of $SmFeO_3$ (which has a reorientation temperature above room temperature) follow very nearly the same curve of intrinsic Faraday rotation *vs.* wavelength in the range $0.55\mu m < \lambda < 1.8\mu m$.

The garnets are basically cubic and therefore do not exhibit the phenomenon of birefringence in the usual sense. However, Dillon (Ref.246and247), in his initial reports of optical transparency in the garnets, noted a magnetic birefringence for light traveling perpendicular to the direction of the magnetization. (See also ref.248) While this effect is useful for pathologic samples with the easy axis in the plane, it will not concern us for device quality magnetic bubble films. Birefringence

associated with growth induced anisotropy has also recently been reported by Dillon, et al (Ref.249).

Dillon (Ref.246) also made initial measurements of the Faraday rotation of several iron garnets for light traveling along the magnetization direction and reported those for YIG in the 7700 to 5300Å range. The results show some broad line structure on a generally rising curve as λ decreases (800 to 4000 degrees /cm over this range). In this case the measurement consists simply of determining the angle between the extinction condition with and without the sample in the beam (for a single domain area of the sample). A separate measurement of the thickness is required to yield the Faraday rotatory power quoted above. For the polished platelets used by Dillon very standard techniques for this thickness measurement sufficed.

Since these initial reports a number of Faraday studies in the garnets have been reported. Krinchik and Chetkin (Ref.228and250) have reported results on yttrium-, erbium-, and holmium iron garnets at 77°K and 300°K from less than 1μm wavelength to ~ 8μm. These show a wavelength independent range beyond 5μm with rising rotation and some rare earth associated structure at shorter wavelengths. Johnson and Tebble (Ref.251and252) have reported results in the 1 to 5μm wavelength range for the iron garnets of Y, Y-Gd, Gd, Tm, Dy and have derived g factors for the ions involved. The experimental system involved recording

the light output as a function of polarizer angle near extinction as described by Austin (Ref.253).

LeCraw, et al (Ref.254) were concerned with the ratio of Faraday rotation to light absorption in the near infrared for YIG, determining a value of 800 degrees/decibel loss. MacDonald, et al (Ref.255) indicate that, for a very thin polycrystalline GdIG film, this value is less than unity. Dillon (Ref.256) has reviewed the properties of a number of magnetic materials for potential applications as Faraday rotators, modulators, lasers, etc. Almasi (Ref.221) has considered the practicalities of magneto-optic display and bubble sensing systems for $DyFeO_3$, YIG and Ga-YIG, and $PbFe_9Al_3O_{19}$. Further Faraday effect data have been given for Ga-YIG by Matthews, et al (Ref.257) and for GdIG films by Sawatzky and Kay (Ref.258). Sawatzky and Horne (Ref.259) have described a highly automated system for the direct recording of Faraday rotation and coercivity which employs sampling techniques at various points on the optical hysteresis loop.

17.3 Other Optical Properties

The Kerr effect - the transformation of plane polarized light upon reflection into either elliptically polarized light or into a different plane of polarization - is of some usefulness in observing domain patterns. The amount of change in the incident light is very much smaller, however, than in the Faraday effect so that the latter

will doubtless continue to be used wherever possible. A few references on the Kerr effect in magnetic bubble materials are: orthoferrites - References 260 and 230; garnets - References 230 and 261. These papers contain references to the relevant experimental techniques.

Optical and magneto-optical absorption studies in the orthoferrites and garnets have been actively pursued since the first reports of optical transparency. They provide considerable insight into the ionic and magnetic structure of these crystals. The transmitted light intensity is governed by the law $I = I_0 \exp(-\alpha x)$ where I_0 is the incident intensity (less that part which is reflected), I is the intensity after a distance x is traversed in the sample, and α is the absorption coefficient. Except for line structure associated with specific rare earth ions, all of the garnets display basically the same wavelength dependence as shown in Figure 23. The apparatus and methods involved are generally those which are standard for all forms of spectrometry, frequently making use of commercially available spectrometers with facilities for dual beam operation and chopped light beam lock-in amplification for noise suppression. Some representative publications dealing with material of interest to the magnetic bubble worker are: orthoferrites - References 262, 263, and 264; garnets - References 265, 266, 267, 268, 269, 270, and 271.

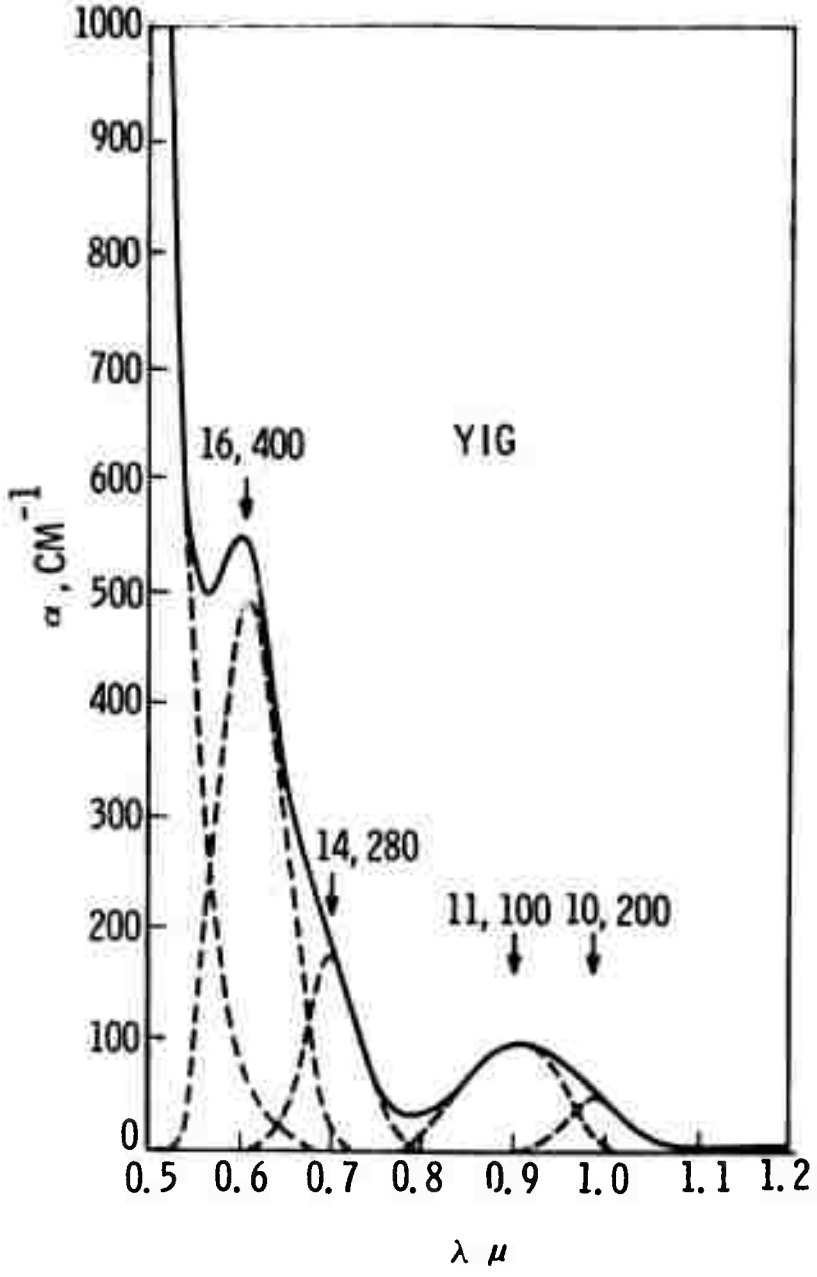

Figure 23. Optical absorption coefficient for YIG in the visible and near-infrared. After Wood, ref. 270.

18. ELECTRICAL PROPERTIES

The magnetic garnets and orthoferrites are highly insulating crystals having a resistivity in excess of 10^{12} ohm-cm when pure. Wood and Remeika (Ref.272) studied the effect of Ca doping (leading to compensating Fe^{4+} ions) and Si doping (leading to Fe^{2+} ions) on optical and electrical properties of YIG. In both cases the resistivity dropped to $\sim 10^{6}$ ohm cm for 0.002 impurity atoms per formula and leveled off at $\sim 10^{5}$ ohm cm for higher concentrations. In addition, they found that Fe^{4+} corresponds to p-type conductivity and Fe^{2+} to n-type by means of the thermoelectric effect. Thus the electrical properties of garnets are demonstrated to be potentially useful as a semi-quantitative check of purity. Similar measurements of Sn doping of Gd and Tm orthoferrites (Ref.264) show very similar pure resistivities with decreases to $\sim 10^{4}$ ohm cm with doping.

Experimental precautions in the measurement of resistivity of such insulating materials have been discussed many times in the literature (Ref.273,274, and275). They consist primarily of 1) avoiding shunting paths due to surface effects and instrumentation, 2) avoiding spurious effects of contact resistance and, 3) avoiding error in the measurement of the very small currents involved. For the garnet films on more massive substrates there are the additional questions of the contribution of the substrate and the interfacial layer to the total conductivity. When all of this is considered it

appears unlikely that electrical measurements will find much use in the characterization of magnetic bubble materials.

Other electrical measurements which have been carried out in bubble materials include photoconductivity in GdIG (Ref.276), the generation of bubbles by resistive heating (Ref.277) and the detection and study of a current controlled negative resistance in Si doped YIG (Ref.278 and279). These last measurements also indicate the Si impurity provides an electrically active level with an activation energy of 0.3eV.

19. SUMMARY

In this report we have presented the results of a study of the physical properties of magnetic bubble materials. Discussions of the known methods for measuring these properties have been given, and recommendations, wherever possible, as to which measurement techniques seem "best" at this time have been made. In order to recommend a "best" technique among all those which have been cited in the literature for measuring a given material parameter, one really needs to have had experience with all the techniques. Lacking that, we have considered such things as the simplicity, accuracy, and economy of the various methods along with our experience with some of the characterization techniques in making recommendations as to which methods are "best". Not all of the physical properties of bubble materials discussed are felt to be worthy of routine characterization. The report has been written from the general viewpoint of someone just beginning to set up a bubble garnet materials characterization facility. In those laboratories where a strong capability already exists in a certain important measurement technique, such as ferrimagnetic resonance for example, the "best" technique for measuring, say, anisotropy field, at that laboratory, may not be the technique which we recommend here. The results of this study are summarized briefly in table III. The reader is directed to the appropriate section of this report for a more detailed discussion.

TABLE III
SUMMARY OF RECOMMENDED CHARACTERIZATION TECHNIQUES

Material Property	Frequency of Measurement*	"Best" Measurement Technique †
Substrate Composition	S	Electron Microprobe
Film Composition	S	Electron Microprobe
Substrate Lattice Constant	S	X-Ray Diffraction from High Index Planes
Film-Substrate Lattice Mismatch	S	X-Ray Diffraction from High Index Planes
Substrate Defects	R	Etching and Microscopic Examinations
Film Defects	R	Magneto-Optical Scanning in an Oscillating Bias Field
Film Thickness	R	Interference of Reflected Light
Thickness Variations	R	Photograph in Monochromatic Light
Characteristic Length	R	Strip Domain Period plus Thickness
Magnetization	R	Characteristic Length plus Collapse Field
Wall Energy	R	Derive from Characteristic Length and $4\pi M_s$
Wall Dynamics	R	Strip Domain Step-Field Response
Anisotropy	S	AC Magneto-Optical Response in Crossed Fields
Coercivity	S	Lock-in Detection of Partial Hysteresis Loop

TABLE III (Cont.)

SUMMARY OF RECOMMENDED CHARACTERIZATION TECHNIQUES.

Material Property	Frequency of Measurement*	"Best" Measurement Technique †
Magnetostriction Coefficients	I	Strain Gauge Technique on Bulk Samples
Neel & Compensation Temperatures	S	Magneto-Optical: Wall Susceptibility vs. Temp.
Temperature Variations	S	Themoelectric Microscope Stage
Thermal Conductivity	N	Use Literature Value for YIG
Index of Refraction	I	Brewster Angle in Monochromatic Light
Faraday Rotation	N	Use Literature Values
Electrical Conductivity	N	See Discussion in Section 18

* R: Routine Measurement
S: Measurement on Selected Samples
I: Infrequent Measurement
N: No Measurement Should be Made

† See Discussion of Section 19

REFERENCES

1. M. Robinson, A. H. Bobeck, and J. W. Nielsen, "Chemical Vapor Deposition of Mangetic Garnets for Bubble-Domain Devices," IEEE Trans. Mag., p. 464, September 1971.

2. H. J. Levinstein, R. W. Landorf, and S. J. Licht, "Rapid Technique for the Heteroepitaxial Growth of Thin Magnetic Garnet Films," IEEE Trans. Mag., Volume MAG-7, p. 470 (1971).

3. J. E. Mee, G. R. Pulliam, J. L. Archer, and P. J. Besser, "Magnetic Oxide Films," IEEE Trans. Mag., Volume MAG-5, p. 717 (1969).

4. L. S. Birks, Electron Probe Microanalysis, Interscience Publishers, New York (1963).

5. A. E. Paladino and B. D. Roiter, "Czochralski Growth of Yttrium Gallium Garnet," J. Amer. Cer. Soc., 49, 51 (1966).

6. G. H. Morrison, Editor, Trace Analysis, Physical Methods, Interscience Publishers, New York (1966).

7. W. W. Meinke and B. F. Scribner, Editors, "Trace Characterization, Chemical and Physical," National Bureau of Standards Monograph 100, U. S. Government Printing Office, Washington, D. C. (1967).

8. M. S. Wang, W. T. Cave, and W. S. Coakley, Chapter 8 - Qualitative and Semiquantitative Analysis, E. L. Groves, Editor, "Analytical Emission Spectroscopy," Marcel Dekker Inc., New York (1972).

9. A. I. Braginski, T. R. Oeffinger, and W. J. Takei, "Compositional Variation in YIG Films," to be published.

10. C. D. Brandle, D. C. Miller, and J. W. Nielsen, "The Elimination of Defects in Czochralski Grown Rare-Earth Gallium Garnets," J. Cryst. Growth, 12,195 (1972).

11. B. D. Cullity, Elements of X-Ray Diffraction, Addison-Wesley Publishing Company, Inc., Palo Alto, California (1967).

12. E. D. Pierron and J. B. McNeely, "Precise Cell Parameters of Semiconductor Crystals and Their Applications," Adv. X-Ray Analysis 12, 343 (1969).

13. D. M. Heinz, J. L. Archer, P. J. Besser, P. E. Elkins, B. J. Huffman, J. E. Mee, L. A. Moudy, and L. R. Tocci, "Single Crystal Orthoferrites for Memory Applications," Technical Report ECOM-0258-2, February (1972) p. 24.

14. L. K. Shick, J. W. Nielsen, A. H. Bobeck, A. J. Kurtzig, P. C. Michaelis, and J. P. Reekstin, "Liquid Phase Epitaxial Growth of Uniaxial Garnet Films, Circuit Deposition and Bubble Propagation," Appl. Phys. Letters, Volume 18, pp. 89-91 (1971).

15. S. Geller, G. P. Espinosa, and P. B. Crandall, "Thermal Expansion of Yttrium and Gadolinium Iron, Gallium and Aluminum Garnets," J. App. Cryst., 2, 86 (1969).

16. W. D. Kingery, Property Measurements at High Temperatures, John Wiley and Sons, Inc., New York (1959), p. 136.

17. J. E. Mee, P. J. Besser, P. E. Elkins, H. L. Glass, and E. C. Whitcomb, Investigation of Single Crystal Ferrite Thin Films, NASA CR-112012 Report, Contract No. NAS12-522, p. 56.

18. P. Chaudhari, "Defects in Garnet Films Suitable for Magnetic Bubble Domain Devices," Paper 10.3, International Magnetics Conference, Kyoto, Japan, April 1972, and to be published.

19. M. Born and E. Wolf, Principles of Optics , MacMillan Company, New York (1959).

20. E. W. Sucov, "Evaluation of Specially Grown Ruby Laser Rods," Appl. Opt. 4, 1107 (1965).

21. R. F. Belt, "YAG - A Versatile Host," Laser Focus Magazine, April 1970.

22. R. C. Linares, "Growth of Garnet Laser Crystals," Solid State Comm., 2, 229 (1964).

23. O. H. Nestor, Production Engineering Measure for Ruby Laser Rods - Final Report, Contract No. DA-36-039-AMC-06168(E), June 28, 1965-October 23, 1967.

24. D. C. Miller, "Defects in Garnet Substrates and Epitaxial Magnetic Garnet Films Revealed by Phosphoric Acid Etching," Paper 5, Spring Meeting - Electrochemical Society, Houston, Texas, May 1972.

25. A. R. Lang, "Direct Observation of Individual Dislocations by X-Ray Diffraction," J. App. Phys., 29, 597 (1958).

26. V. K. Bonse, M. Hart and J. B. Newkirk, "X-Ray Diffraction Topography," Adv. X-Ray Analysis, 10, 1 (1967).

27. J. E. Mee, P. J. Besser, P. E. Elkins, H. L. Glass, and E. C. Whitcomb, Investigation of Single-Crystal Ferrite Thin Films, Final Report, NASA Contract NAS12-522, CR-112012 (1971).

28. H. L. Glass, "X-Ray Double Crystal Topography of Epitaxial Magnetic Bubble Domain Garnets," Mat. Res. Bull., 7, 385 (1972).

29. A. A. Thiele, "The Theory of Cylindrical Magnetic Domains," Bell System Tech. J. 48, 3287 (1969).

30. A. A. Thiele, "Theory of the Static Stability of Cylindrical Domains in Uniaxial Platelets," J. Appl. Phys., 41, 1139 (1970).

31. A. A. Thiele, "Device Implications of the Theory of Cylindrical Magnetic Domains," Bell System Tech. J. 50, 725 (1971).

32. A. H. Bobeck, R. F. Fischer, and J. L. Smith, "An Overview of Magnetic Bubble Domains Material-Device Interface," C. D. Graham, Jr. and J. J. Rhyne, Editors, Magnetism and Magnetic Materials-1971, Amer. Inst. Phys., New York (1972), p. 45.

33. J. E. Mee, P. J. Besser, and F. A. Pizzarello, Epitaxial Growth of Ferromagnetic Garnets, Technical Report AFAL-TR-70-194 Air Force Avionics Lab.

34. D. M. Heinz, P. J. Besser, and J. E. Mee, "Bubble Domains in CVD Films of Gallium-Substituted Erbium Iron Garnet," Magnetism and Magnetic Materials 1971, p. 96.

35. D. M. Heinz, P. J. Besser, J. M. Owens, J. E. Mee, and G. R. Pulliam, "Mobile Cylindrical Magnetic Domains in Epitaxial Garnet Films," J. Appl. Phys. 42, 1243 (1971).

36. B. J. Roman, R. R. Spiwak, and S. A. Baron, "Epitaxial Garnet Thickness Determinations from Near Infrared Interferometry," Bell Laboratories Internal Memorandum of May 25, 1971.

37. F. A. Jenkins and H. E. White, Fundamentals of Optics, Second Edition, McGraw-Hill, New York (1950), p. 254.

38. A. Vasicek, "Optics of Thin Films," (North-Holland, Amsterdam, 1960).

39. R. W. Shaw, R. M. Sandfort, and J. W. Moody, Magnetic Bubble Materials: Initial Characterization Report, Technical Requirement No. 1533, ARPA Order 1999, Contract No. DAAH01-72-C-0490.

40. P. W. Shumate, Jr., "Techniques for Evaluating Magnetic Bubble Materials," Paper 2, Spring Meeting - Electrochemical Society, Houston, Texas, May 1972.

41. B. Johnson and A. K. Walton, "The Infrared Refractive Index in Garnet Ferrites," Brit. J. Appl. Phys., 16, 475 (1965).

42. P. M. Grant, "Reflectivity of YIG and YGaG: Observation of Charge Transfer and Crystal Field Transitions," Appl. Phys. Letters, 11, 166 (1967).

43. R. C. Linares, "Epitaxial Growth of Narrow Linewidth Yttrium Iron Garnet Films," J. Crystal Growth, 3, 443 (1968).

44. A. J. Kurtzig and J. R. Patel, "Interaction of Magnetic Domain Walls and Individual Dislocations," Phys. Letters, 33A, 123 (1970).

45. T. L. Felmlee and R. Hiskes, Magnetic Rare-Earth Compounds, Final Technical Report. Contract No. DAAH01-70-C-1106, Program Code No. OD10 Advanced Research Project Agency, June 1971, p. 70.

46. E. A. Giess, D. C. Cronemeyer, L. L. Rosier, and J. D. Kuptsis, "Orthoferrite Crystal Flux-Growth Morphology and Perfection Effects," Mat. Res. Bull. 5, 495 (1970).

47. P. W. Shumate, Jr., "Magneto-Optic Measurement Techniques for Magnetic Bubble Materials," IEEE Trans. Mag., 7, 586 (1971).

48. R. A. Burmeister, T. L. Felmlee, and R. Hiskes, Magnetic Rare-Earth Compounds, Semiannual Technical Report, Contract No. DAAH01-70-C-1106, Program Code No. OD10, Advanced Research Project Agency, December 1970.

49. Reference 45, p. 64.

50. A. J. Kurtzig, "Interaction of Magnetic Domain Walls with Twin and Grain Boundaries in Orthoferrites," IEEE Trans. Mag., Volume MAG-6, 497 (1970).

51. J. W. Nielsen, "Properties and Preparation of Magnetic Materials for Bubble Domains," Metall. Trans., 2, 625 (1971).

52. F. B. Hagedorn, "Instability of an Isolated Straight Magnetic Domain Wall," J. Appl. Phys., 41, 1161 (1970).

53. P. P. Luff, private communication.

54. P. J. Shumate, Jr., "An Operational Method for Locating and Mapping Imperfections in Single Crystal Platelets of Rare-Earth Orthoferrites," J. Appl. Phys., 42, 1274 (1971).

55. V. I. Nikitenko, L. M. Debukh, S. Sh. Gendelev, and N. G. Shcherbak, "Possibility of Direct Investigation of the Influence of Dislocations on the Processes of Magnetization of Yttrium Iron Garnet Crystals," JETP Lett., 8, 288 (1968).

56. J. E. Geusic, H. J. Levinstein, S. J. Licht, L. K. Shick, and C. D. Brandle, "Cylindrical Magnetic Domain Epitaxial Films with Low Defect Density," Appl. Phys. Letters 19, 93 (1971).

57. R. Hiskes, Magnetic Rare-Earth Compounds, Semiannual Technical Report, Contract No. DAAH01-71-C-1259, Program Code No. OD10, Advanced Research Projects Agency, February 1972.

58. F. B. Hagedorn, W. J. Tabor, J. E. Geusic, H. J. Levinstein, S. J. Licht, and L. K. Shick, "Cylindrical Magnetic Domain Epitaxial Film Characterization: Device and Growth Implications," Appl. Phys. Letters 19, 95 (1971).

59. D. C. Fowlis and J. A. Copeland, "Rapid Method for Determining the Magnetization and Intrinsic Length of Magnetic Bubble Domain Material," C. D. Graham, Jr. and J. J. Rhyne, Editors, Magnetism and Magnetic Materials-1971 , Amer. Inst. Phys., New York (1972), p. 240.

60. R. W. Shaw, D. E. Hill, R. M. Sandfort, and J. W. Moody, "Determination of Magnetic Bubble Film Parameters from Strip Domain Measurements," Bull. Am. Phys. Soc., Series II, 17, 108 (1972).

61. Z. Malek and V. Kambersky, "On the Theory of the Domain Structure of Thin Films of Magnetically Uniaxial Materials," Czech. J. Phys., 8, 416 (1958).

62. C. Kooy and V. Enz, "Experimental and Theoretical Study of the Domain Configuration in Thin Layers of $BaFe_{12}O_{19}$," Philips Res. Reports 15, 7 (1960).

63. F. B. Hagedorn, "Domain Wall Motion in Bubble Domain Materials," C. D. Graham, Jr. and J. J. Rhyne, Editors, Magnetism and Magnetic Materials-1971 Amer. Inst. Phys., New York (1972), p. 72.

64. L. G. VanUitert, E. M. Gyorgy, W. A. Bonner, W. H. Grodkiewicz, E. J. Heilner, and G. J. Zydzik, "Control of Bubble Domain Properties in Garnets," Mat. Res. Bull. 6, 1185 (1971).

65. A. J. Kurtzig, R. C. LeCraw, A. H. Bobeck, E. M. Walters, R. Wolfe, H. J. Levinstein, and S. J. Licht, "Correlation of Domain Wall Mobility with Gallium Concentration in Bubble Garnets," C. D. Graham, Jr. and J. J. Rhyne, Editors, Magnetism and Magnetic Materials-1971, Amer. Inst. Phys., New York (1972) p. 180.

66. Y. S. Lin and Y. O. Tu, "Micromagnetic Solutions for Bubble Domains," Appl. Phys. Letters 18, 247 (1971).

67. W. J. DeBonte, "Theory of the Static Stability of Thick Walled Cylindrical Domains in Uniaxial Platelets," C. D. Graham, Jr. and J. J. Rhyne, Editors, Magnetism and Magnetic Materials-1971, Amer. Inst. Phys., New York (1972), p. 140.

68. D. E. Hill, private communication.

69. D. C. Mattis, "The Theory of Magnetism," Harper and Row, New York (1965), p. 5.

70. L. R. Maxwell, "Ferromagnetism and Ferrimagnetism," K. Lark-Horovitz and V. A. Johnson, Editors, Methods of Experimental Physics: Volume 6B: Solid State Physics, Academic Press, New York (1959), p. 193.

71. T. R. McGuire and P. J. Flanders, "Direct Current Magnetic Measurements," A. E. Berkowitz and E. Kneller, Editors, Magnetism and Metallurgy, Volume 1, Academic Press, New York (1969), p. 123.

72. H. J. Oguey, "Alternating Current Magnetic Measurements," A. E. Berkowitz and E. Kneller, Magnetism and Metallurgy, Volume 1, Academic Press, New York (1969), p. 189.

73. G. N. Rathenau and J. L. Snoek, "Apparatus for Measuring Magnetic Moments," Philips Res. Reports 1, 239 (1946).

74. C. A. Domenicali, "A Null-Coil Pendulum Magnetometer," Rev. Sci. Instr. 21, 327 (1950).

75. R. M. Bozorth, H. J. Williams, and D. E. Walsh, "Magnetic Properties of Some Orthoferrites and Cyanides at Low Temperatures," Phys. Rev. 103, 572 (1956).

76. S. Geller, H. J. Williams, R. C. Sherwood, J. P. Remecka, and G. P. Espinosa, "Magnetic Study of the Lighter Rare-Earth Ions in the Iron Garnets," Phys. Rev. 131, 1080 (1963).

77. S. Geller, H. J. Williams, G. P. Espinosa, and R. C. Sherwood, "Importance of Intrasublattice Magnetic Interactions and of Substitutional Ion Type in the Behavior of Substituted Yttrium Iron Garnets," Bell Systems Tech. J. 43, 565 (1964).

78. F. W. Harrison, J. F. A. Thompson, and G. K. Lang, "Single Crystal Magnetization Data for Anisotropic Rare-Earth Iron Garnets at Low Temperatures," J. Appl. Phys. 36, 1014 (1965).

79. R. Pauthenet, "Les Proprietés Magnétiques des Ferrites D'Yttrium et de Terres Rares des Formule $5Fe_2O_3 \cdot 3M_2O_3$," Ann. Phys. (Paris) 3, 424 (1958).
See also R. Pauthenet Ann. Phys. [12] 7, 710 (1952), Aimantation Spontanée des Ferrites.

80. S. Geller, H. J. Williams, R. C. Sherwood, and G. P. Espinosa, "Magnetic and Crystallographic Studies of Substituted Gadolinium Iron Garnets," J. Appl. Phys. 36, 88 (1965).

81. S. Foner, "Versatile and Sensitive Vibrating Sample Magnetometer," Rev. Sci. Inst. 30, 548 (1959).

82. P. J. Flanders and W. D. Doyle, "Motor Driven Magnetometer for Thin Magnetic Films," Rev. Sci. Instr. 33, 691 (1962).

83. D. O. Smith, "Development of a Vibrating Coil Magnetometer," Rev. Sci. Instr. 27, 261 (1956).

84. K. Dwight, N. Menyuk, and D. Smith, "Further Development of the Vibrating Coil Magnetometer," J. Appl. Phys. 29, 491 (1958).

85. D. M. Heinz, P. J. Besser, P. E. Elkins, H. L. Glass, J. E. Mee, L. A. Moudy, Epitaxial Film Growth of Bubble Domain Materials, Technical Report AFML-TR-71-126, June 1971, p. 20.

86. G. T. Croft, F. J. Donahoe, and W. F. Love, "Automatic Recording Torsional Magnetic Susceptibility Balance," Rev. Sci. Instr. 26, 360 (1955).

87. R. F. Penoyer, "An Automatic Torque Balance for Magnetic Anisotropy Measurements," Rev. Sci. Instr. 30, 711 (1959).

88. W. S. Byrnes and R. G. Crawford, "Improved Torque Magnetometer," J. Appl. Phys. 29, 493 (1958).

89. S. Chikazumi, "Physics of Magnetism," Wiley, New York (1964).

90. R. C. Sherwood, J. P. Remeika, and H. J. Williams, "Domain Behavior in Some Transparent Oxides," J. Appl. Phys. 30, 217 (1959).

91. D. Treves, "Magnetic Studies of Some Orthoferrites," Phys. Rev. 125, 1843 (1962).

92. D. Treves, "Studies on Orthoferrites at the Weizmann Institute of Science," J. Appl. Phys. 36, 1033 (1965).

93. J. Sosniak, "Magnetic Properties of Sputtered Single-Crystal Films of Terbium Orthoferrite," J. Appl. Phys. 42, 1802 (1971).

94. R. W. Teale, R. F. Pearson, and M. J. Hight, "Ferrimagnetic Resonance and Torque Measurements on Ytterbium-Substituted Yttrium Iron Garnet," J. Appl. Phys. 32, Suppl., 150S (1961).

95. R. F. Pearson and R. W. Cooper, "Torque Measurements on Rare-Earth Doped Yttrium Iron Garnet," J. Appl. Phys. 32, Suppl., 265S (1961).

96. R. F. Pearson, "Magnetocrystalline Anisotropy of Rare-Earth Iron Garnets," J. Appl. Phys. 33, Suppl., 1236 (1962).

97. R. F. Pearson and K. Tweedale, "Field Dependence of Anisotropy in Ytterbium-Doped Yttrium Iron Garnet," J. Appl. Phys. 35, 1061 (1964).

98. N. I. Sudakov, N. I. Vershinino, A. I. Drokin, and N. D. Ursulyak, "Magnetic Anisotropy of Bi-Ca-Fe-V Garnets," Bull. Acad. Sci. USSR, 34, 962 (1970).

99. R. Lacey, private communication.

100. Reference 57, p. 50.

101. A. H. Bobeck, "Recent Developments in Magnetic Bubble Technology," Paper 1, Spring Meeting - Electrochemical Society, Houston, Texas, May 1972.

102. R. Clover, private communication.

103. J. W. Beck, "Faraday Effect Hysteresigraph," Rev. Sci. Instr. 38, 1031 (1967).

104. C. D. Mee, "Recent Measurements of the Magneto-Optical Properties of Some Garnets," Contemp. Phys. 8, 385 (1967).

105. C. D. Mee, "The Magnetization Mechanism in Single-Crystal Garnet Slabs Near the Compensation Temperature," IBM Journal 11, 468 (1967).

106. D. J. Craik, "The Derivation of "Bubble" Material Parameters from Magnetization Curves," Physics Letters, 39A, 45 (1972).

107. F. Bloch, "Zur Theorie des Austauschproblems und der Remanenzerscheinung der Ferromagnetika", Z. Physik 74, 295 (1932).

108. Reference 89, p. 186.

109. A. J. Kurtzig and W. Shockley, "Measurement of the Domain-Wall Energy of the Orthoferrites," J. Appl. Phys. 39, 5619 (1968).

110. J. M. Nemchik, "Circular Domain Configuration in GdIG," J. Appl. Phys. 40, 1086 (1969).

111. S. H. Charap and J. M. Nemchik, "Behavior of Circular Domains in GdIG," IEEE Trans. Mag., Volume MAG-5, 566 (1969).

112. J. A. Cape and G. W. Lehman, "Magnetic Bubble Domain Interactions," Solid State Comm., 8, 1303 (1970).

113. J. A. Cape and G. W. Lehman, "Magnetic Domain Structures in Thin Uniaxial Plates with Perpendicular Easy Axis," J. Appl. Phys. 42, 5732 (1971).

114. J. Kaczér, "Ferromagnetic Domains in Uniaxial Materials," IEEE Trans. Mag., Volume MAG-6, 442 (1970).

115. B. A. Calhoun, E. A. Giess, and L. L. Rosier, "Dynamic Behavior of Domain Walls in Low-Moment Yttrium-Gallium-Iron Garnet Crystals," Apply. Phys. Letters 18, 287 (1971).

116. W. A. Bonner, J. E. Geusic, D. H. Smith, F. C. Rossol, L. G. VanUitert, and G. P. Vella-Coliero, "Characteristics of Temperature-Stable Eu-Based Garnet Films for Magnetic Bubble Applications," J. Appl. Phys. 43, 3226 (1972).

117. J. F. Dillon, Jr., "Domains and Domain Walls," edited by G. Rado and H. Suhl, Magnetism, Volume III, Academic Press, New York (1963), p. 415.

118. C. Kittel and J. K. Galt, "Ferromagnetic Domain Theory," F. Seitz and D. Turnbull, Editors, Solid State Physics, Volume 3, Academic Press, Inc., New York (1956), p. 437.

119. J. K. Galt, "Motion of Individual Domain Walls in A Nickel-Iron Ferrite," Bell Systems Tech. J. 33, 1023 (1954).

120. J. F. Dillon, Jr. and H. E. Earl, Jr., "Domain Wall Motion and Ferrimagnetic Resonance in a Manganese Ferrite," J. Appl. Phys. 30, 202 (1959).

121. H. Umebayashi and Y. Ishikawa, "Motion of a Single Domain Wall in a Parasitic Ferromagnet $YFeO_3$," J. Phys. Soc. Japan, 20, 2193 (1965).

122. F. B. Hagedorn and E. M. Gyorgy, "Domain Wall Mobility in Single-Crystal Yttrium Iron Garnet," J. Appl. Phys. Suppl. 32, 282S (1961).

123. M. A. Wanas, "Domain Wall Motion in Yttrium-Iron Garnets," J. Appl. Phys. 38, 1019 (1967).

124. H. Harper and R. W. Teale, "Magnetic Domain Wall Mobility Limitation by Anisotropic Impurity Ions in Ferrimagnetic Insulators," J. Phys. Chem. Sol., 28, 1781 (1967).

125. H. Harper and R. W. Teale, "The Influence of Erbium Doping on the Velocity of Magnetic Domain Wall Propagation in Yttrium Iron Garnet," J. Phys. C (Proc. Phys. Soc.) Series 2, Volume 1, 1046 (1968).

126. G. Asti, M. Colombo, M. Giudici and A. Levialdi, "Magnetization Dynamics in $BaO:6Fe_2O_3$ Single Crystals Using Pulsed Magnetic Fields," J. Appl. Phys. 36, 3581 (1965).

127. G. Asti, M. Colombo, M. Giudici, and A. Levialdi, "Domain Wall Motion in Barium Ferrite Single Crystals," J. Appl. Phys. 38, 2195 (1967).

128. G. Asti, F. Conti, and C. M. Maggi, "Domain Wall Mobility in High Uniaxial Anisotropy Ferrites," J. Appl. Phys. 39, 2039 (1968).

129. G. P. Vella-Coliero, D. H. Smith, and L. G. VanUitert, "Domain Wall Mobility in Some Rare-Earth Iron Garnets," IEEE Trans. Mag., Volume MAG-7, 745 (1971).

130. G. P. Vella-Coliero, D. H. Smith, and L. G. VanUitert, "Resonant Motion of Domain Walls in Yttrium Gadolinium Iron Garnet," J. Appl. Phys. 43, 2428 (1972).

131. F. N. H. Robinson, "Nuclear Resonance Absorption Circuit," J. Sci. Instr., 36, 481 (1959).

132. G. R. Henry, "Effects of Wall Inertia on Cylindrical Magnetic Domains," J. Appl. Phys. 42, 3150 (1971).

133. S. Middelhoek, "Domain Wall Velocities in Thin Magnetic Films," IBM Journal 10, 351 (1966).

134. S. Konishi, S. Yamada, and T. Kusuda, "Domain Wall Velocity, Mobility, and Mean-Free-Path in Permalloy Films," IEEE Trans. Mag., Volume MAG-7, 722 (1971).

135. J. A. Seitchik, W. D. Doyle, and G. K. Goldberg, "Simple Method of Measuring Mobility in Cylindrical Domain Materials," J. Appl. Phys. 42, 1272 (1971).

136. J. M. Nemchik and S. H. Charap, "Measurement of Domain Wall Mobility in GdIG," Metall. Trans., 2, 635 (1971).

137. A. H. Bobeck, I. Danylchuk, J. P. Remeika, L. G. VanUitert, and E. M. Walters, "Dynamic Properties of Bubble Domains," presented at 1970 Int. Conf. Ferrites, Kyoto, Japan.

138. H. Callen and R. M. Josephs, "Dynamics of Magnetic Bubble Domains with Application to Wall Mobilities," J. Appl. Phys. 42, 1977 (1971).

139. A. H. Bobeck, "Properties and Device Applications of Magnetic Domains in Orthoferrites," Bell Systems Tech. J. 46, 1901, (1967).

140. A. A. Thiele, A. H. Bobeck, E. Della Torre, "The Energy and General Translation Force of Cylindrical Magnetic Domains," Bell Systems Tech. J. 50, 711 (1971).

141. B. E. Argyle, J. C. Slonczewski, and A. F. Mayadas, "Domain Wall Motion in Rare-Earth Substituted Ga:YIG Epitaxial Films," C. D. Graham and J. J. Rhyne, Editors, Magnetism and Magnetic Materials-1971, Amer. Inst. Phys., New York (1972), p. 175.

142. H. Callen, R. M. Josephs, J. A. Seitchik, and B. F. Stein, "Wall Mobility and Velocity Saturation in Bubble Domain Materials," to be published.

143. J. C. Slonczewski, "Dynamics of Magnetic Domain Walls," C. D. Graham and J. J. Rhyne, Editors, Magnetism and Magnetic Materials-1971, Amer. Inst. Phys., New York (1972), p. 170.

144. J. A. Cape, "Dynamics of Bubble Domains," J. Appl. Phys. 43, to be published.

145. F. C. Rossol, "Domain Wall Mobility in Rare-Earth Orthoferrites by Direct Stroboscopic Observation of Moving Domain Walls," J. Appl. Phys. 40, 1082 (1969).

146. F. C. Rossol, "Domain Wall Mobility in Yttrium Orthoferrite," Phy. Rev. Letters 24, 1021 (1970).

147. P. W. Shumate, Jr., "Anisotropy in the Domain Wall Mobility of Rare-Earth Orthoferrites," J. Appl. Phys. 42, 5770 (1971).

148. A. Marsh, R. J. Fairholme, and G. P. Gill, "Domain Wall Mobility in Orthoferrite Crystals Grown by Float-Zone Technique," IEEE Trans. Mag., Volume MAG-7, 470 (1971).

149. P. W. Shumate, Jr., "Annealing-Induced Mobility Changes in Rare-Earth Orthoferrites," J. Appl. Phys. 43, 27 (1972).

150. E. M. Gyorgy and F. B. Hagedorn, "Analysis of Domain Wall Motion in Canted Antiferromagnets," J. Appl. Phys. 39, 88 (1968).

151. P. W. Shumate, Jr. and P. M. Eisenberger, "Domain Wall Mobility Enhancement Through X-Ray Irradiation Compared with Thermal Annealing," J. Appl. Phys. 43, 1299 (1972).

152. P. M. Eisenberger, P. H. Schmidt, and E. M. Walters, "Improved Magnetic Bubble Mobility by X-Ray Irradiation," Appl. Phys. Letters 17, 533 (1970).

153. A. H. Bobeck, R. F. Fischer, A. J. Perneski, J. P. Remeika, and L. G. VanUitert, "Application of Orthoferrites to Domain Wall Devices," IEEE Trans. Mag., Volume MAG-5, 544 (1969).

154. J. A. Copeland and R. R. Spiwak, "Circular Domain Velocity Versus Force," IEEE Trans. Mag., Volume MAG-7, 749 (1971).

155. P. W. Shumate, Jr., private communication.

156. F. C. Rossol and A. A. Thiele, "Domain Wall Dynamics Measured Using Cylindrical Domains," J. Appl. Phys. 41, 1163 (1970).

157. F. C. Rossol, "Stroboscopic Observation of Cylindrical Domain Propagation in a T-Bar Structure," IEEE Trans. Mag., Volume MAG-7, 142 (1971).

158. G. P. Vella-Coleiro and W. J. Tabor, "Measurement of Magnetic Bubble Mobility in Epitaxial Garnet Films," to be published.

159. J. A. Copeland, J. P. Edward, W. A. Johnson, and J. G. Ruch, "Single Conductor Magnetic Bubble Propagation Circuits," J. Appl. Phys. 42, 1266 (1971).

160. G. E. Moore, Jr., "High-Speed Stroboscopic Analysis of a Current-Drive Magnetic Domain Propagating Circuit," IEEE Trans. Mag., Volume MAG-7, 751 (1971).

161. R. M. Goldstein and J. A. Copeland, "Permalloy Rail-Cylindrical Magnetic Domain System," J. Appl. Phys. 42, 2361 (1971).

162. R. E. DeWames and T. Wolfram, "Dipole Exchange Spin Waves in Ferromagnetic Films," J. Appl. Phys. 41, 987 (1970).

163. R. E. DeWames and T. Wolfram, "Experimental Test for Pinned Spins in Ferromagnetic Resonance," Phys. Rev. Letters 26, 1445 (1971).

164. T. Wolfram and R. E. DeWames, "Magneto-Exchange Branches and Spin-Wave Resonance in Conducting and Insulating Films: Perpendicular Resonance," Phys. Rev. B4, 3125 (1971).

165. M. Sparks, "Ferromagnetic Resonance in Thin Films:
I. Theory of Normal Mode Frequencies.
II. Theory of Linewidths.
III. Theory of Mode Intensities."
Phys. Rev. B1, 3831, 3856, 3869 (1970).

166. R. F. Soohoo, Magnetic Thin Films, Harper and Row, New York (1965), p. 184ff.

167. R. C. LeCraw, R. Wolfe, A. H. Bobeck, R. D. Pierce, and L. G. VanUitert, "Radio-Frequency Determination of New Growth-Induced Anisotropy in Garnets for Bubble Devices," J. Appl. Phys. 42, 1641 (1971).

168. F. W. Harrison, R. F. Pearson, and K. Tweedale, "Single Crystal Research on Ferrites and Garnets," Philips Tech. Rev. 28, 135 (1967).

169. A. M. Clogston, H. Suhl, L. R. Walker, and P. W. Anderson, "Ferromagnetic Resonance Linewidth in Insulating Materials," J. Phys. Chem. Sol. 1, 129 (1956).

170. J. F. Dillon, Jr. and J. W. Nielsen, "Ferrimagnetic Resonance in Rare-Earth Doped Yttrium Iron Garnet: I. Field for Resonance," Phys. Rev. 120, 105 (1960).

171. J. F. Dillon, Jr. and L. R. Walker, "Ferrimagnetic Resonance in Rare-Earth Doped Yttrium Iron Garnet: II. Terbium Substitution," Phys. Rev. 124, 1401 (1961).

172. J. F. Dillon, Jr., "Ferrimagnetic Resonance in Rare-Earth Doped Yttrium Iron Garnet: III. Linewidth," Phys. Rev. 127, 1495 (1962).

173. G. P. Rodrigue, H. Meyer, and R. V. Jones, "Resonance Measurements in Magnetic Garnets," J. Appl. Phys. 31, 376S (1960).

174. A. F. Kip, "Resonance Phenomena," Lark Horowitz and Johnson, Editors, Methods of Experimental Physics - Volume 6B - Solid State Physics (Academic Press, New York, 1959), p. 227.

175. P. E. Seiden,"Magnetic Resonance," A. E. Berkowitz and E. Kneller, Editors, Magnetism and Metallurgy, Academic Press, New York (1969), p. 93.

176. R. S. Anderson, "Electron Spin Resonance," L. Marton, Editor, Methods of Experimental Physics, Volume 3, Academic Press, New York (1962).

177. Reference 89, p. 128.

178. J. Kanamori, "Anisotropy and Magnetostriction of Ferromagnetic and Antiferromagnetic Materials," G. T. Rado and H. Suhl, Editors, Magnetism, Volume 1, Academic Press, New York (1963), p. 127.

179. S. Reich, S. Shtrickman, and D. Treves, "Angular Variation of Coercivity in Orthoferrite Single Crystals," J. Appl. Phys. 36, 140 (1965).

180. K. P. Belov, A. M. Kadomtseva, and R. Z. Levitin, "On the Nature of the Magnetization Curves of a Single Crystal of $SmFeO_3$ near the Reorientation Temperature," Sov. Phys. JETP 24, 878 (1967).

181. R. M. Bozorth, V. Kromer, and J. P. Remeika, "Magnetization in Single Crystals of Some Rare-Earth Orthoferrites," Phys. Rev. Letters 1, 3 (1958).

182. R. C. Sherwood, L. G. VanUitert, R. Wolfe, and R. C. LeCraw, "Variation of the Reorientation Temperature and Magnetic Crystal Anisotropy of the Rare-Earth Orthoferrites," Phys. Letters 25A, 297 (1967).

183. A. H. Bobeck, E. G. Spencer, L.G. VanUitert, S. C. Abrahams, R. L. Barns, W. H. Grodkiewicz, R. C. Sherwood, P. H. Schmidt, D. H. Smith, and E. M. Walters, "Uniaxial Magnetic Garnets for Domain Wall "Bubble" Devices," Appl. Phys. Letters 17, 131 (1970).

184. A. Akselrad and H. Callen, "Growth-Induced Non-Cubic Anisotropy Arising from the Tetrahedral Sites in Garnets," Appl. Phys. Letters 19, 464 (1971).

185. A. H. Bobeck, D. H. Smith, E. G. Spencer, L. G. VanUitert, and E. M. Walters, "Magnetic Properties of Flux Grown Uniaxial Garnets," IEEE Trans. Mag., Volume MAG-7, 461 (1971).

186. P. J. Flanders, "Utilization of a Rotating Sample Magnetometer," Rev. Sci. Instr. 41, 697 (1970).

187. W. D. Doyle and P. J. Flanders, "The Magnetic Anisotropy in Polished GdIG Platelets," C. D. Graham and J. J. Rhyne, Editors, Magnetism and Magnetic Materials-1971, Amer. Inst. Phys., New York (1972), p. 707.

188. A. J. Kurtzig and F. B. Hagedorn, "Non-Cubic Magnetic Anisotropics in Bulk and Thin Film Garnets," IEEE Trans. Mag., Volume MAG-7, 473 (1971).

189. P. W. Shumate, Jr., D. H. Smith, and F. B. Hagedorn, "The Temperature Dependence of the Anisotropy Field and Coercivity in Epitaxial Films of Mixed Rare-Earth Iron Garnets," to be published.

190. A. Sano and A. Serra, "Static and Dynamic Properties of a Gadolinium Garnet," IEEE Trans. Mag., Volume MAG-4, 646 (1968).

191. B. F. Stein, "Magnetic Properties of GdIG Films Grown by Chemical Vapor Deposition," J. Appl. Phys. 41, 1262 (1970).

192. B. F. Stein and M. Kestigian, "Effect of Lattice and Thermal Mismatch on the Coercive Force of GdIG Films," J. Appl. Phys. 42, 1806 (1971).

193. L. Reimer, "Eine neue Method zur Messung der Magnetischen Eigenshaften dünner Schichten mit Hilfe des Faraday Effektes," Z. Naturforsch 11, 611 (1956).

194. D. J. Craik and M. J. Wood, "Apparatus for Quasi-Static and Dynamic Measurements on Magnetic Films," J. Sci. Instr. 42, 410 (1965).

195. T. Collins, "Temperature Dependence of the Hysteresis Properties of Polycrystalline Spinel, Ferrite, and Garnet Materials," IEEE Trans. Mag., Volume MAG-3, 513 (1967).

196. J. P. Hanton and A. H. Morrish, "Coercive Force of Single Crystal GdIG as a Function of Temperature," J. Appl. Phy. 36, 1007 (1965).

197. L. L. Rosier and B. A. Calhoun, "Dynamic Behavior of Domain Walls in Yttrium-Gallium-Iron Garnets," IEEE Trans. on Magn., MAG-7, 747-748 (1971).

198. E. A. Giess, B. E. Argyle, B. A. Calhoun, L. C. Cronemeyer, E. Klokholm, L. R. McGuire, and T. S. Plaskett, "Rare-Earth Yttrium-Iron-Gallium Garnet Epitaxial Films for Magnetic Bubble Domain Applications," Mat. Res. Bull., Volume 6, pp. 1141-1150 (1971).

199. E. R. Callen, A. E. Clark, B. DeSavage, and W. Coleman, "Magnetostriction in Cubic Neel Ferrimagnets, with Application to YIG," Phys. Rev. 130, pp. 1735-1740 (1963).

200. J. E. Goldman, "Magnetostriction of Annealed and Cold Worked Nickel Rods," Phys. Rev. 72, 529 (1947).

201. S. Iida, "Anomolous Magnetostriction of $Tb_3Fe_5O_{12}$ and $Eu_3Fe_5O_{12}$," Phys. Letters 6, pp. 165-167 (1963).

202. A. E. Clark and B. F. DeSavage, "Magnetostriction of Dyprosium, Holium and Erbium Iron Garnets," JAP 37, pp. 1324-1326, (1966).

203. S. Iida, "Magnetostriction Constants of Rare-Earth Iron Garnets," J. Phys. Soc. Japan, Volume 22, pp. 1201-1209 (1967).

204. K. P. Belov, A. M. Kadomtseva, T. L. Ovchinnikova, and V. V. Uskov, "Magnetostriction of Thulium Orthoferrite Single Crystals in the Region of the Temperature of Reorientation of the "Weak" Ferromagnetic Moment," JETP Letters 4, pp. 170-171 (1966).

205. E. M. Gyorgy, L. G. VanUitert, E. C. Heisler, Jr., and W. H. Grodkiewicz, "Magnetostriction of Some Rare-Earth Orthoferrites," JAP 42, pp. 482-485 (1971).

206. G. A. Petrakovskii, E. M. Smokotin, and A. G. Titava, "Temperature Dependence of the Magnetostriction Constants of Single Crystals of Yttrium-Gallium Ferrites Measured by the Microwave Method," Soviet Physics-Solid State, 9, pp. 1820-1824, (1960).

207. E. M. Gyorgy, J. P. Remeika, and F. B. Hagedorn, "Magnetic Behavior of Some Orthoferrites in the Anisotropy Change Region," JAP 39, pp. 1369-1370 (1968).

208. F. C. Rossol, "Temperature Dependence of Magnetic Domain Structure and Wall Energy in Single Crystal Thulium Orthoferrite," JAP 39, pp. 5263-5269 (1968).

209. W. C. Koehler, E. O. Wollan, and M. K. Wilkinson, "Neutron Diffraction Study of the Magnetic Properties of Rare-Earth Iron Perovskites," Phys. Rev. 118, pp. 58-70 (1960).

210. E. O. Wollan and W. C. Koehler, "Neutron Diffraction Study of the Magnetic Properties of the Series of Perovskite-Type Compounds," Phys. Rev. 100, pp. 545-563 (1955).

211. M. Eibschütz, S. Shtrikman, and D. Treves, "Mössbauer Studies of Fe^{57} in Orthoferrites," Phys. Rev. 156, pp. 562-577 (1967).

212. M. Eibschütz, G. Gorodetsky, S. Shtrikman, and D. Treves, "Differential Thermal Analysis and Mössbauer Studies in Rare-Earth Orthoferrites," JAP 35, pp. 1071-1072 (1964).

213. W. H. VonAulock, Handbook of Microwave Ferrite Materials, Academic Press, New York (1965).

214. Ta-Lin Hsu and D. W. Bellavance, "The Variation of $4\pi M_s$, Tc, and Ga/Fe Ratio with LPE Growth Temperature in Bubble Domain Films," Paper 1.4, Intermag Conference, Kyoto, Japan (1972).

215. D. H. Smith and A. W. Anderson, "The Temperature Dependence of Bubble Parameters in Some Rare-Earth Garnet Films," C. D. Graham and J. J. Rhyne, Editors, Magnetism and Magnetic Materials-1971, Amer. Inst. Phys., New York (1972), p. 120.

216. B. Lüthi, "Thermal Conductivity of Yttrium Iron Garnet," J. Phys. Chem. Solids 23, pp. 35-38 (1962).

217. P. L. Douglas, "Heat Transport by Spin Waves in Yttrium Iron Garnet," Phys. Rev. 129, pp. 1132-1135 (1963).

218. G. A. Slack and D. W. Oliver, "Thermal Conductivity of Garnets and Phonon Scattering by Rare-Earth Ions," Phys. Rev. 4, 592-609 (1971).

219. G. A. Slack, "Thermal Conductivity of CaF_2, MnF_2, CoF_2 and ZnF_2 Crystals," Phys. Rev. 122, pp. 1451-1464 (1961).

220. W. Strauss, "Detection of Cylindrical Magnetic Domains," J. Appl. Phys. 42, 1251 (1971).

221. G. S. Almasi, "Magneto-Optic Bubble Domain Devices," IEEE Trans. Mag., Volume MAG-7, 370 (1971).

222. R. J. Meltzer, "Spectrographs and Monochromators," R. Kingslake, Editor, Applied Optics and Optical Engineering, Academic Press, New York (1969), p. 47.

223. J. R. Benford and H. E. Rosenberger, "Microscopes," R. Kingslake, Editor, Applied Optics and Optical Engineering, Academic Press, New York (1967), p. 31.

224. M. W. P. Cann, "Light Sources in the 0.15-20μ Spectral Range," Applied Optics 8, 1645 (1969).

225. N. S. Kapany, Fiber Optics, Principles and Applications, Academic Press, New York (1967).

226. W. P. Siegmund, "Fiber Optics," R. Kingslake, Editor, Applied Optics and Optical Engineering, Academic Press, New York (1967), p. 1.

227. R.C.A. Phototubes and Photocells, Technical Manual PT-60, Staff Members of Radio Corporation of America (Radio Corporation of America, Lancaster, Pennsylvania, 1963).

228. G. S. Krinchik and M. V. Chetkin, "Magneto-Optical Properties of Garnet Ferrites in the Infrared Region," Sov. Phys. - JETP 13, 509 (1961).

229. Reference 37, p. 26.

230. F. J. Kahn, P. S. Pershan, and J. P. Remeika, "Ultraviolet Magneto-Optical Properties of Single Crystal Orthoferrites, Garnets, and Other Ferric Oxide Compounds," Phys. Rev. 186, 891 (1969).

231. F. L. Grismore, Jr. and J. E. Rhodes, Jr., "Fine Structure Absorption Measurements of Bulk Rare-Earth IG Single Crystals by Reflectivity Techniques," IEEE Trans. Mag., Volume MAG-5, 457 (1969).

232. Reference 37, p. 489.

233. F. Abeles, "La Determination de l'Indice et de l'Epaisseur des Couches Minces Transparentes," J. Phys. Radium 11, 310 (1950).

234. G. Hass and A. F. Turner, "Optical Measurements on Thin Films," Lark-Horovitz and Johnson, Editors, Methods of Experimental Physics, Volume 6B, Academic Press, New York (1959), p. 278.

235. A. V. Antonov, A. M. Balbashov, and A. Ya, Chervonenkis, "Optical Properties of Rare-Earth Orthoferrites," Sov. Phys. - Solid State 12, 1363 (1970).

236. W. Jung, "Dielectric Permittivity Tensor of $ErFeO_3$ for Radiation in the Visible Spectrum," J. Appl. Phys. 36, 1249 (1965).

237. P. N. Argyres, "Theory of the Faraday and Kerr Effects in Ferromagnetics," Phys. Rev. 97, 334 (1955).

238. G. S. Krinchik and M. V. Chetkin, "The Problem of Determining the Dielectric Permittivity and Magnetic Permeability Tensors of a Medium," Sov. Phys. - JETP 36, 1368 (1959).

239. W. Brewer and J. Jaumann, "Der Zusammenhang zwischen dem magnetooptischen Kerr- und Faraday Effect und die optischen Konstanten von dicken Ansdampfschichten aus Eisen, Kobalt, and Nickel," Z. Physik 173, 117 (1963).

240. F. Seitz, "The Modern Theory of Solids," McGraw-Hill, New York (1940), p. 629.

241. W. J. Tabor and F. S. Chen, "Electromagnetic Propagation Through Materials Possessing Both Faraday Rotation and Birefringence: Experiments with Ytterbium Orthoferrites," J. Appl. Phys. 40, 2760 (1969).

242. W. J. Tabor, A. W. Anderson, and L. G. VanUitert, "Visible and Infrared Faraday Rotation and Birefringence of Single Crystal Rare-Earth Orthoferrites," J. Appl. Phys. 41, 3018 (1970).

243. R. Wolfe, A. J. Kurtzig, and R. C. LeCraw, "Room Temperature Ferromagnetic Materials Transparent in the Visible," J. Appl. Phys. 41, 1218 (1970).

244. M. V. Chetkin, Ya. I. Shcherbakov, and A. Ya. Chervonenkis, "Magneto-Optical Properties of the Orthoferrites of Y, Sm, and Eu in the Infrared," Bull. Acad. Sci. USSR 34, 929 (1970).

245. R. B. Clover, C. Wentworth, and S. S. Mroczkowski, "Low Birefringent Orthoferrites for Optical Devices," IEEE Trans. Mag., Volume MAG-7, 480 (1971).

246. J. F. Dillon, Jr., "Optical Properties of Several Ferrimagnetic Garnets," J. Appl. Phys. 29, 539 (1958).

247. J. F. Dillon, Jr., "Observation of Domains in the Ferrimagnetic Garnets by Transmitted Light," J. Appl. Phys. 29, 1286 (1958).

248. J. F. Dillon, Jr., J. P. Remeika, and C R. Staton, "Linear Magnetic Birefringence in Cubic Magnetic Crystals," J. Appl. Phys. 40, 1510 (1969).

249. J. F. Dillon, Jr., E. M. Gyorgy, and J. P. Remeika, "Optical Birefringence and Anisotropy in a Uniaxial Ferrimagnetic Garnet," C. D. Graham and J. J. Rhyne, Editors, Magnetism and Magnetic Materials-1971, Amer. Inst. Phys., New York (1972), p. 190.

250. G. S. Krinchik and M. V. Chetkin, "Exchange Interaction and Magneto-Optical Effects in Ferrite Garnets," Sov. Phys. - JETP 14, 485 (1962).

251. B. Johnson and R. S. Tebble, "The Infrared Faraday Effect and g Values in Rare-Earth Garnets," Proc. Phys. Soc. 87, 935 (1966).

252. B. Johnson, "The Faraday Effect at Near Infrared Wavelengths in the Rare-Earth Garnets," Brit. J. Appl. Phys. 17, 1441 (1966).

253. I. G. Austin, "Infrared Faraday Rotation and Free Carrier Absorption in Bi_2Te_3," Proc. Phys. Soc. 76, 169 (1960).

254. R. C. LeCraw, D. L. Wood, J. F. Dillon, Jr., and J. P. Remeika, "The Optical Transparency of Yttrium Iron Garnet in the Near Infrared," Appl. Phys. Letters 7, 27 (1965).

255. R. E. MacDonald, O. Voegeli, and C. D. Mee, "Magneto-Optical Properties of Garnet Films," J. Appl. Phys. 38, 4101 (1967).

256. J. F. Dillon, Jr., "Origin and Uses of the Faraday Rotation in Magnetic Crystals," J. Appl. Phys. 39, 922 (1968).

257. H. Matthews, S. Singh, and R. C. LeCraw, "Sublattice Contributions to the Infrared Rotary Dispersion in YIG," Appl. Phys. Letters 7, 165 (1965).

258. E. Sawatzky and E. Kay, "Magnetic and Structural Properties of Epitaxial and Polycrystalline GdIG Films Prepared by RF Sputtering," J. Appl. Phys. 42, 367 (1971).

259. E. Sawatzky and D. H. Horne, "Apparatus for Direct Recording of Magneto-Optic Rotation and Magnetic Hysteresis," Rev. Sci. Instr. 41, 1284 (1970).

260. C. A. Fowler, Jr., E. M. Fryer, B. L. Brandt, and R. A. Isaacson, "Magnetic Domains in Orthoferrites by the Kerr Effect," J. Appl. Phys. 34, 2064 (1963).

261. F. J. Kahn, P. S. Pershan, and J. P. Remeika, "Ultraviolet Magneto-Optical Properties of Single Crystal Ferrimagnetic Ferric Oxide Compounds," J. Appl. Phys. 40, 1508 (1969).

262. H. Schuchert, S. Hüfner, R. Faulhaber, "Optical Investigations of $DyFeO_3$," Z. Phys. 220, 273 (1969).

263. H. Schuchert, S. Hüfner, and R. Faulhaber, "Optical Investigations of $HoFeO_3$," Z. Phys. 220, 280 (1969).

264. D. L. Wood, J. P. Remeika, and E. D. Kolb, "Optical Spectra of Rare-Earth Orthoferrites," J. Appl. Phys. 41, 5315 (1970).

265. A. P. Malozemoff, "The Optical Spectrum and Magnetic Properties of $TmFeO_3$ in the Single-Ion Model," J. Phys. Chem. Solids 32, 1669 (1971).

266. A. M. Clogston, "Interaction of Magnetic Crystals with Radiation in the Range 10^4-$10^5 cm^{-1}$," J. Appl. Phys. Suppl. 31, 198S (1960).

267. P. C. Bailey, "Absorption and Reflectivity Measurements on Some Rare-Earth Iron Garnets and α-Fe_2O_3," J. Appl. Phys. Suppl. 31, 39S (1960).

268. K. A. Wickersheim, "Optical and Infrared Spectra of the Garnets and Ferrites," J. Appl. Phys. Suppl. 32, 205S (1964).

269. D. L. Wood, "Energy Levels of Yb^{3+} in Garnets," J. Chem. Phys. 39, 1671 (1963).

270. D. L. Wood and J. P. Remeika, "Effect of Impurities on the Optical Properties of Yttrium Iron Garnet," J. Appl. Phys. 38, 1038 (1967).

271. P. Grünberg, S. Hüfner, E. Orlich, and J. Schmitt, "Crystal Field in Somarium and Dysprosium Garnets," J. Appl. Phys. 40, 1501 (1969).

272. D. L. Wood and J. P. Remeika, "Optical Transparency of Rare-Earth Iron Garnets," J. Appl. Phys. 37, 1232 (1966).

273. W. C. Dunlap, Jr., "Conductivity Measurements on Solids," Lark Horovitz, and Johnson, Editors, Methods of Experimental Physics: Solid State Physics, Volume 6B, Academic Press, New York (1959), p. 32.

274. D. E. Hill, "Basic Physics of Semiconductors," J. E. Katon, Editor, Organic Semiconducting Polymers, Dekker, New York (1968), p. 1.

275. J. F. Keithley, "Electrometer Measurements," Instruments and Control Systems 35, 74 (1962).

276. P. W. Grant and W. Ruppel, "Photoconductivity in Garnets," Solid State Comm. 5, 543 (1967).

277. D. C. Bullock and D. J. Epstein, "A New Technique for Generating Magnetic Bubbles," Proc. IEEE 59, 1713 (1970).

278. D. C. Bullock and D. J. Epstein, "Negative Resistance, Conductive Switching and Memory Effect in Silicon-Doped Yttrium-Iron Garnet Crystals," Appl. Phys. Letters 17, 199 (1970).

279. T. Kaplan, D. C. Bullock, D. Adler, and D. J. Epstein, "Thermally Induced Negative Resistance in Si-Doped YIG," Appl. Phys. Letters 20, 439 (1972).